FINAL REPORT

FOR

"ROCKET STUDY OF AURORAL PROCESSES"

NSG-6022


(NASA-CR-164534) ROCKET STUDY OF AURORAL PROCESSES Final Report, 1 May 1978 - 30 Jun. 1981 (New Hampshire Univ.) 77 p
HC A05/MF A01 CSCL 04A

N81-27720

Unclas
G3/46 26754

FINAL REPORT

FOR

"ROCKET STUDY OF AURORAL PROCESSES"

NSG-6022

MAY 1, 1978 - JUNE 30, 1981

NATIONAL AERONAUTICS AND SPACE ADMINISTRATION

WALLOPS FLIGHT CENTER

WALLOPS ISLAND, VA. 23337

LARRY J. EARLY, TECHNICAL OFFICER

Prepared by: Roger L. Arnoldy
Principal Investigator
Space Science Center
University of New Hampshire
Durham, New Hampshire 03824

FINAL REPORT FOR GRANT NSG-6022

## 1. INTRODUCTION

The work supported under NSG-6022 entitled "Rocket Study of Auroral Processes" commenced in 1978 and terminated June 30, 1981. Under NSG-6022 the University of New Hampshire built particle experiments for three rocket flights. These were a joint University of New Hampshire - University of Minnesota Terrier Malemute Flight, NASA 29:014, launched January 27, 1980; University of Minnesota, Echo V Flight, launched November 13, 1979; and the Norwegian Corobier Ferdinand 50 Flight, launched January 24, 1980. This grant also supported the analysis of data obtained from earlier rocket flights, Echo III, Flight 18:165, Flight 18:1004 and Flight 18:1005, and theoretical studies.

The form of this report will discuss each of the items in the work statement in detail starting first with the data analysis of earlier flights and theoretical studies.

## 2. ANALYSIS OF DATA - EARLIER FLIGHTS

### 2.1 Auroral Electrodynmics

2.1.0 Theoretical paper - "Modulation of Terrestrial Ion Escape Flux Composition (by Low-Altitude Acceleration and Charge Exchange Chemistry)", T.E. Moore, J. Geophys. Res., 85 2011, 1980.


Abstract

Motivated by recent observations of highly variable hot plasma composition in the magnetosphere, control of the ionospheric escape flux composition by low-altitude particle dynamics and ion chemistry has been investigated for an $e^-$, $H^+$, $O^+$, ionosphere. Theoretical polar wind results of Banks and Holzer and observations of highly nonthermal ion escape have been used as guides. It is found that the fraction of the steady state escape flux which is $O^+$ can be controlled very sensitively by the occurrence of parallel or transverse ion accel-

eration at altitudes below the altitude where the neutral oxygen density falls rapidly below the neutral hydrogen density and the ionospheric source of $O^+$ tends to be rapidly converted by charge exchange to $H^+$. The acceleration is required both to overcome the gravitational confinement of $O^+$ and to violate charge exchange equilibrium so that the neutral hydrogen atmosphere appears 'optically' thin to escaping $O^+$. Constraints are placed on the acceleration processes, and it is shown that $O^+$ escape is facilitated by observed ionospheric responses to magnetic activity.

2.1.1 Paper published using Flight 18:165 data - "Rocket Observations at the Northern Edge of the Eastward Electrojet", L.J. Cahill, Jr., R.L. Arnoldy, W.W.L. Taylor, J. Geophys. Res., 85, 3407, 1980.

Abstract

A Nike-Tomahawk rocket was launched north over two quiet late evening arcs in March 1975. A northward magnetic disturbance was observed on the ground under the rocket trajectory. South of the arcs the northward electric field was 60 mV/m, indicating strong westward plasma flow. An eastward electrojet current layer was penetrated in the upward flight. Precipitating electrons were observed over each arc. The electric field decreased to below 20 mV/m over each arc and recovered to 50 mV/m between the arcs. Using the observed electron flux and a model of the ionosphere, the Hall and Pedersen conductivities were calculated. These conductivities were used, with the observed electric field, to calculate the eastward and northward components of the horizontal ionospheric currents. The eastward current calculated south of the first arc agreed well with the observed eastward electrojet current. The power disipated by the Pedersen current $\Sigma_P |E|^2$ was also calculated and compared with the power carried by the precipitating electrons. The Joule power decrease abruptly in the auroral arcs, as the precipitating electron power increased. The total dissipated power was approximately the same inside the arcs, between them, and south of the luminosity. North of the aurora the electric field and dissipated power remained low. Field-aligned currents carried by the observed electrons were about a factor of 3 lower than those inferred from the magnetic field measurements. Likewise, current continuity arguments to keep the auroral current system divergence free required a larger field-aligned current than that obtained from the particle detectors.

2.1.2 Paper published using Flight 18:1005 data - "Ionospheric Electrical Currents in the Late Evening Plasma Research", D.A. Behm, F. Primdahl, L.J. Zanetti, Jr., R.L. Arnoldy, and L.J. Cahill, Jr., J. Geophys. Res., 84, 5339, 1979.

"Page missing from available version"

than that from measured precipitating electrons. There were also discrepancies between the ion drift measurement and the other measurements. We conclude that the various techniques are subject to large errors and that measurements of this important quantity be used with caution.

2.2 Electron Gun Dynamics

2.2.1 Paper published using Echo III data - "The Hot Plasma Environment and Floating Potentials of an Electron-Beam-Emitting Rocket in the Ionosphere", R.L. Arnoldy and J.R. Winckler, J. Geophys. Res., 86, 575, 1981.

Abstract

With an extensive array of particle sensors the plasma environment surrounding the Echo III accelerator payload is studied. From measurements of the thermal ion spectrum, negative payload potentials referenced to the unpertured ionospheric plasma are obtained. Multiple detectors determined the electron population from a fraction of an eV up to 40 keV energy. An intense electron population extending up to the energy of injected electrons by the accelerator is produced when the acceleration is turned on. The energetic tail of this population is returned to the payload principally from directions in which the beam was fired, with the most intense fluxes coming from the atmosphere for downward injections of the beam. The atmospheric-scattered beam and secondary electrons are called 'quick echoes'. Electrons of energy less than several keV down to the detector threshold (0.1 eV) are called the suprathermal component. These electrons are produced isotropically around the payload during gun firings and decay away in approximately 32 ms. The largest directional intensities of this component are observed at the higher altitudes. Quick echo electrons are also observed to produce suprathermal electrons when they encounter the payload. The mechanism by which the suprathermal electrons are produced is discussed but remains unknown at the present time. The hot electrons surrounding the accelerator payload during gun injections bring sufficient charge to the payload to neutralize it provided the loss of charge by secondary production on the payload skin is small, presumably owing to a positive payload floating potential during injection. Since the hot population exists for tens of milliseconds after the gun turn off, it results in driving the payload up to 4 volts negative during this time. Secondary production on the payload skin apparently prevents much larger negative potentials after gun turn off when the payload is immersed in the hot population. Quick echo electrons creating suprathermal electrons around the payload also drive the paylaod to a few volts negative. This is an important consideration when discussing the origin of the suprathermal electrons, since electrical discharge and beam plasma discharge mechanisms do not apply to the quick echo beams.

3. TERRIER-MALEMUTE FLIGHT- NASA 19:014

3.1 Description of Payload and Flight 

This rocket payload was launched up to an altitude of ~ 400 km over a quiet,

pre-midnight, auroral arc. It was fully instrumented to measure AC/DC fields, plasma, and energetic particles to investigate the electrodynamics of the aurora and its coupling to the magnetosphere. In addition to these passive measurements the flight contained an active experiment to study the plasma dynamics of firing 80 milliamperes of 60 eV argon ions into the ionosphere under auroral conditions.

AC/DC electric and magnetic fields were measured by the University of Minnesota. In addition the University of Minnesota built the argon plasma generator. Bernard Hallsler of the Max Planck Institute, Garching, provided a search coil magnetometer. Dr. Edward Szuszczwicz of the Naval Research Laboratory diagnosed the electron plasma with a pulsed plasma probe. The University of New Hampshire made the ion plasma measurements, topside photometer observations, and the energetic ion and electron measurements.

Multiple electrostatic analyzers measured the electron and ion distribution function from a few eV to 30 keV every 200 ms in 64 energy steps. In addition, with a peak tracking analyzer, 0.8 ms time resolution was obtained at the energy of the peak in the electron spectrum.

Finally, the University of New Hampshire ion plasma experiment measured the thermal ion population with four detectors positioned on the spinning payload to obtain a distribution function approximately once per second. The detectors were small geometric factor, electrostatic analyzers, sweeping the ion spectrum from 0 → 5 eV in 32 steps once every 25.6 milleseconds.

## 3.2 Flight Summary

The flight was highly successful. All experiments functioned properly with the exception of a great deal of interference in the search coil data. Vehicle performance was nominal, however, the electronic payload timer was late by about 34 seconds. This delay in function timing (see Wallops Report "Post Flight Investigation of the Terrier-Malemute 29:014 UE Delayed Mission Events, May 1980) resulted in 1) loss of 100 km upleg electrojet data, and 2) failure to recover payload.

The flight was in a diffuse aurora on the upleg and, according to ground data, over the eastward electrojet. Just beyond apogee the flight entered discrete aurora and crossed the Harang discontinuity into the westward electrojet. On the downleg of the trajectory and during the period of ion plasma release the flight was in transient discrete aurora.

## 3.3 Results

### 3.3.1 Paper presented at Fall A.G.U. 1980 - "Preliminary Results of Plasma Gun Operation in the Auroral Ionosphere", L.J. Cahill, Jr., R.L. Arnoldy, and D.A. Behm, EOS, 61, 1082, 1980.

Abstract

A sounding rocket instrumented with a full set of particles and fields detectors was launched from Poker Flats into the evening auroral ionosphere in January 1980. A 60 volt Argon ion gun on the rocket was operated intermittently during the last third of the flight. Immediately when the ion gun was turned on a number of effects were noted in the detectors. The signal from the electric field booms was saturated during part of each spin

period while the gun was on but displayed the normal sine wave modulation during the remainder of the period. A strong 2 to 4 kHz signal was received in an AGC receiver connected to the set of electric field booms. This signal was also spin modulated with large amplitude during only part of each spin period and amplitude lower by at least one order of magnitude during the remainder of the period. There was also a large increase in the waves observed with a 1 to 10 mHz swept frequency receiver.

The gun operation also produced dramatic changes in the charged particle fluxes. Two new populations of electrons appeared. The first was an enhancement betwee 100 and 1000 eV with the peak flux at 300 eV. The flux increased from $10^8$ to $10^9$ $(cm^2$ sec sr keV$)^{-1}$ at 300 eV. This population was isotropic with as many electrons coming up the field line as down. The second population was below 150 eV, increasing by a factor of five for electrons streaming down the field line and decreasing for particles coming back up.

3.3.2 Invited paper presented at "Chapman Conferences on the Formation of Auroral Arcs", R.L. Arnoldy, College, Alaska, July, 1981.

Abstract

Auroral electron and ion precipitation measured by sounding rockets and low altitude satellites will be reviewed. The two observing platforms provide a different perspective of the aurora. An attempt will be made to relate the two data sets to establish the precipitation signature of an auroral arc. Energy spectra and pitch angle distributions of precipitating particles have provided the basis for most auroral acceleration mechanisms. The altitude and particle mass dependence of these parameters as well as their spatial relationship to the visual aurora will be reviewed.

Although optical data have shown the fine structure (temporal and spatial) of an arc, improved response of particle detectors is just beginning to reveal this structure in particle precipitation. For example, intense fluxes of field aligned electrons are often observed having a duration on the order of a second as seen by rocket detectors. Similar field aligned bursts fluctuate at a few Hertz in satellite data. The intent of this paper is to summarize the observations that may aid in the formation of an auroral arc theory and which ultimately must be explained by such a theory.

This paper is to be published in the "Proceedings of Chapman Conference on the Formation of Auroral Arcs", A.G.U. Publication, Washington, D.C., S.-I. Akasofu, Editor, 1981. (This paper is presented in its entirety in Appendix A).

3.4 Work In Progress

Much of the data from the flight are still being analyzed, particularly, the aspect of combining the AC/DC field, plasma, and energetic particle results in a consistent model. Interesting observations we are currently pursuing at UNH are the following:

3.4.1. Natural Aurora Measurements

Using large geometric factor detectors capable of obtaining good statistics in measuring the weak diffuse aurora particle precipitation we find:

Ions < 1 keV undergo significant heating in the direction transverse to B during diffuse aurora. Diffuse aurora conics?

The diffuse auroral electron background shows little evidence of acceleration when the discrete aurora peaked spectum "grows" out of the diffuse precipitation.

Energetic (> 10 keV) ions and electrons having a trapped pitch angle distribution show nearly an order of magnitude increase in directional intensity when the rocket moves from the diffuse to discrete aurora.

These results suggest AC acceleration mechanisms might be important. In addition, the third result above casts some doubt on using the trapped pitch angle distribution as evidence of closed field lines. Why should trapped radiation increase on auroral field lines?

3.4.2 The Argon Plasma Releases:

Created a down-streaming electron population (< 150 eV) much like that often observed at the edges of auroral arcs.

Created a suprathermal population of electrons between 100 and 1000 eV energy with a peak flux at ∿ 300 eV which was isotropic in direction.

Triggered the release of a short burst of > 15 keV ions apparently from the trapped radiation.

Given the fact that the plasma generator was a very low power instrument, it seems imperative that the plasma releases triggered instabilities in the natural auroral environment to produce the effects observed. Finally, the results suggest that local ionospheric conditions could play an important role in discrete arc formation.

4. ECHO V (NASA 12:037)

4.1 Description of Payload and Flight

The Echo V payload launched by a Strypi II vehicle out of the Poker Flat, Alaska range carried an electron gun capable of injecting 40 keV electron bursts into the magnetosphere at a current of about 0.5 ampere. Earlier

flights in this program successfully detected electrons that have echoed from the conjugate hemisphere. The primary objective of the Echo V flight was to employ this technique to probe the magnetospheric configuration of the auroral oval. Are the auroral field lines closed, how far into the tail do they extend, are they equipotentials? Additional objectives were to continue to study the plasma dynamics associated with the gun injections.

The Principal Investigator for this program was Professor John Winckler at the University of Minnesota. The University of Minnesota furnished the electron gun, neutral gas release experiment and various sensors to diagnose the beam and its echo, these included scintillators for x-ray and energetic particle detection and photometers. Professor Paul Kellogg at the University of Minnesota performed plasma diagnostic measurements aboard the spacecraft with a Langmuir probe and wave measurements from the ground. Both the University of Minnesota and Professor Neil Davis from the University of Alaska conducted optical measurements for beam detection from the ground. Finally, the University of New Hampshire provided energetic ion and electron detectors and thermal ion sensors.

Four electrostatic analyzers measuring ions and electrons in the energy ranges, few eV to 2 keV and 50 eV to 30 keV, comprised the University of New Hampshire's energetic particle package. These detectors swept their respective energy range once every 200 milliseconds sampling 64 energy levels per sweep. The objective of these detectors was to measure the auroral precipitation and any perturbation of it due to the gun firing. Scattered beam electrons and secondary electrons produced by the beam and/or by the beam plasma discharge mechanism have also been studied by these sensors.

The UNH thermal ion sensors were identical to those discussed above for the Terrier-Malemuteflight except that they were rotated by a motor driven platform to obtain the distribution function since the payload did not spin. The motion of gun electrons in traversing the magnetosphere is sensitive to the convection electric fields they experience. The prime objective of the thermal ion sensors was to obtain a measure of these fields in the ionosphere.

## 4.2 Flight Summary

The flight was successfully launched with its trajectory over a weak aurora and just south of a bright auroral band. The UNH detectors all collected data, however, just before apogee the energetic particle detectors did not sweep the spectrum but were locked at one energy. Although this was a "failure" mode, valuable high time resolution data were collected as a result of it. No return Echo electrons were measured optically by the University of Alaska-University of Minnesota experiments. It is believed that the beam electrons were scattered to trapped orbits as a result of wave activity on the auroral field lines.

## 4.3 Results

Some preliminary results on the cross B dimension of the space charge region created by the electron gun were presented in an invited review paper authored by J.R. Winckler at the"NATO Advanced Research Institute on Artificial Particle Beams Ultilized in Space Plasma Studies"held in Norway, April, 1981.

The size of the electrostatically perturbed region transverse to the magnetic field around an electron-beam-emitting payload may exceed a kilometer as measured by the reduction in the thermal ion population reaching the payload just after beam emission.

4.4 Work In Progress

A major area of current study involves the electron-beam interactions with the ionosphere between 100 - 200 km.

Beams are a strong source of secondary electrons < 1 keV in energy (suprathermal population). The intensity of these electrons increases with altitude. This beam-plasma interaction is quenched by the release of neutral gas. Fluctuations in the suprathermal electron component can be excited at ambient heavy ion gyrofrequencies by the beam.

The scattering of beam electrons between 100 and 200 km is due primarily to beam-neutral collisions. A weak, neutral density independent, mechanism is observed above 200 km altitude.

## 5. COROBIER (F-50)

5.1 Description of Payload and Flight

Corobier is an acronum for "Coordinated Rocket and Backscatter Investigation of the E-Region". The program was a Norwegian one with Dr. Jan Holtet of the University of Oslo, the Principal Investigator, and Dr. Ray Greenwald of the Max-Planck Insitute, Lindau, a Co-Investigator. The general objective of the program was to study plasma instabilities and irregularities in the auroral E-region with a combination of ground-based probing of the ionosphere with radar and in-situ measurements. Enhanced ionospheric electric fields excite plasma instabilities in the auroral zone E-region. Although these waves are thought to be produced by the two stream and gradient drift instabilities there are a number of questions that remain.

A host of AC/DC wave experiments and plasma particle sensors were flown. Investigators included Holtet, Troym, Soraas and Stadenes from Norway; Falthamar and Bostrom from Sweden, Primdahl and Unstrup from Denmark and Evans and Arnoldy from the United States. The flight was launched out of the Norway Andoya rocket range on January 24, 1980. The UNH experiment consisted of thermal ion detectors identical to those that were flown aboard Flight 29:014. The objectives were to measure the ion temperatures and the E-region convective electric field in aspect of the specific program objectives.

5.2 Flight Summary

The UNH detectors worked normally during the flight although they did not fully deploy due to the anomalously low spin rate. The low spin rate resulted in all of the payload doors (except the UNH door) not to deploy, hence the flight was a failure. No attempt has been made to analyze the UNH data primarily because no other (except the DC magnetometer) experiment operated properly and also no support data are available.

# APPENDIX A

# REVIEW OF AURORAL PARTICLE PRECIPITATION

R. L. Arnoldy

Space Science Center, University of New Hampshire, Durham, N. H. 03824

Abstract. Auroral electron and ion precipitation measured by sounding rockets and satellites will be reviewed. The two observing platforms provide a different perspective of the aurora. An attempt will be made to relate the two data sets to establish the precipitation signature of an auroral arc. Energy spectra and pitch angle distributions of precipitating particles have provided the basis for most auroral acceleration mechanisms. The altitude and particle mass dependence of these parameters, as well as their spatial relationship to the visual aurora will be reviewed. Although optical data have shown the fine structure (temporal and spatial) of an arc, improved response of particle detectors is just beginning to reveal this structure in particle precipitation. For example, intense fluxes of field aligned electrons are often observed having a duration on the order of a second as seen by rocket detectors. Similar field-aligned bursts fluctuate at a few Hertz in satellite data. The intent of this paper is to summarize the observations that may aid in the formulation of an auroral arc theory.

## Introduction

Particle precipitation associated with discrete auroral arcs will be reviewed in this paper, emphasizing those observations which are pertinent to theories of auroral arc formation. Because of the large quantity of auroral particle precipitation data available, only observations by rockets and satellites generally made in the evening sector will be considered. Recent reviews of hot magnetospheric ions and electrons associated with optical auroras have been made by Hultqvist (1979, 1974).

This review will be organized according to observations made in three regions of space: Region 1 accessible to rockets and low altitude satellites (few hundred to a few thousand kilometers); Region 2 extending from 4000 → 8000 km (S3-3 satellite range); and Region 3 near the equatorial plane (geosynchronous satellite measurements).

## Inverted V Precipitation

The signature of an auroral arc in electron precipitation data is an inverted V structure in an electron spectrogram (Heikkila, 1970; Frank and Ackerson, 1971). In an inverted V the peak in the electron spectrum (monoenergetic peak) increases in energy toward the arc center resulting in an inverted V structure in an energy versus time spectrogram. Arcs or inverted V's are typically a few hundred km in latitudinal width when detected aboard satellites, whereas rocket observations, capable of better spatial resolution, reveal inverted V structures down to several km in width. There is some confusion in terminology in the literature concerning the identification of arcs with inverted V structures. Satellite papers refer to arcs imbedded in inverted V's, whereas from the perspective of rocket measurements any auroral form steady enough in time to traverse with a rocket payload has an inverted V structure. The difference appears to be one of measurement resolution. In fact, rockets have yet to identify the small scale structure (tens of meters) associated with optical arcs (Maggs and Davis, 1968). Finally, the relationship of electrostatic shocks seen by the S3-3 satellite (Mozer et. al., 1977) to inverted V's or auroral arcs also remains unclear at the present time.

Inverted V's occur on open as well as closed field lines. Figure 1 gives the latitudinal and longitudinal distribution of inverted V's seen by the AE-D satellite (Lin and Hoffman, 1979). They primarily occur in the evening sector auroral oval but are also present in the polar cap where field lines are normally considered to be open. Using the definition that field lines are closed if they can support trapped radiation, inverted V's detected at satellite altitudes occur on both open and closed field lines (Frank and Ackerson, 1972; Mizera et. al., 1976; Eliasson et. al., 1978; Lin and Hoffman, 1979). At rocket altitudes, however, inverted V's are generally seen coincident with a mirroring population of energetic ions and/or electrons suggesting closed field lines (Venkatarangan et. al., 1975; Whalen and Daley, 1979).

The monoenergetic peak in the inverted V electron spectrum is generally taken as evidence for electron acceleration by a quasi-static electric potential. There are a number of observations,

however, that suggest the inverted V electrons have passed through a turbulent region. The pitch angle distribution of the monoenergetic peak electrons is isotropic minus the loss cone at low altitudes (Arnoldy et. al., 1974; Lin and Hoffman, 1979). The temperature of precipitating electrons with energies above the spectral peak is proportional to the peak energy suggesting that they are heated in the acceleration region (Lin and Hoffman, 1979). The monoenergetic peak of inverted V's represents a stable electron distribution when observed at rocket altitudes (Kaufmann et. al., 1978) as the example in Figure 2 shows. Finally, the V-shaped pitch angle distributions observed by the AE-D satellite for energies below the monoenergetic peak has been explained as due to a field-aligned component combined with isotropic backscattered electrons and a significant number of electrons with energies slightly below the peak energy trapped between their mirror points and an electric potential structure (Lin and Hoffman, 1979).

The field-aligned electrons in an inverted V occur at energies below the monoenergetic peak producing double peaked spectra as seen in Figure 3 (Arnoldy et. al., 1974; Lin and Hoffman, 1979; Kaufmann, 1980). The 5 keV peak in the spectra of Figure 3 is isotropic in pitch angle, whereas the 2 - 3 keV peak is field-aligned and observed only at small pitch angles. This field-aligned component will be discussed in more detail later in this review.

Ion Precipitation

The ESRO I data showed that ions and electrons simultaneously precipitated on the same field line, but keV ion fluxes and spectra were less variable than those of the electrons in the same energy range (Hultqvist, 1979). The ESRO I data also showed that keV electrons were frequently field-aligned in the same region as ions, however, more sporadic and narrower in space/time than the ion field-aligned fluxes. Field-aligned keV ions occur at the edge of inverted V's with spectral softening at the center and a tendency toward isotropy (Hultqvist, 1971). In contradiction to the ESRO I results cited above, the ESRO 4 and IMJUN 5 data show no field-aligned ions and rarely any hot ions in inverted V's, respectively (Frank and Ackerson, 1972; Eliasson et. al., 1979). Hultqvist (1971) has interpreted the different results in terms of a solar cycle effect. ESRO I, operating during solar maximum, observed both ions

electrons accelerated by a potential above the satellite. The potential accelerating the ions occurred below the electron potential and was created by the precipitating electrons interacting with an elevated neutral atmosphere during solar maximum conditions.

Rocket measurements of ion precipitation are more limited because of the low altitude obtained by many of the flights. Spectral and intensity changes are generally anticorrelated when ions and electrons precipitate simultaneously (Bryant et. al., 1977; Edwards et. al., 1978). A notable exception is the case of general ion and electron anticorrelation until the center of an electron inverted V is reached where suddenly a band of 6 keV ions appeared simultaneously with the electrons (Bryant et. al., 1977). Ion data from a number of Canadian rocket flights (Miller and Whalen, 1976) show relative independence of energy spectra from auroral activity. Pitch angle distributions were observed to be either isotropic over the upper hemisphere or trapped, and there was, in general, little correlation with electron precipitation.

## Field-Aligned Precipitation

As discussed above, the monoenergetic peak in the electron spectrum is generally isotropic in pitch angle. The electrons discussed here are sporadic bursts of intense field-aligned precipitation. The field-aligned electrons are usually less than a few keV in energy and are below the monoenergetic peak in the spectrum (Arnoldy et. al., 1974; Lin and Hoffman, 1979). Figure 4 shows a flux ratio spectrogram of a satellite inverted V event. The heavy line tracing the spectral peak lies in a region of general pitch angle isotropy whereas the field-aligned fluxes are transient and of lower energy. The field-aligned fluxes generally occur over a range of energies (Arnoldy et. al., 1974; Raitt and Sojka, 1977; Lin and Hoffman, 1979).

Field-aligned electrons are generally seen during active auroras (McEwen, 1972; Arnoldy et. al., 1974; Bosqued et. al., 1974) and are localized on edges of arcs in regions between different plasmas (Whalen and McDiarmid, 1972; Bryant et. al., 1973; Maehlum and Moestue, 1973; Arnoldy, 1974; Lundin, 1974; Pulliam et. al., 1980). Figure 5 gives two energy channels of a rocket electron detector along with ground photometer measurements in the lower panel. The rapid oscillations in the 1.4 keV detector at 195 and 310 seconds are a spin

modulation as the detector swept through the field-aligned precipitation localized near the northern and southern borders of the aurora.

The field-aligned precipitation occurs in bursts or fluctuates at a few Hertz (McEwen, 1971; Arnoldy et. al., 1974; Bosqued et. al., 1974; Boyd and Davis, 1977; Raitt and Sojka, 1977). If fluctuating, all energies field-aligned fluctuate in phase (Lin and Hoffman, 1979). This later observation rules out an energy dependent process for producing the field-alignment. Finally, the field-alignment is generally within 20° of the field line at rocket altitudes and on occasion less than 10° (Bryant et. al., 1973; Arnoldy et. al., 1974; Bosqued et. al., 1974). To maintain such a degree of field-alignment the mechanism could not be too far removed from the measurements. This combined with their short-lived nature and field-alignment over a range of energies suggests that the phenomena is the result of the acceleration of ambient electrons in a large scale transient electric field. The relationship of the field-aligned fluxes to the inverted V acceleration region remains unclear at the present time.

## Low Energy Electron Precipitation

The electron differential directional intensity below the monoenergetic peak in the precipitating electron spectrum can be fit to a power law as $E^{-\gamma}$ where $\gamma$ varies between 1 and 2 (Reasoner and Chappell, 1973; Arnoldy and Choy, 1973). Over an inverted V or a discrete auroral arc these low energy electrons are generally isotropic over the full 180° range of pitch angles. Evans (1974) has interpreted this result in terms of an electric field trapping secondaries and degraded primaries between the potential region and the atmosphere. Recent efforts by Pulliam et. al., (1980) to fit this model to rocket data have been quite successful.

Recent measurements over a diffuse aurora have revealed similar isotropic low energy electrons (Evans and Moore, 1979). Since the diffuse aurora electron precipitation has no peak in the spectrum the electrons apparently have not fallen through a potential region. There is, therefore, no mechanism to reflect the backscattered electrons at 1 - 2 earth radii above the aurora. To achieve the measured isotropic distributions, Evans and Moore (1979) have postulated that the backscattered electrons fill the entire flux tube and as a result of pitch angle scattering could be a source for the plasma sheet electron population.

Evans and Moore (1979) have modeled the plasma sheet spectrum and presumably the spectrum precipitated during diffuse aurora are due to a primordial Maxwellian (Figure 6) and the atmospheric backscattered electrons that are in equilibrium with this Maxwellian. In the model spectrum the Maxwellian electrons dominate at high energies and the atmospheric electrons dominate at low energies giving a spectrum which approximates that measured quite well. This topic will be discussed further under Region 3.

When not over visible aurora the low energy precipitated electrons often remain but are not isotropic in pitch angle. Figure 7 gives down and up-going electron energy spectra measured by a sounding rocket in the region between two visible auroras. There is a definite downward streaming population of suprathermal electrons between 100 and 500 eV energy which are not secondarily related to any higher energy component. Figure 8 gives data from another rocket flight where a very narrow arc (spatially coincident with the 3 keV fluxes) was imbedded in widespread low energy precipitation. Above the arc, at 145 seconds flight time, the electrons below 1 keV were isotropic in pitch angle while outside the arc, at 200 seconds there was a net downward streaming of the less than 1 keV electrons. This net precipitation of less than 1 keV electrons carries significant current out of the atmosphere and could represent the high energy tail of the precipitation responsible for the large scale evening sector Region 1 currents except when over an arc where the Region 1 current is carried predominantly by the accelerated energetic electrons.

There is a growing body of evidence that suprathermal electrons are rather easily heated by wave interactions. Measurements from both the Polar V and Echo III electron accelerator payloads give an intense background of suprathermal electrons that remained after the energetic beam injections. These electrons could not be interpreted in terms of beam secondaries nor as scattered and degraded beam primary electrons (Maehlum et. al., 1979; Arnoldy and Winckler, 1980). The accelerator payloads are known, however, to be intense sources of wave turbulence when operated in the upper ionosphere (Cartwright and Kellogg, 1974). Such turbulence could heat the particle population near the payload. Johnson and Sojka (1980) cite a case of ambient thermal electrons being heated to temperatures as high as $10^5$ K by the passage of a field-aligned beam of a few hundred eV through the ionosphere at altitudes over 660 km. A beam/

plasma interaction is cited as the heating mechanism. Finally, recent results we have obtained from the release of an argon plasma at 200 km altitude show considerable modification of the naturally occurring precipitation below 1 keV. Figure 9 gives some preliminary electron measurements from this experiment. An isotropic population of electrons at a few hundred eV is introduced as well as a component below 100 eV streaming down the field lines. These electrons were closely correlated with plasma injections when wave instruments aboard the payload also measured greatly enhanced intensities. Such modifications of the low energy component can alter the light emission and electrodynamic properties of the upper ionosphere from that expected on the basis of atmospheric collisions above.

## Region 2

The S3-3 spacecraft surveying the region of space from 4000 → 8000 km above the auroral arc has provided considerable evidence for large scale electric fields along the magnetic field from pitch angle and energy distributions of electrons and ions. The satellite is generally found to be immersed in an electric field ∿ 1 volt/km extending over a few thousand kilometers (Chui and Schulz, 1978; Cladis and Sharp, 1979). We now briefly review the different types of particle population measured by the S3-3 mission, not all of which are readily interpretable in terms of quasi-steady field-aligned electric field.

### UFI (Upward Flowing Ions)

UFI with a directional intensity $J > 2 \times 10^6$ $(cm^2 \text{ sec ster keV})^{-1}$ are a common feature seen on approximately 60% of the S3-3 orbits. They coincide with the statistical auroral oval and have a strong dawn-dusk asymmetry with a maximum in the dusk sector (Chielmetti et. al., 1978). The predominant species in the UFI are $H^+$ and $O^+$ ions (Shelley et. al., 1976). UFI and electrostatic hydrogen cyclotron waves coincide in over 90% of the events studied (Kintner et. al., 1979). Finally, UFI are observed to have a beam pitch angle distribution of ($0 \sim 180°$) or a conic pitch angle distribution ($90° < 0 < 180°$).

### UFI Beams

UFI beams have a maximum frequency of occurrence in the dusk sector and are observed prima-

rily above 5000 km altitude (Corney et.al., (1980). Beams are observed primarily in the region of upward field-aligned current and coincide with electrostatic shocks in the evening sector (Cattell et. al., 1979). It would appear that the beams are a phenomena associated with discrete auroral forms.

UFI Conics

Conics are observed at lower altitudes than beams with a tendency to prefer the higher altitudes during disturbed times (Corney et. al., 1980). During magnetically quiet times conics tend to be a daytime cusp phenomena becoming more uniformly spread in local time as the activity increases (Ghielmetti et. al., 1979). Conics are observed in all field-aligned current regions (Cattell et. al., 1979) hence appear to be less associated with inverted V's than beams. Conics are apparently the same ions as the transversely accelerated ions (TAI) seen at lower altitudes (Whalen et. al., 1978; Klumpar, 1979; Ungstrup et. al., 1979).

DFI (Downward Flowing Ions)

DFI occur much less frequently than do UFI in the auroral region and do not display a dawn-dusk asymmetry (Ghielmetti et. al., 1979). DFI occur equatorward of UFI and in regions of inward (evening) and outward (morning) field-aligned currents (Cattell et. al., 1979), hence appear to be associated with the diffuse aurora. DFI are correlated with trapped keV ions and occur preferentially in spatially localized regions of enhanced hot keV plasma ions. Because of this, Ghielmetti, et al. (1979) have associated DFI with the injection of ring current ions in the equatorial plane. Some DFI are associated with retarded electron precipitation suggesting an electric field acceleration opposite to that in inverted V's (Ghielmetti et. al., 1979). The first example of an ion inverted V was presented at this conference by Burgess and Reiff (1980).

Counterstreaming Electron Beams

Counterstreaming electron beams have energies in the keV range. They are often spatially associated with regions of UFI conics (Fennell et. al, 1979). They are field-aligned to within several degrees and are generally comparable in width for both upward and downward beams (Sharp et.al., 1980).

The energy spectra for counterstreaming electron beams are broad and generally unstructured. In the region of counterstreaming electron beams, the electron beams, the loss cone of background electrons is not affected, ruling out a quasi-static parallel electric field. Sharp et. al.(1980) have suggested that the counterstreaming electron beams are locally accelerated ambient electrons by flickering double layers. Counterstreaming electron beams appear to be similar in many respects to the field-aligned electron bursts seen by low altitude satellites and rockets discussed above.

## Region 3

Plasma injections at synchronous orbit are the equatorial plane signature of an auroral substorm. Although much correlative work between ground and synchronous satellite measurements has been done (Akasofu, 1977), how one region maps to the other is still unclear. Moreover, the physics of the injection of particles at synchronous orbit remains to be defined. That there is an exchange of particles between the equatorial plane and the ionosphere is certain, however, the degree to which the ionosphere provides plasma to the equatorial plane (plasma sheet) is yet to be fully explored. As we have seen, measurements at $\sim 1$ $R_E$ (Region 2) reveal many particles leaving the ionosphere. Presumably these particles are those that have been detected at synchronous altitude as "source cone" ions and electrons (McIlwain, 1974; Mauk and McIlwain, 1975). It is to be noted, however, that the source cone particles observed have a wider pitch angle spread than the actual loss cone at 6.6 $R_E$. If the particles were accelerated in Region 2 they must have been diffused in pitch angle before reaching the equator.

An example of an electron injection at synchronous orbit is given in Figure 10. At 0412 UT the intensity of the higher energy electrons increased by one or two orders of magnitude while the low energy electrons (< few keV) decreased by about as much. The injection represented a dramatic change in spectrum from a monotonically decreasing one to nearly a Maxwellian. Following the injection, the spectrum then gradually returned to approximately its old shape and to pre-injection intensity levels. If an aurora was initiated as a result of this injection, then the gradual return of low energy electrons might represent the filling of the plasma sheet with backscattered and secondary electrons from the auroral

ionosphere as suggested by Evans and Moore (1979).

## Concluding Remarks

This review of auroral particle precipitation raises three questions about auroral arc formation. First, what is the role of AC phenomena in auroral particle acceleration? Examples of bursts of field-aligned electrons, simultaneous ion and electron precipitation, counterstreaming electrons, and conics (transversely accelerated ions) all suggest AC phenomena. Second, what is the importance of electrons < 1 keV in the auroral beam? Clearly they are not all secondaries. Inverted V's appear to be imbedded in and possibly develop as a result of this precipitation. Finally, what role does the lower ionosphere have on the formation of arcs? Recent controlled experiments with sounding rockets which have altered the lower ionospheric conductivity often have resulted in some form of anomalous particle precipitation. In addition, there is a growing evidence for fairly low altitude acceleration of particles occurring naturally, such as bursts of low energy field-aligned electrons and transversely accelerated ions.

Acknowledgements. This work was supported by the National Aeronautics and Space Administration under Grant NSG-6022 and by the Division of Atmospheric Sciences, National Science Foundation under Grant ATM-7920484. Many helpful discussions the author has had with Professor Richard Kaufmann and Dr. Thomas Moore at the University of New Hampshire, is gratefully acknowledged.

## References

Akasofu, S.I., Physics of the magnetospheric substorm, D. Reidel, Boston, 1977.

Arnoldy, R.L., and L.W. Choy, Auroral electrons of energy less than 1 keV observed at rocket altitudes, J. Geophys. Res., 78, 2187, 1973.

Arnoldy, R.L., P.B. Lewis, and P.O. Isaacson, Field-aligned auroral electron fluxes, J. Geophys. Res., 79, 4208, 1974.

Arnoldy, R.L., The relationship between field-aligned current, carried by suprathermal electrons, and the auroral arc, J. Geophys. Res. Ltrs., 4, 407, 1977.

Arnoldy, R.L., and J. Winckler, The hot plasma environment and floating potentials of an electron beam-emitting rocket in the ionosphere, accepted, J. Geophys. Res., 84, 1980.

Bosqued, J.M., G. Cardona, and H. Rème, Auroral electron fluxes parallel to the geomagnetic field lines, J. Geophys. Res., 79, 98, 1974.

Boyd, J.S. and T.N. Davis, Rocket measurements of electrons in a system of multiple auroral arcs, J. Geophys. Res., 82, 1177, 1977.

Bryant, D.A., G.M. Courtier, and G. Bennett, Electron intensities over two auroral arcs, Planet. Space Sci., 21, 165, 1973.

Bryant, D.A., D.S. Hill, D.R. Lepine, and R.W.N. Mason, Electrons and positive ions in an auroral arc, Nature, 266, 148, 1977.

Burgess, G.A., and P.H. Reiff, Particle acceleration of an ion inverted V, Program of AGU Chapman Conference on the Formation of Auroral Arcs, 1980.

Cartwright, D.G., P.J. Kellogg, Observations of radiation from an electron beam artificially injected into the ionosphere, J. Geophys. Res., 79, 1439, 1974.

Cattell, C., R. Lynch, R.B. Torbert, and F.S. Mozer, Observations of differences between regions of current flowing into and out of the ionosphere, Geophys. Res. Ltrs., 6, 621, 1979.

Chui, Y.T. and M. Schulz, Self-consistent particle and parallel electrostatic field distributions in the magnetosphere--ionosphere auroral region, J. Geophys. Res., 83, 629, 1978.

Cladis, J.B., and R.D. Sharp, Scale of electric field along magnetic field in an inverted V event, J. Geophys. Res., 84, 6564, 1979.

Edwards, T., D.A. Bryant, and M.J. Smith, Preliminary results of particle measurements from Skylark SL 1421 and Fulra F1, paper presented at MIST, Southampton, 1978.

Eliasson, L., L.A. Holmgren, and K. Ronmark, Pitch angle and energy distributions of auroral electrons measured by the ESRO 4 satellite, KGI Reprint, 1978.

Eliasson, L., L.A. Holmgren and D. Hultqvist, Observations of keV ions in inverted V events by means of the ESRO 4 satellite, KGI Report, 1979.

Evans, D.S., Precipitating electron fluxes formed by a magnetic field-aligned potential difference, J. Geophys. Res., 39, 2853, 1974.

Evans, D.S., and T.E. Moore, Precipitating electrons associated with the diffuse aurora: evidence for electrons of atmospheric origin in the plasma sheet, J. Geophys. Res., 84, 6451, 1979.

Fennell, J.F., P.F. Mizera and D.R. Croley, Jr., Observations of ion and electron distribution during the July 29 and July 30, 1977 storm period, Proceeding of Magnetospheric Boundary

Layer Conference, Alpach, 1979.
Frank, L.A. and K.L. Ackerson, Observations of charged particle precipitation into the auroral zone, J. Geophys. Res., 76, 3612, 1971.
Frank, L.A. and K.L. Ackerson, Local time survey of plasma at low altitudes near the auroral zone, J. Geophys. Res., 77, 4116, 1972.
Ghielmetti, A.G., R.G. Johnson, R.D. Sharp, and E.G. Shelley, The latitudinal diurnal, and altitudinal distributions of upward flowing energetic ions of ionospheric origin, Geophys. Res. Ltrs., 5, 59, 1978.
Ghielmetti, A.G., R.D. Sharp, E.G. Shelley, and R.G. Johnson, Downward fluxing ions and evidence for injections of ionospheric ions into the plasma sheet, J. Geophys. Res., 84, 5781, 1979.
Gorney, D.J., A. Clarke, D.R. Croley, J.F., Fennell, J.M. Luhmann, and P.F. Mizera, The distribution of ion beams and conics below 8000 km, Aerospace Report # ATR-80 (7744)-1, 1980.
Heikkila, W.J., Satellite observations of soft particle fluxes in the auroral zone, Nature, 225, 369, 1970.
Hultqvist, B., On the production of magnetic field-aligned electric field by the interaction between the hot magnetospheric plasma and the cold ionosphere, Planet. Space Sci., 19, 749, 1971.
Hultqvist, B., Rocket and satellite observations of energetic particle precipitation in relation to optical aurora, Ann. Geophys., 30, 223, 1974.
Hultqvist, B., The hot ion component of the magnetospheric plasma and some relations to the electron component--observations and physical implications, Space Science Review, 23, 581, 1979.
Johnson, A.D., and J.J. Sojka, A beam/plasma interaction in the high-altitude auroral ionosphere, accepted, Planet. Space Sci., 26, 1980.
Kaufmann, R.L., P.E. Dusenberry, and B.J. Thomas, Stability of auroral plasma: parallel and perpendicular propagation of electrostatic wave, J. Geophys. Res., 83, 5663, 1978.
Kaufmann, R.L., Electrostatic wave growth: secondary peaks in the measured auroral distribution function, J. Geophys. Res., 84, 1713, 1980.
Kintner, P.M., M.C. Kelley, R.D. Sharp, A.G. Ghielmetti, M. Temerin, C. Cattell, P.F. Mizera, and J.F. Fennell, Simultaneous observations of energetic (keV) upstreaming and electrostatic hydrogen cyclotron waves, J. Geophys. Res., 84, 7201, 1979.
Klumpar, D.M., Transversely accelerated ions: an ionospheric source of hot magnetospheric ions,

J. Geophys. Res., 84, 4229, 1979.
Lin, C.S., and R.A. Hoffman, Characteristics of the inverted-V event, J. Geophys. Res., 84, 1514, 1979.
Lundin, R., Rocket observations of electron spectral and angular characteristics of an inverted V event, Planet. Space Sci., 24, 499, 1976.
Maehlum, B.N. and H. Moestue, High temporal and spatial resolution observations by low energy electrons by mother-daughter rocket in the vicinity of two quiescent auroral arcs, Planet. Space Sci., 21, 1957, 1973.
Maehlum, B.N., B. Grandal, T.A. Jacobsen and J. Troim, Polar 5--an electron accelerator experiment within an aurora 2, scattering of an artificially produced electron beam in the atmosphere, Planet. Space Sci., 28, 279, 1979.
Maggs, J.E., and T.N. Davis, Measurements of the thickness of auroral structures, Planet. Space Sci., 16, 205, 1968.
Mauk, B.H., and C.E. McIlwain, USCD auroral particle experiment, IEEE Trans. on Aerospace and Electronic Systems, AES-11, 1125, 1975.
McEwen, D.J., Rocket measurements of low energy electrons during auroral events, Space Research XII, Bowhill, Jaffee and Rycoft, editors, Akademie-Verlag, Berlin, 1972.
McIlwain, C.E., Auroral electron beams near the magnetic equator, Physics of the hot plasma in the magnetosphere, editors, Hultqvist and Stenflo, Plenum Press, New York, 1975.
Miller, J.R. and B.A. Whalen, Characteristics of auroral proton precipitation observed from sounding rockets, J. Geophys. Res., 81, 147, 1979.
Mizera, P.F., D.R. Croley, Jr., and J. Fennell, Electron pitch angle distributions in an inverted V structure, Geophys. Res. Ltrs., 3, 149, 1976.
Mozer, F.S., C.W. Carlson, M.K. Hudson, R.B. Torbert, B. Parady, J. Yatteau and M.C. Kelley, Observations of paired electrostatic shocks in the polar magnetosphere, Phys. Rev. Ltrs., 38, 1977.
Pulliam, D.M., H.R. Anderson, K. Stammes, and M. H. Rees, Auroral electron acceleration and atmospheric interactions, Rice Preprint, 1980.
Raitt, W.J., J.J. Sojka, Field-aligned suprathermal electron fluxes below 270 km in the auroral zone, Planet. Space Sci., 25, 5, 1977.
Reasoner, D.L. and C.R. Chappell, Twin payload observations of incident backscattered auroral electrons, J. Geophys. Res., 78, 2176, 1973.
Sharp, R.D., E.G. Shelley, R.G. Johnson, and A.G.

Ghielmetti, Counterstreaming electron beams at altitudes of ~ 1 Rg over the auroral zone, J. Geophys. Res., 84, 92, 1980.

Shelley, E.G., R.D. Sharp, and R.G. Johnson, Satellite observations of an ionospheric acceleration mechanism, Geophys. Res., Ltrs., 3, 654, 1976.

Ungstrup, E., D.M. Klumpar, and W.J. Heikkila, Heating of ions to suprathermal energies in the topside ionosphere by electrostatic ion cyclotron wave, J. Geophys. Res., 84, 4289, 1979.

Venkatarangan, P., J.R. Burrows, and I.B. McDiarmid, On the angular distributions of electrons in inverted V substructures, J. Geophys. Res., 80, 1975.

Whalen, B.A., and I.B. McDiarmid, Observations of magnetic field-aligned auroral electron precipitation, J. Geophys. Res., 77, 191, 1972.

Whalen, B.A., W. Bernstein, and P.W. Daley, Low altitude acceleration of ionospheric ions, Geophys. Res. Ltrs., 5, 55, 1978.

Whalen, B.A., and P.W. Daley, Do field-aligned auroral particle distributions imply acceleration by quasi-static parallel electric fields? J. Geophys. Res., 84, 4175, 1979.

## Figure Captions

Fig. 1. Spatial occurrence map of 280 inverted V events. Local time and circles of constant invariant latitude are shown as reference (from Lin and Hoffman, 1979).

Fig. 2. Example to show how a peak in the differential energy spectrum is not necessarily an unstable structure in the distribution function f.

Fig. 3. Sequential electron spectra from flight 18:91. Pitch angle of the electrons is given by the smooth curve. The lower two decades of the flux scale are used to give pitch angles from 1° to 100° (from Arnoldy et. al., 1974).

Fig. 4. Spectrogram displaying the flux ratios $J(-7°)/J(60°)$ of an inverted V event. The flux ratios are separated into four categories as shown in the upper right corner (from Lin and Hoffman, 1979).

Fig. 5. Top two panels, directional intensities 1.4 and 4.5 keV electrons. Bottom panel, ground meridian-scanning photometer looking at foot of rocket field line, energy of peak current (from Arnoldy, 1977).

Fig. 6. Measured electron spectrum during a diffuse aurora together with a model spectrum

which is the sum of a Maxwellian and the distribution of atmospherically produced backscattered and secondary electrons that is in equilibrium with this Maxwellian. The energy spectrum for the Maxwellian of temperature 2.5 keV and density 0.2 $cm^{-3}$ is also plotted for comparison (from Evans and Moore, 1979).

Fig. 7. Spectra of electrons moving up and down the magnetic field line measured simultaneously by rocket detectors.

Fig. 8. Rocket measurements of the precipitation of 0.3 and 3 keV electrons and simultaneous up and down spectra taken at two times during the flight. Visible aurora coincided only with the 3 keV precipitation bursts centered on 150 seconds flight time.

Fig. 9. Background auroral spectrum (heavy line) and three simultaneous spectra taken by detectors scanning the pitch angle ranges indicated during an argon plasma release. The auroral spectrum is dramatically altered below 1 keV.

Fig. 10. ATS-6 electron spectra as a function of time during a substorm injection event. The top eight traces give count rates for eight energy channels as a function of time. The energy in keV is given to the right of each trace.

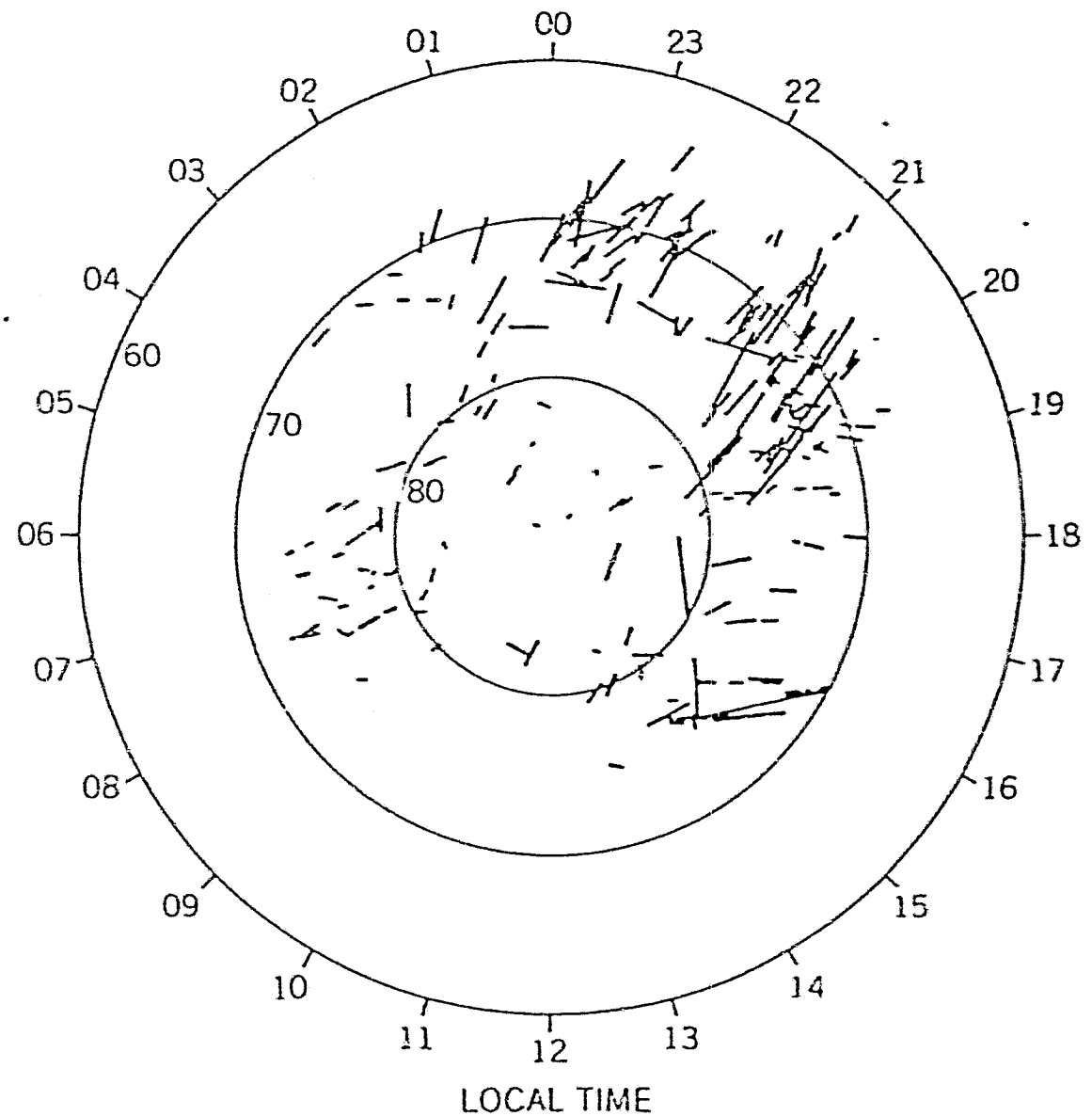
AE-D
"INVERTED V" EVENT OCCURRENCE MAP
00
01
02
03
04
05
06
07
08
09
10
11
12
13
14
15
16
17
18
19
20
21
22
23
60
70
80
LOCAL TIME

Figure 1

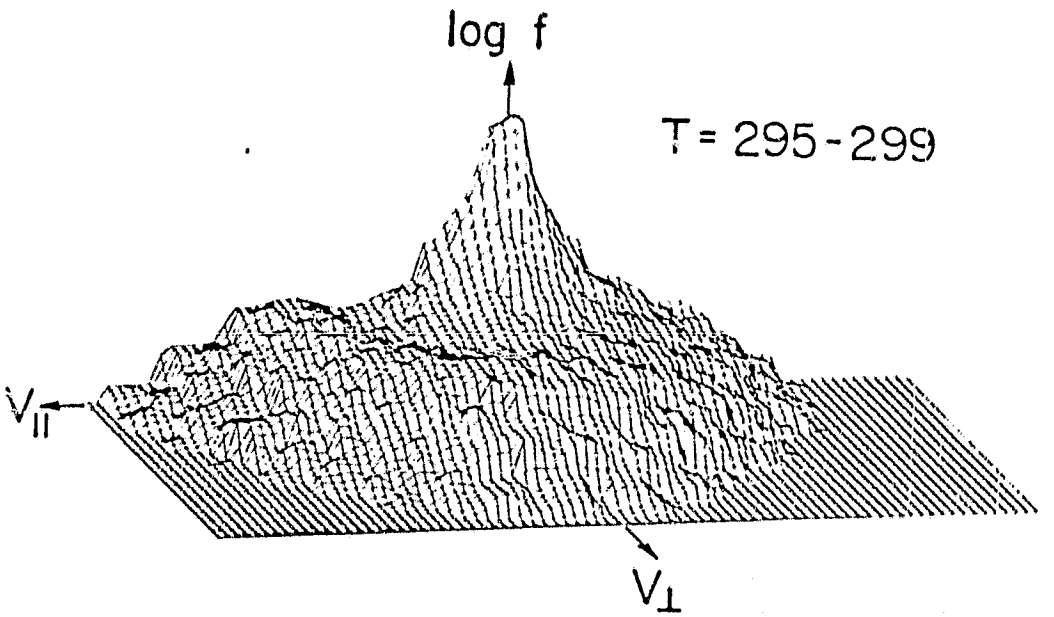
log f
T = 295-299
$V_{\parallel}$
$V_{\perp}$

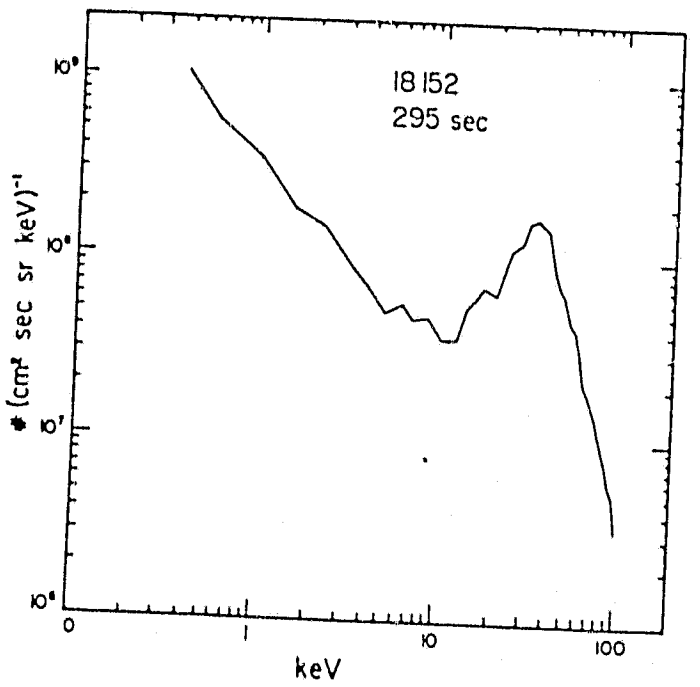
18152
295 sec
# (cm² sec sr keV)⁻¹
10⁰
10⁻¹
10⁻²
0
1
10
100
keV

Figure 2

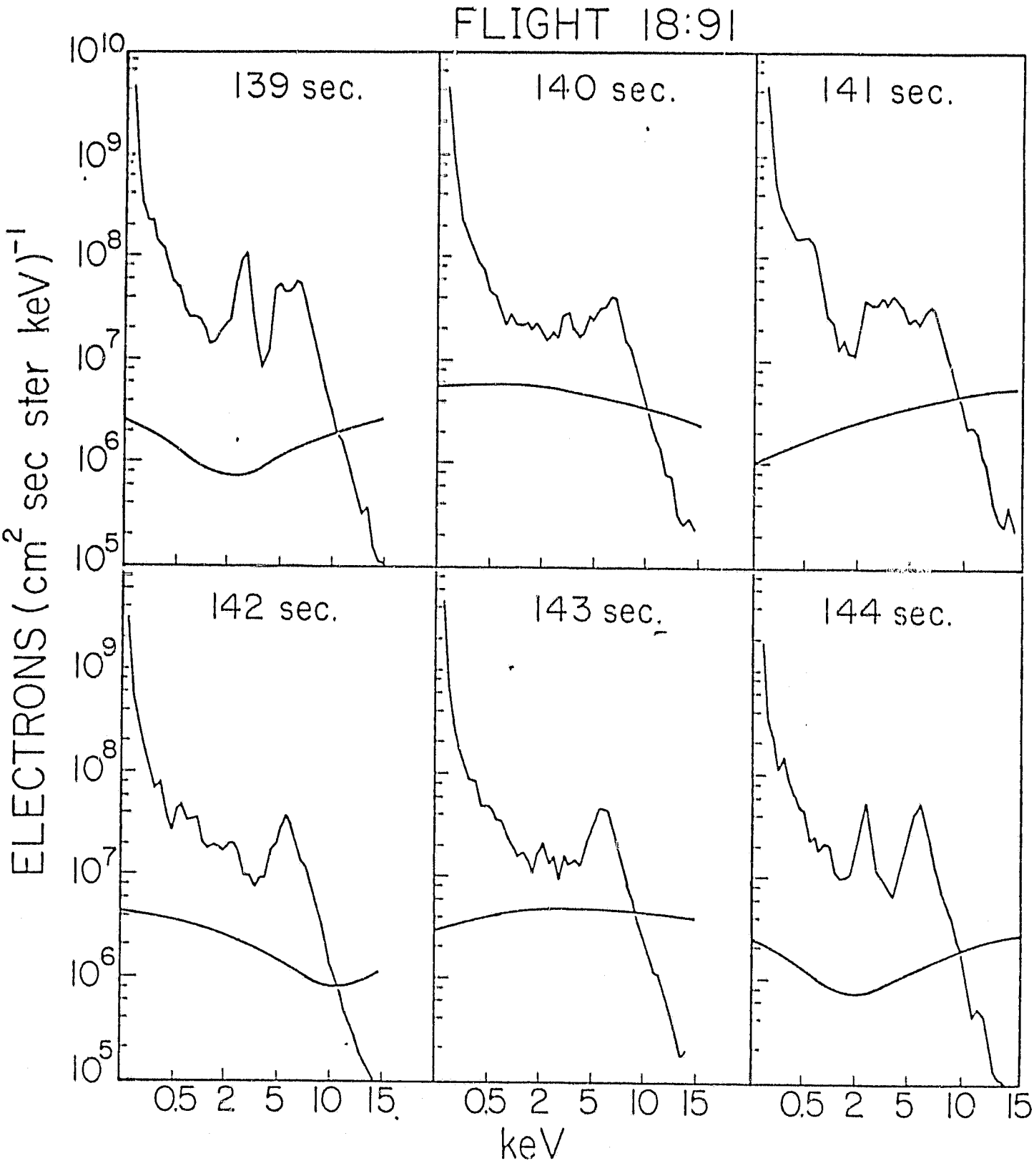
FLIGHT 18:91
139 sec.
140 sec.
141 sec.
142 sec.
143 sec.
144 sec.
ELECTRONS (cm² sec ster keV)⁻¹
10¹⁰
10⁹
10⁸
10⁷
10⁶
10⁵
0.5 2 5 10 15
keV

Figure 3

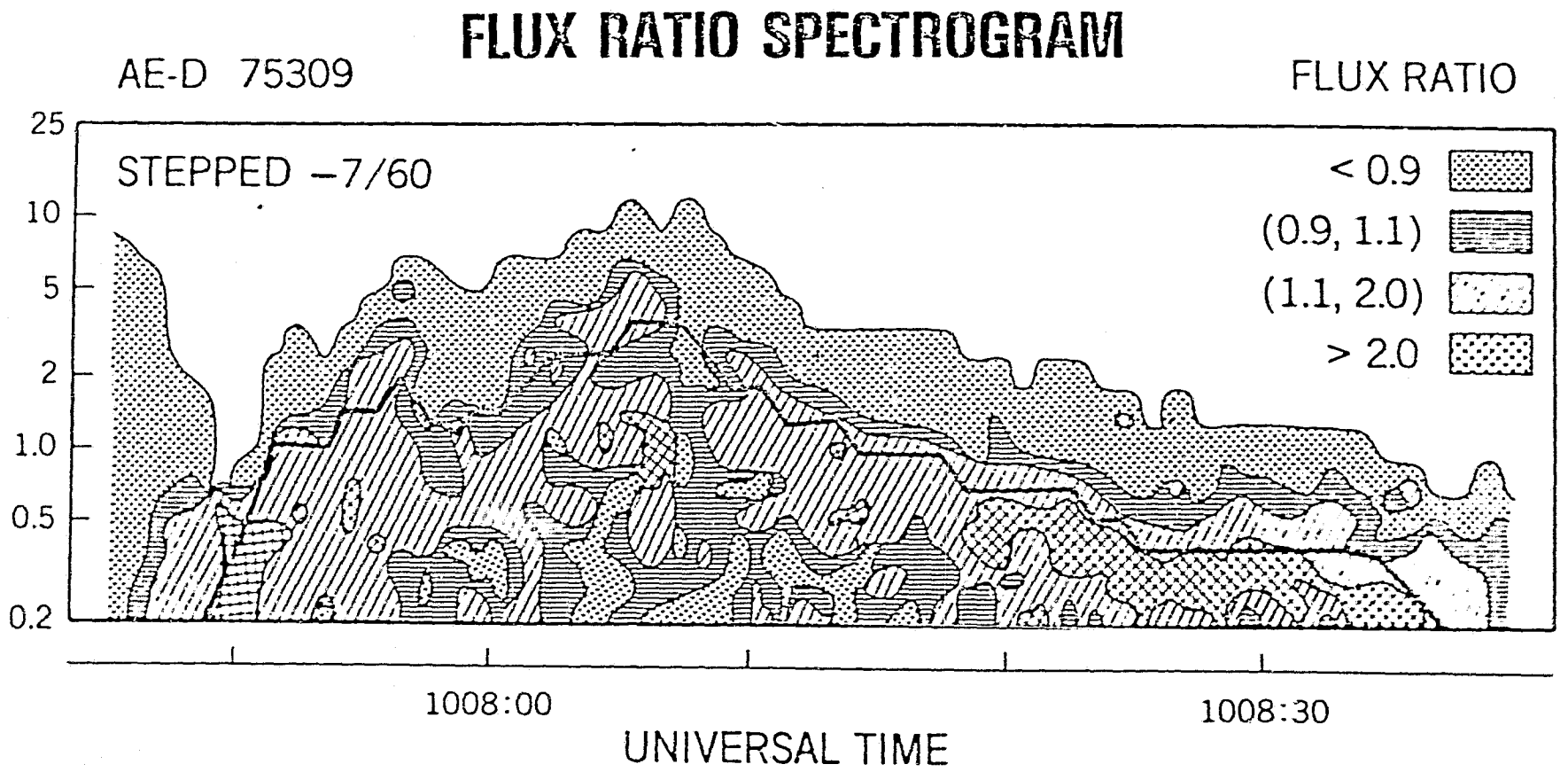
FLUX RATIO SPECTROGRAM
AE-D 75309
FLUX RATIO
STEPPED −7/60
< 0.9
(0.9, 1.1)
(1.1, 2.0)
> 2.0
25
10
5
2
1.0
0.5
0.2
1008:00
1008:30
UNIVERSAL TIME

Figure 4

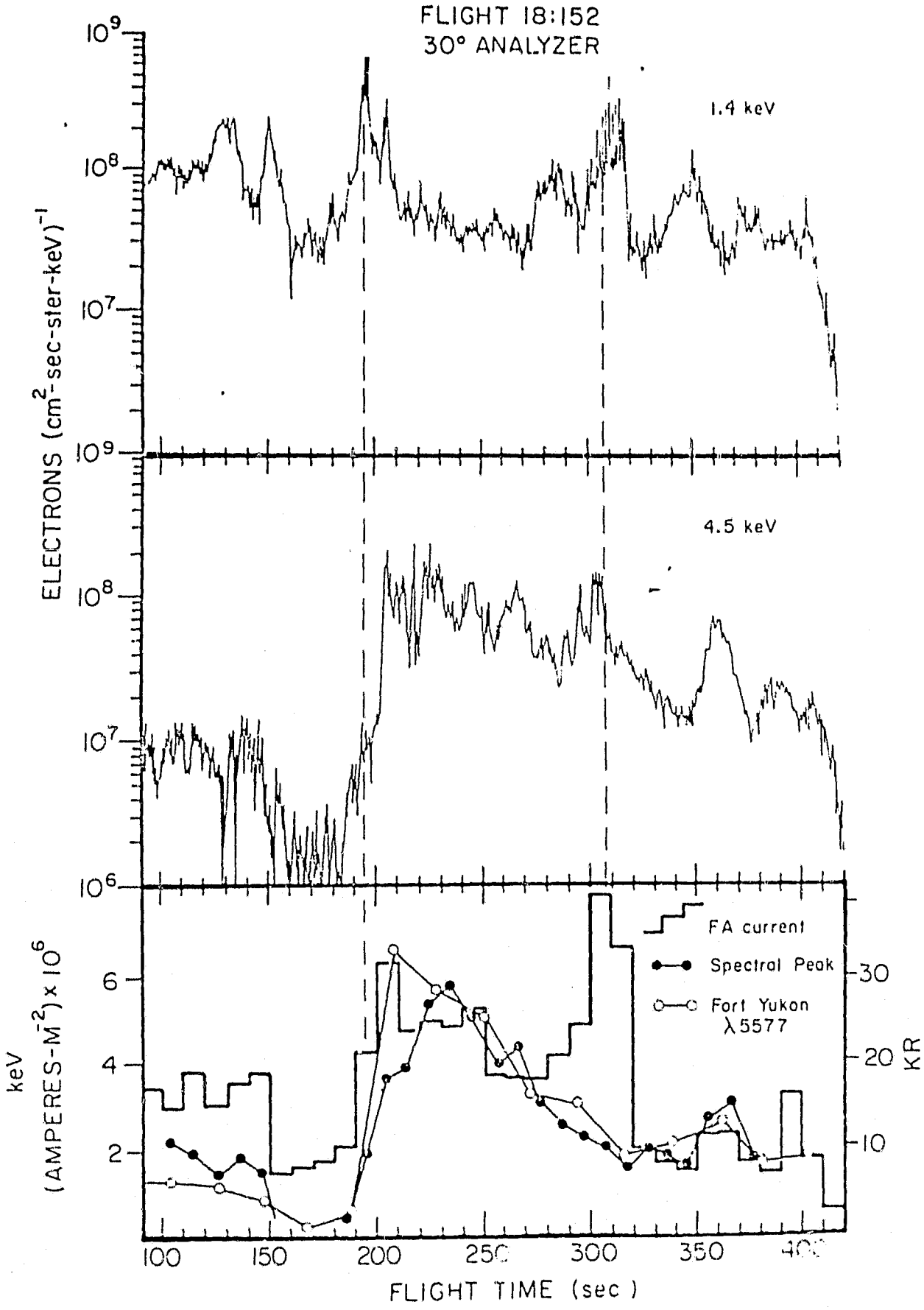
FLIGHT 18:152
30° ANALYZER
1.4 keV
4.5 keV
ELECTRONS (cm²-sec-ster-keV)⁻¹
10⁹
10⁸
10⁷
10⁶
FA current
Spectral Peak
Fort Yukon
λ5577
keV
(AMPERES-M⁻²) x 10⁶
KR
30
20
10
6
4
2
100
150
200
250
300
350
FLIGHT TIME (sec)

Figure 5

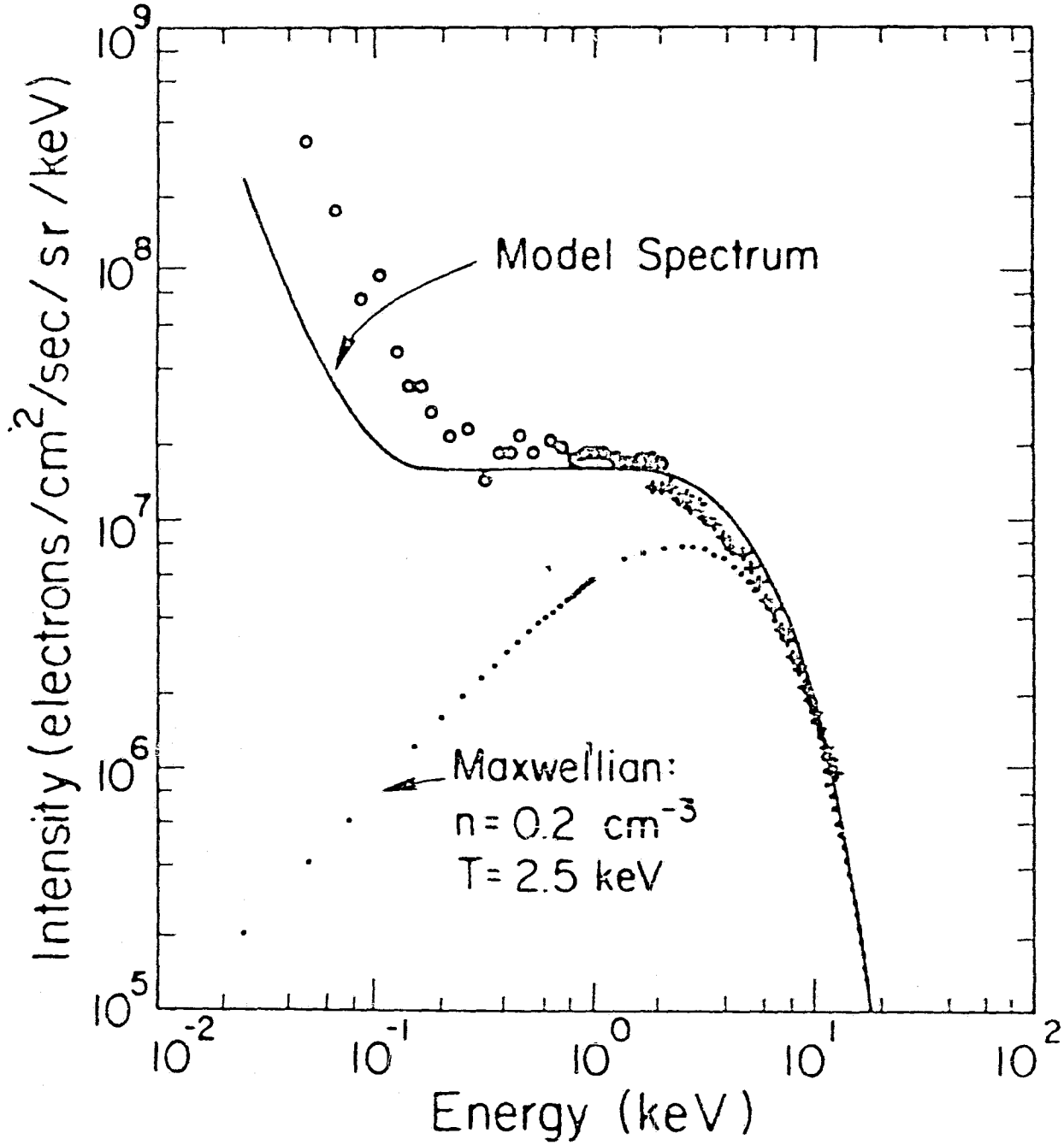
Intensity (electrons/cm²/sec/sr/keV)
Energy (keV)
Model Spectrum
Maxwellian:
n = 0.2 cm⁻³
T = 2.5 keV
10⁹
10⁸
10⁷
10⁶
10⁵
10⁻²
10⁻¹
10⁰
10¹
10²

Figure 6

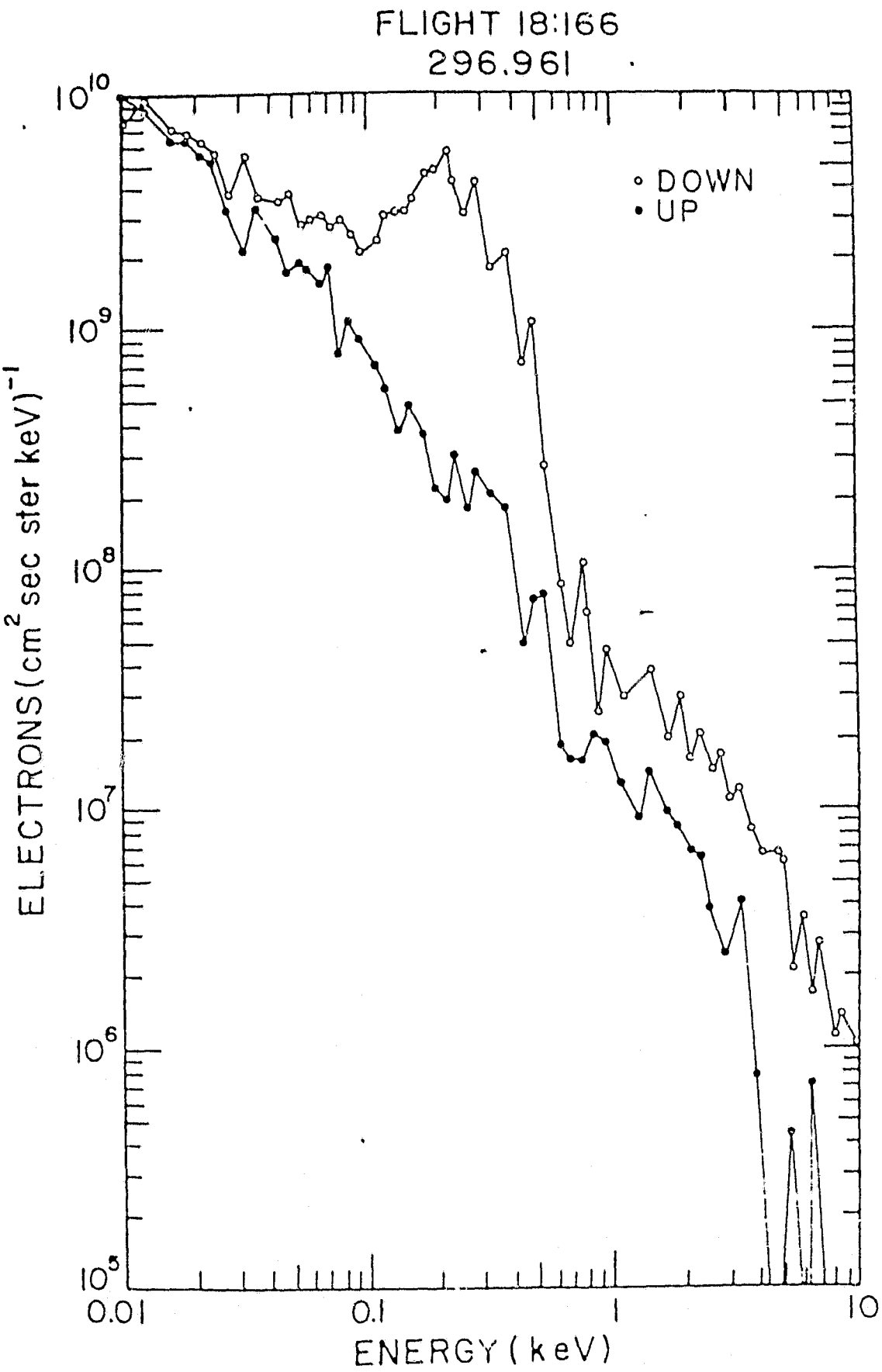
FLIGHT 18:166
296.961
DOWN
UP
ELECTRONS (cm² sec ster keV)⁻¹
10¹⁰
10⁹
10⁸
10⁷
10⁶
10⁵
0.01
0.1
1
10
ENERGY (keV)

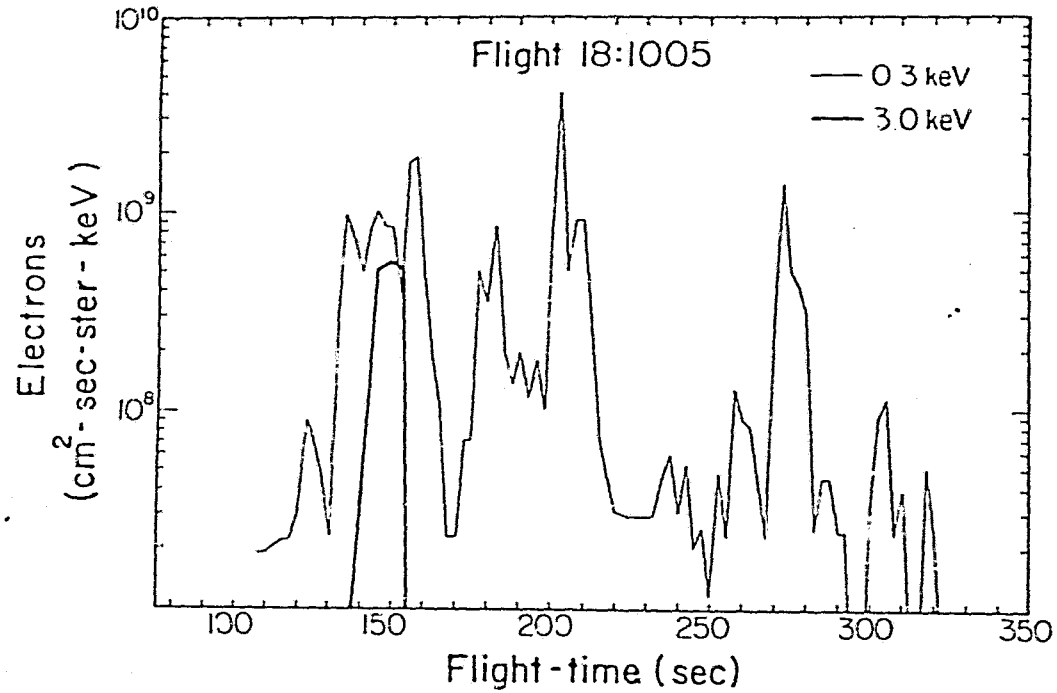
Flight 18:1005
0.3 keV
3.0 keV
Electrons
(cm² - sec - ster - keV)
Flight - time (sec)

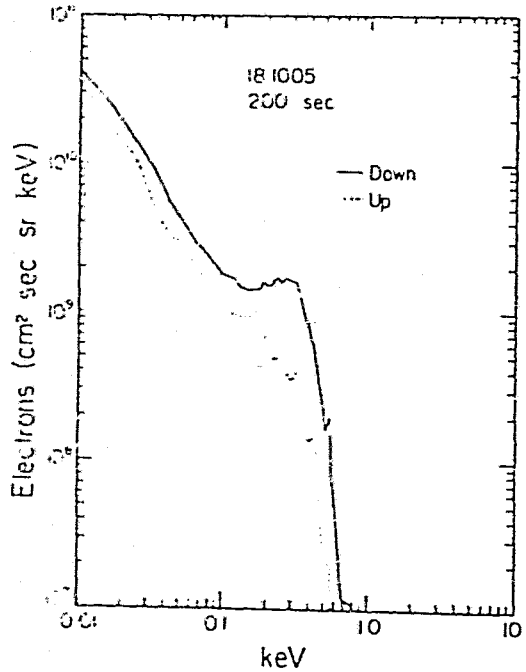
18 1005
200 sec
Down
Up
Electrons (cm² sec sr keV)
keV

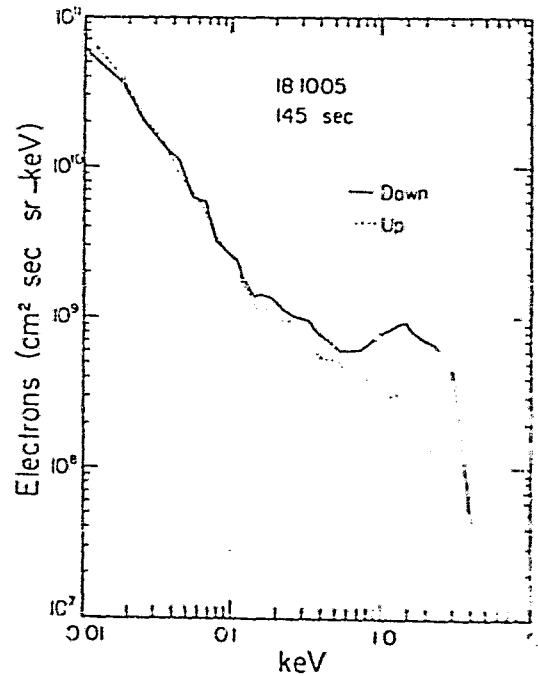
18 1005
145 sec
Down
Up
Electrons (cm² sec sr keV)
keV

Figure 8

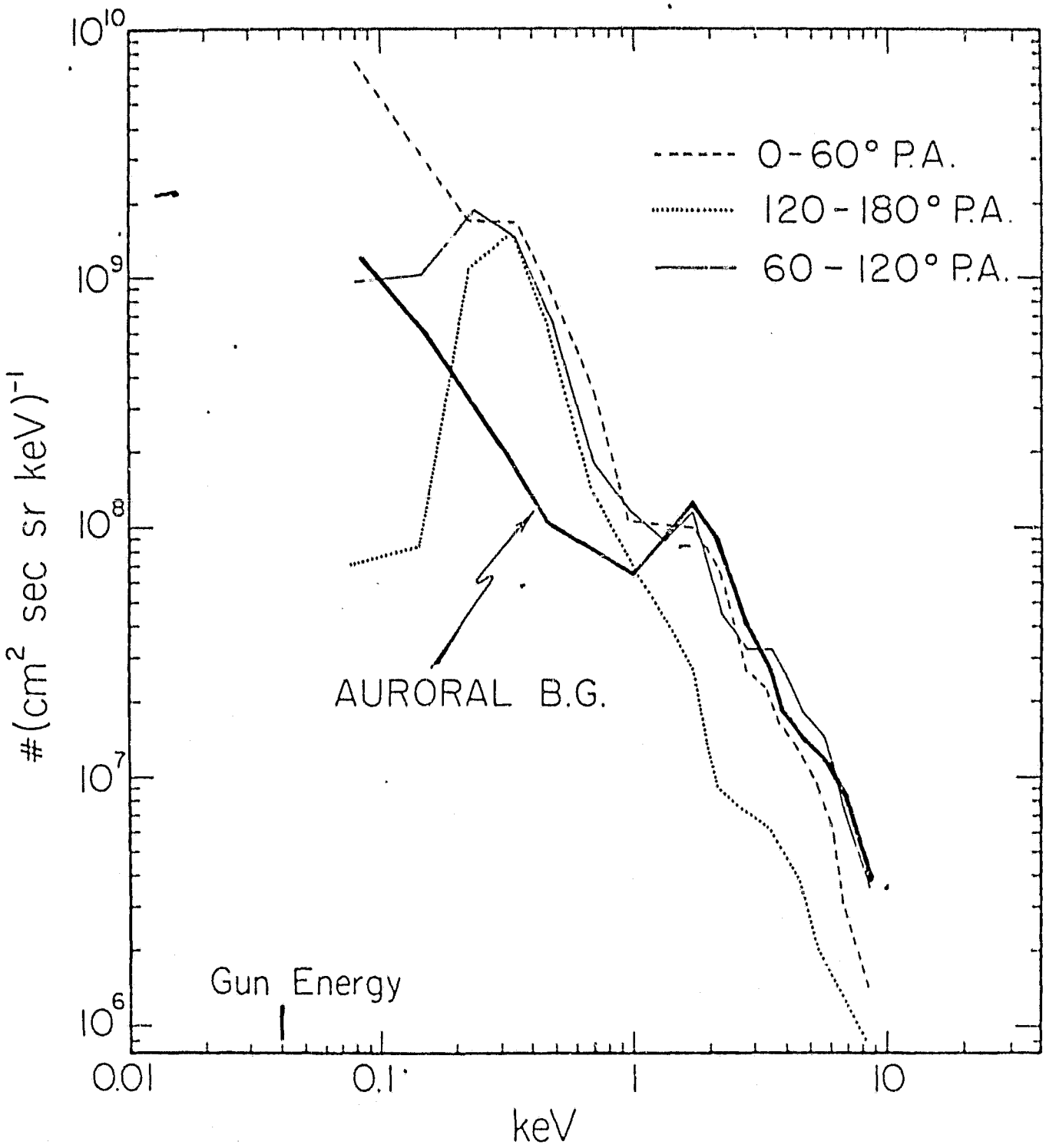
0-60° P.A.
120-180° P.A.
60-120° P.A.
AURORAL B.G.
Gun Energy
#(cm² sec sr keV)⁻¹
keV
10¹⁰
10⁹
10⁸
10⁷
10⁶
0.01
0.1
1
10

Figure 9

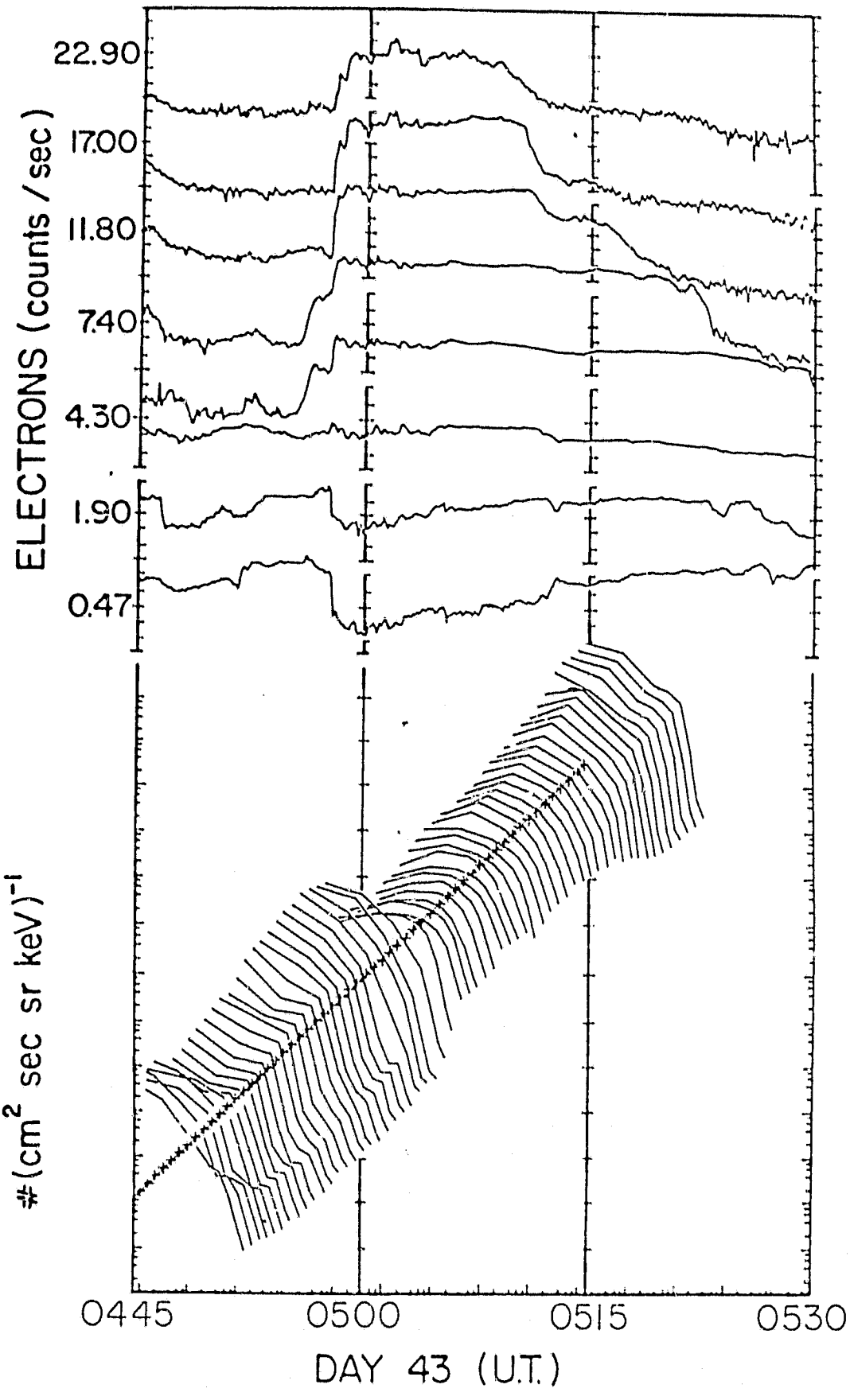
22.90
17.00
11.80
7.40
4.30
1.90
0.47
ELECTRONS (counts / sec)
#(cm² sec sr keV)⁻¹
0445
0500
0515
0530
DAY 43 (U.T.)

Figure 10

JOURNAL OF GEOPHYSICAL RESEARCH, VOL. 85, NO. A5, PAGES 2011-2116, MAY 1, 1980

# Modulation of Terrestrial Ion Escape Flux Composition (by Low-Altitude Acceleration and Charge Exchange Chemistry)

THOMAS E. MOORE

*Space Science Center, University of New Hampshire, Durham, New Hampshire 03824*

Motivated by recent observations of highly variable hot plasma composition in the magnetosphere, control of the ionospheric escape flux composition by low-altitude particle dynamics and ion chemistry has been investigated for an $e^-$, $H^+$, $O^+$ ionosphere. Theoretical polar wind results of Banks and Holzer and observations of highly nonthermal ion escape have been used as guides. It is found that the fraction of the steady state escape flux which is $O^+$ can be controlled very sensitively by the occurrence of parallel or transverse ion acceleration at altitudes below the altitude where the neutral oxygen density falls rapidly below the neutral hydrogen density and the ionospheric source of $O^+$ tends to be rapidly converted by charge exchange to $H^+$. The acceleration is required both to overcome the gravitational confinement of $O^+$ and to violate charge exchange equilibrium so that the neutral hydrogen atmosphere appears 'optically' thin to escaping $O^+$. Constraints are placed on the acceleration processes, and it is shown that $O^+$ escape is facilitated by observed ionospheric responses to magnetic activity.

## INTRODUCTION

The hot magnetospheric plasma has a variable composition which usually includes and is at times dominated by heavy terrestrial ions, most probably $O^+$. Yet models of ionospheric escape (e.g., *Banks and Holzer* [1969*b*], hereafter referred to as BH) predict that only a fraction of order $10^{-3}$ or less of this escaping flux should be $O^+$. This is in accord with a comparison of ionospheric thermal speeds and the gravitational escape velocity. Though auroral zone particle acceleration delivers energies much larger than either thermal or gravitational binding energies, BH have shown that there is another obstacle to $O^+$ escape, namely, the charge exchange $O^+$ flowing up from its source on the neutral H atmosphere. This paper presents an analysis in which ion acceleration is regarded as an imposed free parameter. Steady state conditions are identified under which the ionosphere will respond by releasing primarily $O^+$ rather than $H^+$.

The compositional variability of the hot magnetospheric plasma is illustrated by observations from geosynchronous orbit [*Geiss et al.*, 1978], polar low-altitude orbit [*Shelley et al.*, 1972; *Ghielmetti et al.*, 1978], and rocket altitudes [*Lynch et al.*, 1977; *Moore and Evans*, 1979]. These observations include situations with $O^+/H^+$ ranging from less than a few percent to greater than unity. The correlation of $O^+$ content with magnetic activity reported by *Sharp et al.* [1976] suggests than an ionospheric response to magnetic storms may be involved. Moreover, unusual enrichments of $N^+$ and molecular ions observed in the thermal ionosphere [*Hoffman et al.*, 1974; *Taylor et al.*, 1975] during magnetic storms further support such a hypothesis.

The conceptual separation of energization mechanism and compositional control is supported by observations of keV ions jetting up out of the ionosphere between 1000- and 8000-km altitude above the auroral zone [*Kintner et al.*, 1979; *Klumpar*, 1979; *Sharp et al.*, 1977; *Shelley et al.*, 1976] from a variety of polar orbiters. These ions are generally field aligned to a high degree, sometimes showing 'conical' pitch angle distributions with minima at 90° and 180°. The point of most importance here is that the ion jet composition is highly variable from essentially pure $H^+$ to pure $O^+$ (see especially *Kintner et al.* [1979]). *Ungstrup et al.* [1979] have proposed that these ion flows result from transverse acceleration of ions below the satellite by ion cyclotron waves driven unstable by field-aligned currents. The resulting magnetic mirror force then ejects the ion upward out of the ionosphere. While gyro-resonant preferential acceleration of one or another ion species is an attractive model for the observed composition variations, such effects are ignored in the present treatment, which presumes that acceleration is effective for all species. Instead, attention is focused on ion charge exchange chemistry, with results which have implications for gyro-resonant effects as well.

The approach has been inspired by the results of BH, which represent a solution to the problem of ion dynamics and chemistry when no acceleration is imposed beyond the natural thermal escape of ionospheric plasma. Those results are reviewed in the next section. In subsequent sections, continuity of $O^+$ is considered for the more general case of an arbitrarily imposed vertical flow profile, and the results are evaluated for special cases of (1) parallel acceleration and (2) transverse acceleration. A final section summarizes conclusions which may be drawn from the results obtained.

## POLAR WIND THEORY (HIGH-LATITUDE VERTICAL PLASMA TRANSPORT)

Considerable theoretical work has been done on the escape of ionospheric plasma into the high-latitude magnetosphere beginning with, for example, *Banks and Holzer* [1969*a*], and the escape phenomenon has been termed the polar wind by *Axford* [1968] in recognition of a certain analogy with the solar wind. *Lemaire and Scherer* [1973] have reviewed the lively debate which followed the initial papers. This debate centered on the relative merits of hydrodynamic and kinetic approaches to the problem, and also exhibited some analogies with earlier debate surrounding solar wind theory. Hydrodynamic models are evidently appropriate at low altitudes where collisions are important, while a kinetic approach is appropriate in collisionless regions, the two approaches being of course complementary rather than contradictory. Certain quantitative refinements involving ionization rates and neutral atmosphere models have recently been introduced by *Raitt et al.* [1978], with particular attention to helium escape. The emphasis of the present paper will be on $H^+$ and $O^+$ es-



Paper number 80A0195.
0148-0227/80/080A-0195$01.00

cape and the accidentally resonant charge exchange chemistry which couples these two ions and their neutral atoms.

The hydrodynamic approach has been applied to a polar ionosphere of $H^+$, $He^+$, $O^+$, and $e^-$ by BH, who performed a steady state calculation using continuity and momentum equations for each species. The equations used describe vertical motions taking account of sources and losses of ionization, charge exchange chemistry, and ion-ion, ion-neutral friction. Electron inertia is ignored, and ions and electrons are assumed isothermal except that separate electron and ion temperatures are specified. Pressure is taken to be isotropic and to obey a simple gas law. The neutral atmosphere is described with the model of M. Nicolet et al. (unpublished manuscript, 1969). A dipolar B dependence is used to describe the variation of flux tube cross section with altitude, and the plasma pressure at great altitudes is assumed to be sufficiently low as to force a transonic solution for the light species $H^+$, $He^+$. The result of the calculation is a specification of $n_j(z)$ and $u_j(z)$ for $z$ up to $\sim 1$ $R_A$ and where $j$ enumerates all species.

The results of their calculation can be summarized as follows: A large escape flux of $H^+$ occurs amounting to over $10^8 H^+/cm^2$ s. Escape fluxes of $He^+$ and $O^+$ are much smaller (by $10^{-2}$ and $10^{-3}$, respectively) Most importantly for the present work, a large upward flux of $O^+$ ($>10^8/cm^2$ s) occurs at altitudes below ~600 km which, through charge exchange on neutral H, supplies the escaping $H^+$ flux. It may reasonably be inferred that the ionosphere has a built-in obstacle to the escape of $O^+$ in the form of a neutral hydrogen component which tends to neutralize any upward flowing $O^+$. This result tends to make the observations of escaping $O^+$ cited earlier very difficult to understand.

Wherever the vertical flows are slow enough (much less than the smallest scale height per charge exchange period), charge exchange equilibrium will be maintained, implying that [BH]

$$\frac{n(H^+)}{n(O^+)} \cong \frac{9n(H)}{8n(O)}\left(\frac{T_n}{T_i}\right)^{1/2}$$

where the $n$ are number densities and $T_n$, $T_i$ are neutral and ion temperatures. This condition is satisfied in the BH model below ~600 km, where $n(O)$ drops below $n(H)$ (the 'H, O crossover level') and $O^+$ is converted to $H^+$. One might suspect that a lower H density might shift the equilibrium in favor of $O^+$, but this is not the case. It must be borne in mind that the polar wind $H^+$ escape is driven by the thermal energy of the ions (though it is crucially aided by the $O^+$-$e^-$ gravitational separation E field). Normal thermal escape of $O^+$ is very small. BH have modeled the low H case by considering a higher than normal temperature neutral atmosphere. Figure 1 shows model neutral H atmospheres used by BH and best current models from *Tinsley* [1974], with neutral O crossover levels indicated by dots. A modest temperature increase can clearly produce a dramatic decrease in H above 250 km, due to increased neutral H escape. The result is a reduced source and hence escape of $H^+$. This reduces the demand for and hence the flux of $O^+$. The charge exchange region moves upward to the new $n(H)$, and $n(O)$ crossover level, and $O^+$ escape is still small. The combination of gravitational and chemical obstacles would appear to effectively prevent steady $O^+$ escape, regardless of forces imposed at altitudes above the $n(O) \sim n(H)$ level where $H^+$ is produced.

However, it seems reasonable to inquire whether the ionospheric escape can be driven out of charge exchange equilibrium so as to favor $O^+$ escape by application of acceleration at altitudes where the $O^+$ upflux exists. Auroral acceleration is known to impart energies far in excess of ionospheric thermal energies, thus violating many of the conditions for hydrodynamic flow. As a means of investigating low-altitude acceleration effects, the equation of motion will be ignored and the dynamics regarded as a free parameter. Only a simplified continuity equation for $O^+$ will be considered.

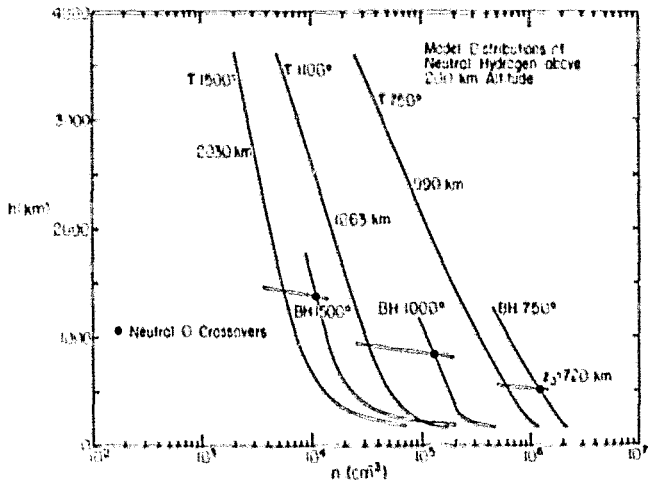


Fig. 1. Model neutral hydrogen atmospheres for altitudes above 200 km, for three temperatures. Profiles from *Banks and Holzer* [1969b] are marked BH. Those from *Tinsley* [1974] are marked T. Rough scale heights are indicated on profiles which are nearly straight lines, and the altitudes at which neutral O (scale height ~70 km) falls below neutral H are indicated with dots.

## ION ESCAPE FROM A CHARGE EXCHANGING ATMOSPHERE

In this section the ion dynamics will be parameterized in terms of a specified vertical velocity profile $v_z(z)$. A continuity equation for some initial upward flux of $O^+$ under the action of forces appropriate to produce $v_z(z)$ will be written including the effects of charge exchange loss and gain due to collisions of the $O^+$ with H and the fast O thus produced with ambient $H^+$. Later, the solution obtained to this equation will be evaluated for some simple assumed upward velocity profiles.

The steady state continuity equation for vertical ion transport in a plane parallel atmosphere is appropriate here in view of the long times over which $O^+$ is observed to vary in the magnetosphere and the fact that most of the charge exchange occurs below 1000 km. It is

$$\frac{dJ_{O^+}}{dz} = Q - L$$

where $J_{O^+} = n_{O^+}v_z$. It is assumed that the $z$ axis is parallel to the magnetic field, which will be assumed essentially vertical, thus restricting this analysis to a high-latitude situation. A term which accounts for field line divergence with altitude has been ignored here, since its effect is to account for geometrically produced changes in $J_{O^+}$ which are not of concern here. All sources and sinks of $O^+$ other than charge exchange will be taken to be in balance everywhere. Neutral hydrogen is present with number density $n_H$, protons with density $n_{H^+}$, and the cross sections for the forward and reverse reactions $O^+ +$

$H + \dot{O} + H^+$ are taken as $\sigma$ and $\sigma_r$, respectively. Continuity then demands

$$\frac{dJ_{O^+}}{dz} = -n_H\langle\sigma v\rangle n_{O^+} + n_{H^+}\langle\sigma_r v\rangle n_O$$

Only the fast O produced by charge exchange of the initial $O^+$ flux ($J_i = (n_{O^+}v_z)_i$) can become a source of $O^+$ flux by reverse charge exchange. Hence the appropriate oxygen number density for the third (source) term is given by

$$(n_O v_z) = J_i - (n_{O^+}v_z)$$

The factor $\langle\sigma v\rangle$ indicates the product of $\sigma$ and the root square sum of ion thermal, neutral thermal, and ion-neutral translation speeds.

Defining $f^+ = J_{O^+}/J_i$ the equation for continuity becomes

$$v_z\frac{df^+}{dz} = -n_H\langle\sigma v\rangle f^+ + n_{H^+}\langle\sigma_r v\rangle(1 - f^+)$$

Solution of this radiative transfer type equation is simplified if one defines a charge exchange depth by analogy with optical depth:

$$\tau = \int_O^\infty n_H\frac{\langle\sigma v\rangle}{v_z}\,dz$$

In radiative transfer the ratio $v_z/v$ is usually taken out of the integral as a cosine factor. However, since it is desired to allow for an ion pitch angle which may vary with $z$, this factor will be retained in the integral here. Note that $\tau$ represents an attenuation depth measured along the path of an $O^+$ ion in escaping from an initial height $z_0$ to large altitudes. With an additional definition,

$$w = \frac{n_{H^+}\langle\sigma_r v\rangle}{n_H\langle\sigma v\rangle}$$

the continuity equation becomes

$$\frac{df^+}{d\tau} = -f^+(1 + w) + w$$

Here $w$ is properly viewed as a function of altitude. A closed form solution does exist and may be integrable for certain simple forms of $w(z)$. Proper calculation of $w$ requires consideration of the continuity and dynamics of $H^+$, which in the calculation of BH had its major source in the $O^+$-H charge exchange. It can be argued from their results that upward escape of $H^+$ occurs so rapidly that $H^+$ densities remain very low and $w$ never becomes large enough to influence the final result for $O^+$. This may be seen as follows: In the case $w$ = constant, the solution for $f^+(0) = 1$ is

$$f^+ = \frac{w}{1 + w}\left(1 + \frac{1}{w}e^{-(1+w)\tau}\right)$$

This in fact is not a bad approximation, since $H^+$ and H have quite similar altitude distributions above 400 km in the BH results. The solution has the appropriate properties for small and large $\tau$, i.e., $f^+(0) = 1$ and $f^+(\infty) \to w/(1 + w)$. Small $f^+$ at high altitudes, as found for the polar wind, carries the implication then of small $w$. In fact, $n_{H^+}$ may be seen to be much smaller than $n_H$ in the BH results. The source term in the continuity equation is evidently kept small by rapid upward loss of $H^+$, even when no external force assists in $H^+$ transport. As more $O^+$ survives, the main source of $H^+$ is removed, and the $O^+$ source term due to the reverse reaction becomes even smaller. For small $w$ the solution for $O^+$ survival when gravitational escape is assured by external forces is just the fraction of initial $O^+$ flux remaining after charge exchange loss:

$$f^+ \simeq e^{-\tau}$$

Here, $\tau$ is the charge exchange depth encountered between some starting altitude and a higher observation point. Clearly, the amount of $O^+$ escaping from the atmosphere under the described dynamical conditions is sensitively dependent on $\tau$. It remains to determine how $\tau$ may vary in response to hypothetical dynamic situations. This requires assumptions about the form of $v_z(z)$.

## PARALLEL ACCELERATION

The simplest possible assumption for $v_z(z)$ is that it is a constant which is imposed by some initial impulsive acceleration and maintained against gravity by some continuing force. This is a very good approximation to a situation including a low-altitude plasma double layer and a useful idealization of a situation involving a distributed vertical potential drop which extends to low altitude. In such a case,

$$\tau = \frac{\langle\sigma v\rangle}{v_z}\int_0^\infty n_H\,dz \simeq \frac{\langle\sigma v\rangle}{v_z}N_H$$

with $N_H$ the column density of neutral hydrogen above the acceleration lower edge. In terms of an assumed exponential atmosphere $n_H = n_0e^{-z/z_0}$; $\tau = z_0/z_i$, where $z_i \equiv [(\langle\sigma v\rangle/v_z)n_0]^{-1}$ defines a 'charge exchange survival height.' Appreciable $O^+$ escape then requires $z_i \gtrsim z_0$, i.e., $\tau \lesssim 1$. That such is not the case in the calculation of BH may be seen by substitution of appropriate values: $N_H \sim 10^{14}$ ($n_0 \sim 1.4 \times 10^6$, $z_0 \sim 750$ km), $v_z \sim 2 \times 10^4$ cm/s, $\langle\sigma v\rangle = 4.3 \times 10^{-11}$ ($T_H + T_{O^+}/16 + 1.2 \times 10^{-8}v_z^2)^{1/2} \sim 1.3 \times 10^{-9}$ with $T_H = 750°$K, $T_{O^+} = 3000°$K. The result for $z_i$ is ~110 km yielding $\tau \simeq 6.6$ and an $O^+$ survival fraction $\sim 10^{-3}$, in rough accord with the complete physical model.

This result indicates the conditions under which an appreciable fraction of the terrestrial ion escape flux can be $O^+$. First, an externally imposed accelerating force must overcome the gravitational confinement (10 eV is required for $O^+$). Next, the charge exchange depth of H must be reduced to a state of 'optical thinness.' This can be accomplished in one or both of two ways: (1) a reduction of the neutral hydrogen column density above the H, O crossover altitude or (2) a reduction of $\langle\sigma v\rangle/v_z$ by acceleration at or below that level.

The first of these possibilities involves an alteration of the neutral hydrogen atmosphere. *Tinsley* [1974] has reviewed current knowledge of the hydrogen 'geocorona' and its variability. Polar wind $H^+$ loss may in time deplete neutral H. Theoretical models predict that the column density above 250 km is tremendously variable with (isothermal) temperature due to escape of fast neutrals (refer to Figure 1). Drops of an order of magnitude result from a temperature rise by only a factor of 2. Storm activity is expected to dominate the auroral ionosphere energy budget producing strong heating at low altitudes. However, Tinsley notes optical measurements indicating maximum column density reduction below 450 km of ~40%. Heating and escape of topside hydrogen may be washed out by flows from other altitudes and latitudes. In any case, with-

out imposed demand for ions (upward acceleration), a reduction of $N_H$ simply reduces the $H^+$ escape flux and hence demand for $O^+$, so that no increase in $O^+$ escape results.

The second possibility is more amenable to analysis. It could be effected by a dependence of $\sigma$ on $v$ or an increase in $v_z$. Figure 2 has been constructed using the BH expression given above and cross-section measurements for keV $O^+$ cited by *Tinsley* [1976] as indicated. In Figure 2, $\langle\sigma v\rangle$ has been plotted versus the energy with which $O^+$ approaches cold neutral H target atoms, though in fact neutral and ion thermal speeds must be root square summed with ion translation speed. The BH expression assumes $\sigma$ is constant with energy, and the keV measurements suggest that $\sigma$ has at most a weak energy dependence ($\sim v^{-0.16}$ or $E^{-0.08}$). An expression for $\tau(v_z)$ may now be written, which is for the BH cross section:

$$\tau = N_H \frac{4.3 \times 10^{-11}(T_{H^+} + T_{O^+}/16 + 1.2 \times 10^{-8} v_z^2)^{1/2}}{v_z}$$

This and the corresponding relation for the keV measurement extrapolation have been plotted in Figure 3 versus the $O^+$ energy corresponding to $v_z$. In both cases, $N_H$ has been taken as $10^{14}$ cm$^{-2}$. Both curves decrease with $E_z$ for $E_z$ below the thermal energy of ~0.1 eV, where they reach a value near unity and begin to saturate between unity and 0.1. Increased thermal energies have the effect of raising the left end of the curves while leaving the right ends stationary, as indicated. The entire curves move upward or downward in proportion to the hydrogen column density $N$, as indicated at center. The curves demonstrate that the ionosphere considered by BH will appear 'optically' thin to $O^+$ ions escaping with translation energy comparable to or larger than their thermal energy, i.e., those escaping with small pitch angles. Hence an acceleration mechanism which can produce supersonic $O^+$ outflow at altitudes below the crossover of neutral O and H densities can totally alter the composition of the escaping ion flux. A surprising aspect of this result is that only a relatively small upward energization (by auroral standards) is needed, provided continued forcing at least maintains the outflow against gravitation.

The most obvious mechanism for such a process is the magnetic field aligned (parallel) electric field thought responsible for downward electron acceleration [*Evans*, 1974]. However, the distribution of such parallel electric fields ($E_\parallel$) at low altitudes is subject to great uncertainty due to a lack of either observations or models of their behavior below ~2000 km. Clearly, a very small fraction of the inferred several kV potential drop can be of importance. It is in the altitude range of interest (200–2000 km) that vertical current conduction makes a transition from resistive to collisionless behavior. If the $E_\parallel$ is associated with the collisionless regime, penetration of $E_\parallel$ to low altitudes may be enhanced by depletions of topside ionization and/or neutrals. Plasma depletions have been observed at auroral and subauroral latitudes [*Taylor et al.*, 1975; *Rao et al.*, 1978; *Roble et al.*, 1971], notably in association with magnetic activity. Further observational and theoretical work on the variability and conduction properties of this transition region is clearly needed to assess the importance of $E_\parallel$ penetration down to charge exchange altitudes.

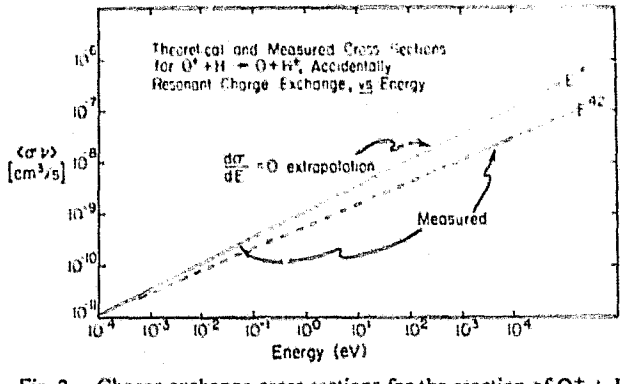


Fig. 2. Charge exchange cross sections for the reaction of $O^+ + H \rightarrow O + H^+$ as a function of energy with which $O^+$ approaches H. The upper line corresponds to an extrapolation of low-energy values under the assumption of constant $\sigma$. The lower curve is an extrapolation of measurements given by *Tinsley* [1976] for keV energies, suggesting $\sigma \sim E^{-0.08}$

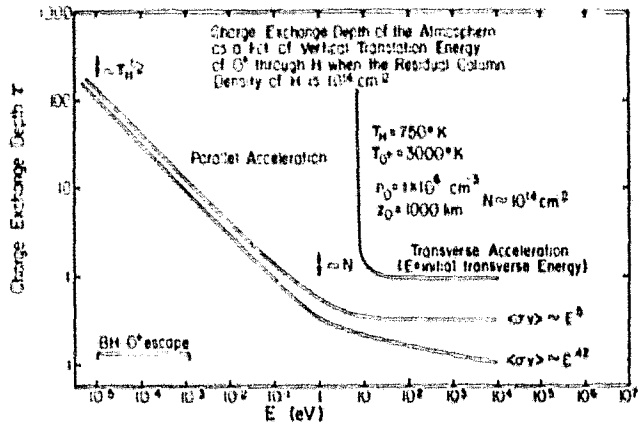


Fig. 3. Charge exchange depth of the hydrogen atmosphere at a column density depth of $10^{14}$ cm$^{-2}$ as a function of $O^+$ energy for two types of ion acceleration. $E$ is the upward translation energy in the parallel acceleration case, the initial transverse energy imparted to the ion in the transverse acceleration case.

## TRANSVERSE ACCELERATION

It is of great interest whether the transverse acceleration by ion cyclotron waves proposed to account for observed conical ion pitch angle distributions can also successfully overcome gravitational and charge exchange barriers hindering $O^+$ removal. It is immediately clear that (1) again, the acceleration must occur below the H, O crossover level to have access to the low-altitude $O^+$ source; (2) the acceleration must occur in a time much shorter than the local charge exchange collision period $[n_H\langle\sigma v\rangle]^{-1} \sim 50$ s for BH parameters. Next, the ion charge exchange depth must be evaluated for $O^+$ ions escaping under the influence of the magnetic mirror force and gravitation. With the following assumptions, (1) $d\sigma/dE = 0$, (2) $n_H = n_0 e^{-z/z_0}$, (3) **B** is parallel to **g** and $\hat{z}$, (4) there is dipole $|B|$ variation with altitude, and (5) ions are rapidly accelerated to $E_{\perp 0}$ and have vanishing initial vertical bulk flow, the result for $\tau$ (see appendix for derivation) is

$$\tau \cong \sigma N_H \frac{p^{1/2}}{[1 - \frac{1}{3}(E_e/E_{\perp 0})]^{1/2}}$$

valid for $p \gg 1$, where $p \cong R_E/z_0$ and is expected to be of order 6.5. $E_{\perp 0}$ is the initial transverse energy, $E_e$ is the $O^+$ escape energy ~10 eV, and $\sigma$, $N_H$ have their usual meaning. This function has a singularity for $E_{\perp 0} = \frac{1}{3} E_e$, due to the impossibility of gravitational escape for $E_{\perp 0}$ at or below that level. The behavior is plotted versus $E$ in Figure 3. For larger energies

the charge exchange depth drops abruptly to approximately unity for BH parameters, where it levels out. This mechanism thus suffers a disadvantage by a factor of order 2.5 compared with the parallel acceleration case in the limit of large acceleration. Moreover, a larger threshold exists for transverse acceleration, since the full escape energy must be provided at once. Heating of $O^+$ at rates slower than 10 eV/min merely hastens their loss by charge exchange, producing fast neutral O. The fast neutral O may transfer energy to neutral H and thus alter its distribution, as discussed above. However, with heating rates much larger than 10 eV/min, occurring at altitudes below the H, O crossover level, the magnetic mirror force can convert an appreciable fraction of the transverse energy to upward translation so that the charge exchange depth drops to approximately unity and $O^+$ escapes without much loss.

One problem with this mechanism is the low altitude at which it must operate for the ionospheric parameters of BH (H, O crossover at ~600 km). *Kindel and Kennel* [1971] have found that the critical current density for ion cyclotron wave growth reaches very high values of $10^{-4}$ to $10^{-2}$ A/m² at 400 km. They identified ionospheric variability as crucial to the minimum altitude at which waves become destabilized by a given current density. The waves are unstable when a critical electron-ion drift is exceeded, i.e., above an altitude which decreases with decreasing electron number density (or increasing current density). Their results indicate that wave growth at 400 km can occur only for the extreme case of an ionospheric trough condition with a current of 160 μA/m². Such conditions may occur during major magnetic storms. However, it still remains to show whether ion transverse heating rates are sufficient to reduce the $O^+$ charge exchange depth, a task which is beyond the scope of this paper. Heating rates of $10$–$150T_i$/ion/s obtained by *Drummond and Rosenbluth* [1962], *Rynn et al.* [1974], and *Palmadesso et al.* [1974] and cited by *Ungstrup et al.* [1979] appear to be ample; and the observations of *Whalen et al.* [1978] indicate that such heating can occur at 400–600 km in the expansive phase of a substorm.

## CONCLUSIONS

The notion that high-latitude ionospheric escape flux composition may be influenced by the interaction of ion dynamics and charge exchange chemistry has been explored for an $H^+$, $O^+$, $e^-$ ionosphere. The polar wind model of *Banks and Holzer* [1969*b*] for the thermal escape of plasma and observations of very nonthermal ion escape have been used as guides. A simple description of ion continuity with arbitrarily imposed dynamics has been used to argue that

1. Appreciable steady escape of $O^+$ from the ionosphere requires ion acceleration at altitudes below that where the neutral O density falls rapidly below the neutral H density and the ionospheric $O^+$ source is converted by charge exchange to $H^+$. This level is normally in the 500- to 1000-km range, according to atmospheric models. The acceleration is required both to overcome the gravitational confinement of $O^+$ and to violate charge exchange equilibrium so that the neutral H atmosphere appears 'optically' thin to escaping $O^+$.

2. Parallel vertical acceleration to ≳0.1 eV will suffice if continued forcing insures gravitational escape. Such continued forcing is automatic if a kilovolt parallel potential drop exists.

3. Transverse acceleration must occur at a rate much larger than 0.2 eV/ion/s in order that gravitational and charge exchange barriers be overcome. Rates still larger than this will not achieve much additional increase in $O^+$ escape. The transverse acceleration must stop as soon as the ion begins to move rapidly upward.

4. Depletion of the neutral H atmosphere by heating and/or escape may play a crucial role by (*a*) raising the H, O crossover level so that $O^+$ persists to higher altitudes where acceleration mechanisms are known to be operative and (*b*) decreasing the H column density above the level where acceleration begins.

5. Depletion of the topside thermal plasma may alternatively serve as an $O^+$ 'throttle' by lowering the region where acceleration occurs.

This analysis shows that ionospheric charge exchange chemistry is an important factor which can effect strong modulation of ionospheric escape flux composition by interaction with low-altitude acceleration processes. Resonant preferential acceleration of a particular ion species need not occur for this modulation to be effective, and this mechanism may mask effects of such selective acceleration by consuming the accelerated ions to produce fast neutrals. It can easily be appreciated that an analysis of a more complex ionosphere containing $NO^+$ or other ions should reveal other interesting effects due to changes of chemistry with varying dynamics. These results point to a bona fide interaction between magnetosphere and ionosphere which can potentially influence the oxygen chemistry of the ionosphere over storm or solar cycle time scales and that of the atmosphere over geologic time scales. Determination of the relative importance of plasma and neutral depletion or of low-altitude acceleration requires a better understanding of ionospheric response to magnetic activity and of parallel current conduction in the topside ionosphere. Additional observations of dc fields, waves, and particles in the altitude range from 500 to 1500 km, i.e., above current rocket or radar altitudes and below most satellite altitudes, would be most helpful. A desirable theoretical goal would be an extension of polar wind theory to situations with vertical currents and particle acceleration to well above thermal energies.

## APPENDIX: CHARGE EXCHANGE DEPTH FOR TRANSVERSELY ACCELERATED IONS

Beginning with the definition for charge exchange depth,

$$\tau \equiv \int_0^\infty \frac{\langle \sigma v \rangle}{v_z} n(z)\, dz$$

and expressing in terms cos $\theta$, where $\hat{z}$ is taken parallel to **B** so $\theta$ is the ion pitch angle; and $n$, the 'target atom' number density, is taken to be $n = n_0 e^{-z/z_0}$, we have, with the change of variable $t = z/z_0$,

$$\tau = \sigma N \int_0^\infty dt\, e^{-t}/\cos\theta$$

Now $\cos\theta = [1 + (v_\perp^2/v_z^2)]^{-1/2}$. A dipolar field is appropriate at altitudes of interest, so that

$$v_\perp^2 = v_{\perp 0}^2 \frac{B}{B_0} = v_{\perp 0}^2 \left(\frac{r_0}{r}\right)^3$$

Here, $r_0$ is the geocentric radius at which ions are accelerated to initial transverse speed $v_{\perp 0}$. To get $v_z^2$, we assume that $\mathbf{B} \cdot \mathbf{g} = 1$ and write an effective potential for field-aligned motion under the influence of gravity and the magnetic mirror force.

Here, $g_0$ is the acceleration of gravity at the starting radius $r_0$, and $\theta_0$ is chosen such that $\phi_z = 0$ there:

$$\phi_z = mg_0r_0\left(\frac{1-r_0}{r}\right) - \tfrac{1}{2}mv_{\perp 0}^2\left[1-\left(\frac{r_0}{r}\right)^3\right]$$

At $r > r_0$, $E_z + \phi_z = 0$ expresses vertical energy conservation for ions with $v_z = 0$ at $r_0$. Thus

$$v_z^2 = \frac{2}{m}E_z = v_{\perp 0}^2\left[1-\left(\frac{r_0}{r}\right)^3\right] - 2g_0r_0\left(1-\frac{r_0}{r}\right)$$

and

$$\cos\theta = \left[1 + \frac{v_{\perp 0}^2\,(r_0/r)^3}{v_{\perp 0}^2[1-(r_0/r)^3] - 2g_0r_0[1-(r_0/r)]}\right]^{1/2}$$

with the substitutions $r = r_0 + z$, $t = z/z_0$, $p = r_0/z_0$, so that $z$ is measured from $r_0$, some manipulation of the expression for $\tau$ gives

$$\tau = \sigma N\int_0^\infty dt\, e^{-t}\left[1 - \frac{(1+t/p)^{-3}}{1-(2g_0r_0/v_{\perp 0}^2)(1-p/t)^{-1}}\right]^{-1/2}$$

Expanding this for small $t/p$ and retaining terms to first order only, one obtains

$$\tau \cong \sigma N\int_0^\infty dt\, e^{-t}\left[\left(3 - \frac{4g_0r_0}{v_{\perp 0}^2}\right)\frac{t}{p}\right]^{-1/2}$$

valid for $p$ large, or

$$\tau \cong \sigma N\frac{p^{1/2}\Gamma(1/2)}{\sqrt{3}[1-(2E_e/3E_{\perp 0})]^{1/2}} \cong \sigma N\frac{p^{1/2}}{[1-(2E_e/3E_{\perp 0})]^{1/2}}$$

where $E_e = 1/2\ mv_e^2 = mg_0r_0$ is the gravitational escape energy from radius $r_0$, $E_{\perp 0}$ is the initial transverse ion energy, and $N$ is the column density of target atoms above $r_0$; $p$ is the ratio of $r_0$ to the target atom scale height and is expected to be larger than 5.

*Acknowledgments.* This work was supported in part by NASA grant NSG-6022. Part of the work was done while the author was a guest of the Kiruna Geophysical Institute. The hospitality of the staff there is greatly appreciated. The author is grateful for stimulating discussions with D. S. Evans, T. E. Holzer, R. L. Kaufmann, D. Klumpar, M. A. Lee, E. Leer, and R. Lundin.

The Editor thanks T. E. Holzer and W. J. Raitt for their assistance in evaluating this paper.

## REFERENCES

Axford, W. I., The polar wind and the terrestrial helium budget, *J. Geophys. Res.*, *73*, 6855, 1968.

Banks, P. M., and T. E. Holzer, Features of plasma transport in the upper atmosphere, *J. Geophys. Res.*, *74*, 6304, 1969*a*.

Banks, P. M., and T. E. Holzer, High-latitude plasma transport: The polar wind, *J. Geophys. Res.*, *74*, 6317, 1969*b*.

Drummond, W. E., and M. N. Rosenbluth, Anomalous diffusion arising from microinstabilities in a plasma, *Phys. Fluids*, *5*, 1507, 1962.

Evans, D. S., Precipitated electron fluxes formed by a magnetic field aligned potential difference, *J. Geophys. Res.*, *79*, 2853, 1974.

Geiss, J., H. Balsiger, P. Eberhardt, H. P. Walker, L. Weber, D. T. Young, and H. Rosenbauer, Dynamics of magnetospheric ion composition as observed by the GEOS mass spectrometer, *Space Sci. Rev.*, *22*, 537, 1978.

Ghielmetti, A. G., R. G. Johnson, R. D. Sharp, and E. G. Shelly, The latitudinal, diurnal, and altitudinal distributions of upward flowing energetic ions of ionospheric origin, *Geophys. Res. Lett.*, *5*, 59, 1978.

Hoffman, J. H., W. H. Dodson, C. R. Lippincott, and H. D. Hammack, Initial ion composition results from the Isis 2 satellite, *J. Geophys. Res.*, *79*, 4246, 1974.

Kindel, J. M., and C. F. Kennel, Topside current instabilities, *J. Geophys. Res.*, *76*, 3055, 1971.

Kintner, P. M., M. C. Kelley, R. D. Sharp, A. G. Ghielmetti, M. Temerin, C. Cattell, and P. Mizera, Simultaneous observations of energetic (keV) upstreaming ions and electrostatic hydrogen cyclotron waves, *J. Geophys. Res.*, *84*, 7201, 1979.

Klumpar, D. M., Transversely accelerated ions: An ionospheric source of hot magnetospheric ions, *J. Geophys. Res.*, *84*, 4229, 1979.

Lemaire, J., and M. Scherer, Kinetic models of the solar and polar winds, *Rev. Geophys. Space Phys.*, *11*, 427, 1973.

Lynch, J., R. Leach, D. Pulliam, and F. Sherb, Composition and energy spectrum variations of auroral ions, *J. Geophys. Res.*, *82*, 1951, 1977.

Moore, T. E., and D. S. Evans, Distribution of energetic positive ion species above a diffuse midnight aurora, *J. Geophys. Res.*, *84*, 6443, 1979.

Palmadesso, F. J., T. P. Coffey, S. L. Ossakow, and K. Papadopoulos, Topside ionospheric heating due to electrostatic ion cyclotron turbulence, *Geophys. Res. Lett.*, *1*, 105, 1974.

Raitt, W. J., R. W. Shunk, and P. M. Banks, Quantitative calculations of helium ion escape fluxes from the polar ionospheres, *J. Geophys. Res.*, *83*, 5617, 1978.

Reiff, L. D. V., W. J. Burke, M. Kanal, and R. C. Sagalyn, Injun 5 low-energy plasma observations during a major magnetic storm, *J. Geophys. Res.*, *83*, 3217, 1978.

Roble, R. G., R. B. Norton, J. A. Findlay, and E. Marovitch, Calculated and observed features of stable auroral red arcs during three geomagnetic storms, *J. Geophys. Res.*, *76*, 5648, 1971.

Rynn, N., D. R. Dakin, D. L. Correll, and G. Benford, Ion heating by the current driven electrostatic ion cyclotron instability, *Phys. Rev. Lett.*, *33*, 765, 1974.

Sharp, R. D., R. G. Johnson, and E. G. Shelley, The morphology of energetic $O^+$ ions during two magnetic storms: Temporal variations, *J. Geophys. Res.*, *81*, 3283, 1976.

Sharp, R. D., R. G. Johnson, and E. G. Shelley, Observations of ionospheric acceleration mechanism producing energetic (keV) ions primarily normal to the geomagnetic field direction, *J. Geophys. Res.*, *82*, 3324, 1977.

Shelley, E. G., R. D. Sharp, and R. G. Johnson, Satellite observations of energetic heavy ions during a geomagnetic storm, *J. Geophys. Res.*, *77*, 6104, 1972.

Shelley, E. G., R. D. Sharp, and R. G. Johnson, Satellite observations of an ionospheric acceleration mechanism, *Geophys. Res. Lett.*, *3*, 654, 1976.

Taylor, H. A., Jr., J. M. Grebowski, and A. J. Chen, Ion composition irregularities and ionosphere-plasmasphere coupling: Observations of a high latitude ion trough, *J. Atmos. Terr. Phys.*, *37*, 613, 1975.

Tinsley, B. A., Hydrogen in the upper atmosphere, *Fund. Cosmic Phys.*, *1*, 201, 1974.

Tinsley, B. A., Evidence that the recovery phase ring current consists of helium ions, *J. Geophys. Res.*, *81*, 6193, 1976.

Ungstrup, E., D. M. Klumpar, and W. J. Heikkila, Heating of ions to suprathermal energies in the topside ionosphere by electrostatic ion cyclotron waves, *J. Geophys. Res.*, *84*, 4289, 1979.

Whalen, B. A., W. Bernstein, and P. W. Daly, Low altitude acceleration of ionospheric ions, *Geophys. Res. Lett.*, *5*, 55, 1978.

(Received November 29, 1979;
revised February 8, 1980;
accepted February 11, 1980.)

JOURNAL OF GEOPHYSICAL RESEARCH, VOL. 85, NO. A7, PAGES 3407-3413, JULY 1, 1980

# Rocket Observations at the Northern Edge of the Eastward Electrojet

LAURENCE J. CAHILL, JR.[1]

*Max Planck Institut für Physik und Astrophysik, Institut für Extraterrestrische Physik 8046 Garching b. Munich, West Germany*

R. L. ARNOLDY

*Space Science Center, University of New Hampshire, Durham, New Hampshire 03824*

WILLIAM W. L. TAYLOR[2]

*Space Science Center, University of Minnesota, Minneapolis, Minnesota 55455*

A Nike-Tomahawk rocket was launched north over two quiet, late evening auroral arcs in March 1975. A northward magnetic disturbance was observed on the ground under the rocket trajectory. South of the arcs the northward electric field was 60 mV/m, indicating strong westward plasma flow. An eastward electrojet current layer was penetrated in the upward flight. Precipitating electrons were observed over each arc. The electric field decreased to below 20 mV/m over each arc and recovered to 50 mV/m between the arcs. Using the observed electron flux and a model of the ionosphere, the Hall and Pedersen conductivities were calculated. These conductivities were used, with the observed electric field, to calculate the eastward and northward components of the horizontal ionospheric currents. The eastward current calculated south of the first arc agreed well with the observed eastward electrojet current. The power dissipated by the Pedersen current $\Sigma_p|E|^2$ was also calculated and compared with the power carried by the precipitating electrons. The Joule power decreased abruptly in the auroral arcs, as the precipitating electron power increased. The total dissipated power was approximately the same inside the arcs, between them, and south of the luminosity. North of the aurora the electric field and dissipated power remained low. Field-aligned currents carried by the observed electrons were about a factor of 3 lower than those inferred from the magnetic field measurements. Likewise, current continuity arguments to keep the auroral current system divergence free required a larger field-aligned current than that obtained from the particle detectors.

## INTRODUCTION

Plasma in the ionosphere drifts toward the west in the evening auroral oval under the influence of a northward electric field. In the lower ionosphere, near 110-km altitude, where the positive ions are retarded by collisions, the westward electron motion constitutes an eastward ionospheric current. A region of eastward drifting plasma is sometimes observed, to the north of the westward drift, with an associated westward ionospheric current [*Maynard,* 1974]. Discrete, quiet, auroral arcs are also observed in the late evening close to the region of plasma flow reversal [*Kamide and Rostoker,* 1977].

*Evans et al.* [1977] and *Maynard et al.* [1977] reported on electric fields and ionospheric currents, observed by rocket, near an auroral arc at the northern edge of the westward plasma flow. We report here on a very similar rocket flight over late evening auroral arcs. *Arnoldy and Lewis* [1977] have described the electron measurements on this flight and have shown that they can be used to predict the auroral light intensity. In this report we will describe measurements of electric fields, ionospheric currents, and field-aligned currents in and near the arcs and will discuss the spatial relations between the arcs, the electric field, and the currents.

## INSTRUMENTATION

The payload included instruments to measure the electric field and the magnetic field (in order to detect electrical currents) as well as the electron flux and the auroral light. Electric double probes were extended, on booms perpendicular to the spin axis, to a separation distance of 3 m. As the booms rotated in the electric field plus $\vec{v} \times \vec{B}$ from rocket motion, a sinusoidal signal was generated which yielded the field amplitude and direction. The electric field perpendicular to $\vec{B}$ was obtained, assuming $\vec{E}$ parallel to $\vec{B}$ to be zero, after removing the $\vec{v} \times \vec{B}$ component. The estimated accuracy of an individual measurement of $\vec{E}$ was ±5 mV/m and ±5°, for a northward field of 50 mV/m. The sensitivity to changes in this field was 2 mV/m and 2°.

Changes in magnetic field, observed as the rocket passed through electrical current sheets, allowed detection and measurement of these sheets. A proton precession magnetometer, which provides total field magnitude measurements, was flown to detect east-west horizontal ionospheric current sheets (electrojet currents). These sheets produce north-south magnetic fields $H$ of order 100 nT. Such fields have components $H \cos I$ parallel to the earth's field (55,000 nT), where $I$, the field inclination, is 77° at Poker Flat. Changes in the parallel components can be observed as changes in total field magnitude. The proton magnetometer had an effective sensitivity, limited by rocket magnetic field and by signal noise, of about 10 nT. North-south ionospheric current sheets or field-aligned current sheets produce east-west magnetic fields $D$, perpendicular to the earth's field and therefore resulting in small magnitude

[1] Present address: Space Science Center, University of Minnesota, Minneapolis, Minnesota 55455.

[2] Present address: TRW Systems Group, Redondo Beach, California 90278.



Paper number 80A0359.
0148-0227/80/080A-0359$01.00

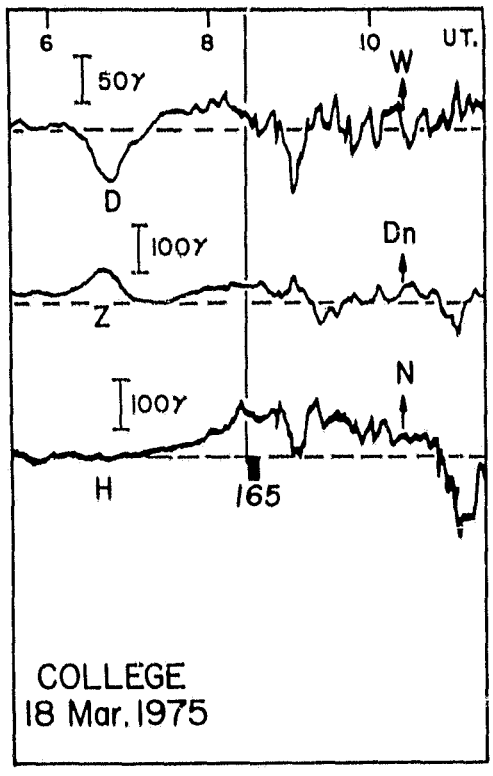


Fig. 1. College magnetogram, 0600–1030 UT, March 18, 1975. The period of flight 18:165 is denoted by the bar under the *H* trace. The approximate quiet time base levels of *H*, *D*, and *Z* are shown by dashed lines.

changes, ~0.1 nT, not observable with the proton magnetometer.

In order to observe more easily the relatively small changes in magnitude of order 10 nT, due to passage through current sheets, in the presence of much larger changes in magnitude of order 1000 nT, due to the inverse cube decrease of the earth's field with altitude, it was necessary to calculate the earth's field magnitude along the trajectory and to subtract this from the observations. Possible errors in the trajectory could produce a cumulative error in the difference magnitude $\Delta B$ as large as 100 nT on the downleg. Of course, it was the change in $\Delta B$ on passing through the relatively thin electrojet current sheet that was essential to the current measurement and not the absolute accuracy of $\Delta B$.

A sensitive flux gate magnetometer was mounted perpendicular to the spin axis to detect changes in the east magnetic field component due to field-aligned current sheets [*Kintner et al.*, 1974]. The times, twice per spin, when the transverse flux gate magnetometer (TFM) was perpendicular to the spin plane field component, ~25,000 nT, were measured with an uncertainty of ±0.1 ms. Since the spin rate above 120 km was nearly constant, the perpendicular times could also be predicted. Penetration of a field-aligned current sheet, with resulting changes in the east magnetic field component, would change the direction of the spin plane magnetic field and thus cause a cumulative deviation of the observed perpendicular times from those predicted. A slow decrease in the spin rate during the flight, slow changes in direction of the earth's field along the trajectory, and periodic variations due to rocket precession were modeled, and the record was corrected for these effects. After smoothing to decrease random fluctuations we estimated that an east component change greater than 200 nT, associated with a current sheet less than 100 km thick, could be detected. Smaller or more gradual changes could not be clearly identified, since they might be due to uncertainties in modeling. The component of $\bar{B}$ along the rocket spin axis was also measured. These measurements agreed with the proton magnetometer results, considering the angle between the spin axis and the magnetic field. They were useful in determining the spin axis direction but did not contribute to the determination of the current sheets. The axial measurements will therefore not be discussed in this report.

The electron flux and auroral light measurements have been described by *Arnoldy and Lewis* [1977]. Electrons between 25 eV and 15 keV were measured with energy resolution of 10% and flux resolution of $10^5$ (cm$^2$ s sr keV)$^{-1}$. The lower energy limit to the electron measurement is difficult to specify, since it depends on the unmeasured rocket potential. The 25-eV estimate is conservatively high. Auroral light measurements were estimated to be accurate to within 1 kR for the data shown.

## Launch Conditions

Flight 18:165 was launched from the Poker Flat Rocket Range, Alaska, in local evening, on March 18, 1975. There was a positive magnetic bay (90 nT at launch) and two quiet auroral arcs to the north (Figures 1 and 2). The flight lasted over 440 s (0827–0834 UT), traveled 270 km north on magnetic azimuth 4° west, and reached 224-km peak altitude. The spin rate after 100 s was 4.75 rps; there was a 49-s precession with half angle 2.4°; and the angular momentum vector was approximately in the magnetic meridian, 16° north of vertical and 29° from the magnetic field. The magnetic local time at launch was ~2100.

## Observations

The auroral arcs shown in Figure 2 were clearly visible in the Ester Dome and Fort Yukon meridian scanning photometer records. In addition, auroral photometers mounted on the rocket allowed measurement of auroral light, looking directly down the magnetic field line below the rocket, once during each spin period (Figure 3). The energy flux of precipitated electrons was 10 ergs cm$^{-2}$ s$^{-1}$ over the first arc and reached 20

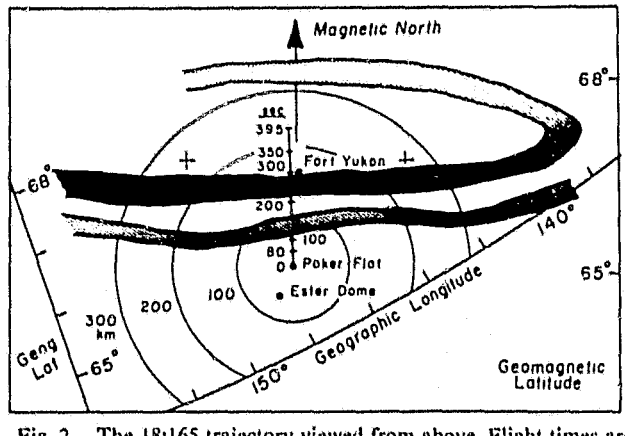


Fig. 2. The 18:165 trajectory viewed from above. Flight times are labeled along the trajectory. The shaded regions indicate the locations of auroral arcs, intense electron precipitation, and electric field amplitude decrease. The crosses show two locations of the radar drift velocity measurements. A third location not marked is just north of Fort Yukon.

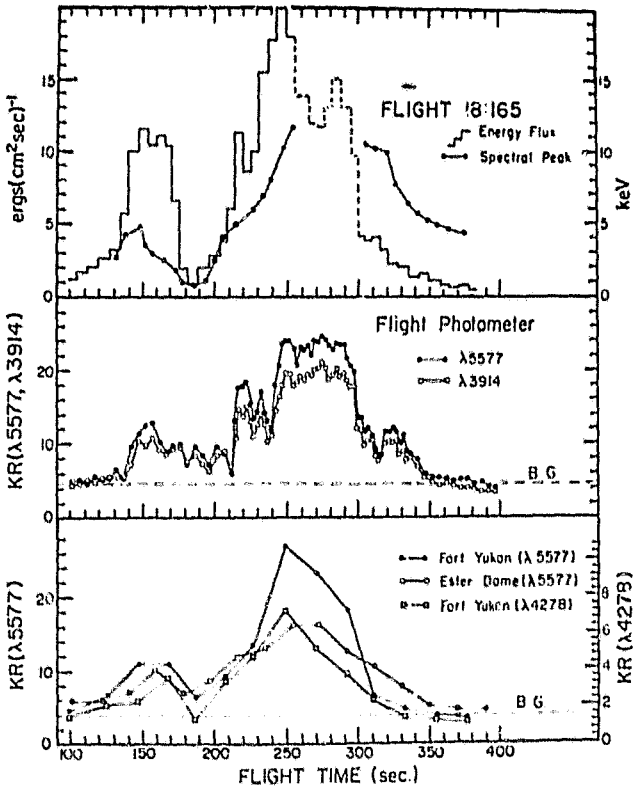


Fig. 3. Particle energy flux and auroral light. (top) The energy flux of precipitating electrons (a few electron volts to 15 keV) is shown together with the energy of a high energy peak in the electron spectrum. (middle) The auroral light intensity as seen by on board photometers looking directly down the magnetic field line is shown. (bottom) The auroral light intensity on the rocket field lines as observed by meridian scanning photometers at Fort Yukon and Ester Dome. This figure is a corrected version of Figure 3 of *Arnoldy and Lewis* [1977], where the measured energy flux over the second arc is in error.

over the second, while the spectral peak in the electron energy spectrum was less than 5 keV for the first arc and over 10 keV for the second. The two arcs were clearly associated with 'inverted V' structures. The spectral peak moved beyond the energy range of the detectors for the second arc. Calculations using the measured spectra during this time will therefore represent lower limits.

In Figure 4 the electric field is compared with the electron energy flux, showing that the field magnitude dropped abruptly as the rocket passed over the arcs where the energy flux was greatest. At the beginning of the flight the field magnitude was relatively high, over 60 mV/m, and pointed approximately toward magnetic north. As the magnitude dropped over the first auroral arc, the direction rotated toward the northwest. Between the arcs the field recovered to 50 mV/m. The field magnitude remained low (~5–15 mV/m) as the rocket passed over the intense arc, with direction generally in the southeast. After 310 s the magnitude increased slowly to 20 mV/m, and the direction returned to northwest. Observations of plasma flow velocity with the Chatanika radar during the flight allowed an independent determination of the electric field. The radar was pointed, in sequence, toward the magnetic north, northwest, and northeast. Measurement intervals, along each beam direction, were chosen to provide line-of-sight plasma drift velocity components at 190-km altitude at three points along a line 170 km north of Chatanika (R.

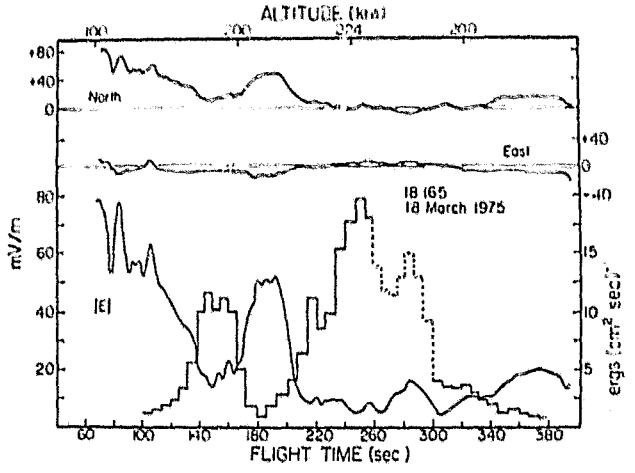


Fig. 4. The electric field magnitude, north component and east component, all in millivolts per meter, measured with the double probe electric field meter on 18:165. The $v \times B$ field has been subtracted. The abrupt decreases in $E$ at 130 and 200 s occur as the rocket enters the regions of intense electron energy flux. Precipitated energy flux is shown as a histogram.

Vondrak, private communication, 1975). The locations, shown in Figure 2, were just north of the bright arc. The velocity components, measured in the interval 0822 to 0833 UT, were used to determine the electric field, 18 mV/m north and 4 mV/m west. The rocket measurement, north of the bright arc (350–390 s) was 15 mV/m north and 8 mV/m west. The agreement between the two measurements was good, considering that the radar measurement was an average over space and time.

The College magnetogram (Figure 1) indicated an eastward electrojet current with the current center north of College. The Fort Yukon magnetogram for the same period showed that the electrojet center was to the south of that station. Figure 5 shows the magnetic field magnitude, measured with a proton magnetometer during the flight, after subtracting the internal reference field. The 160-nT decrease from 70 to 110 s was caused by penetration of the eastward electrojet current layer, while the relatively slow return of the magnitude to zero from 300 to 400 s suggested that the electrojet was not directly penetrated on the downward portion of the flight. The magnitude change, 160 nT, corresponds to a horizontal component $H$ change of 700 nT.

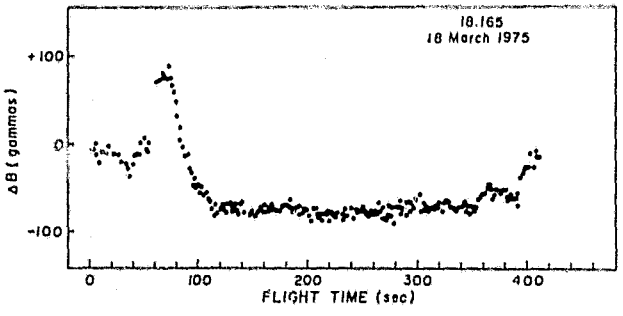


Fig. 5. Magnetic signature of the eastward electrojet. The magnitude of the earth's internal field has been subtracted from the proton precession magnetometer record to emphasize the field changes due to ionospheric currents. The abrupt change between 70 and 110 s indicates passage upward through an eastward directed electrical current sheet. The absence of a similar abrupt transition in the downward flight record suggests that the rocket came down to the north of the electrojet northern boundary.

In addition to the eastward electrojet current, field-aligned currents carried by electrons (a few electron volts to 15 keV) were measured, as shown in Figure 6. The net field-aligned current was calculated from the measured upward and downward electron fluxes. The upward (conventional) current density over the weaker arc, $4 \times 10^{-6}$ A/m$^2$, was about twice that over the more intense arc, $2 \times 10^{-6}$ A/m$^2$. The average current over the 100-km-thick current sheet was $2.5 \times 10^{-6}$ A/m$^2$. This should produce a total transverse (east to west) field change of 320 nT. The direct particle measurements of field-aligned currents were supplemented by sensitive measurement of the direction of the magnetic field component perpendicular to the rocket spin axis by the transverse flux gate magnetometer. The cumulative change, between 150 and 300 s flight time, in the time, each spin, of observing the transverse magnetic field was $2.6 \times 10^{-3}$ s and was equivalent to a change (east to west) in magnetic field of over 1000 nT, as shown in Figure 6. Assuming this field change resulted from penetration of an upward flowing field-aligned current sheet (extending east-west) 100 km thick, the (uniform) current density was $\sim 8 \times 10^{-6}$ A/m$^2$:

$$J_{\parallel} = \frac{\Delta B_{east}}{\mu_0 \, \Delta y} \text{ A/m}^2$$

where $\Delta B_{east}$ is the change in the east component shown in Figure 6 and $\Delta y$ is the sheet thickness. This measurement of field-aligned current gives a result about 3 times greater than the particle measurements. The disagreement between the two techniques for measuring field-aligned current could be due to errors in the modeling or to field-aligned current carried by ions or thermal electrons not measured by the particle detectors.

## CALCULATIONS

Height-integrated Hall and Pedersen conductivities are shown in Figure 7. These were calculated using the incoming measured electron flux, the neutral model atmosphere of *Rees et al.* [1977], the temperature profile of *Jones and Rees* [1973], and the ion composition of an auroral arc given by *Rees and Walker* [1968]. First the electron production rate $q(Z)$ resulting from the electron flux impinging on the atmosphere at each altitude level was calculated according to the work of *Rees* [1963]. Equation 1 in Rees's paper was modified to apply to a measured directional intensity of electrons $J(E)$, as follows:

$$q(Z) = 2\pi \int_0^{\pi/2} \int_{E_{min}}^{E_{max}} \frac{qz}{F} J(E) \sin\theta \cos\theta \, d\theta dE$$

where the ratio $qz/F$ is equation 1 of *Rees* [1963], using the isotropic, normalized energy dissipation distribution function of that paper. The electron density was obtained from the production rate under equilibrium conditions by using the effective recombination coefficients tabulated by *Evans et al.* [1977]. Finally, the collision frequencies and the Hall and Pedersen conductivities were obtained as outlined by *Evans et al.* [1977]. Note in Figure 7 that the Pedersen conductivity $\Sigma_p$ exceeds the Hall conductivity $\Sigma_H$ for the first arc. The reverse is true for the second and brighter arc, which is produced by more energetic electrons that deposit their energy deeper in the atmosphere.

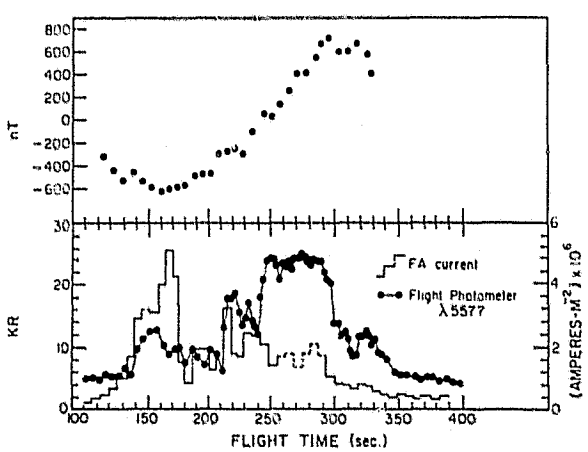


Fig. 6. Field-aligned current from electron flux and magnetic measurements. The difference between upward and downward moving electrons is a net downward electron flux. This constitutes the upward electrical current density shown in the bottom panel. The flight photometer record (5577 Å) is also plotted to show the relation of field-aligned current to the auroral arcs. In the top panel the change in the eastward magnetic field component, as deduced from the transverse flux gate measurements, is shown.

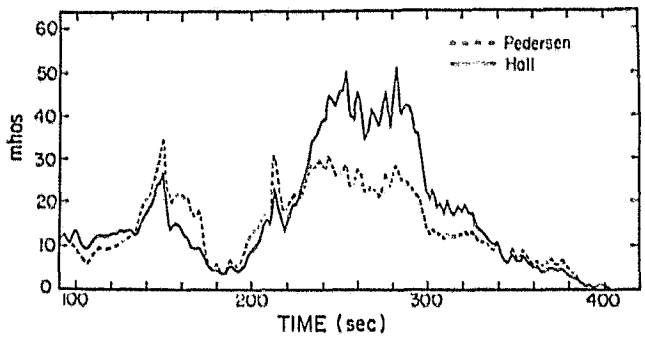


Fig. 7. Height-integrated Hall and Pedersen conductivities calculated from the precipitating electron flux.

One may calculate the Joule power dissipated by the ionospheric current component parallel to $E$ from the calculated Pedersen conductivity and the measured electric field as $\Sigma_p E^2$ [*Evans et al.*, 1977]. This Joule power as a function of flight time is given in Figure 8 along with the power carried into the atmosphere by the precipitating electrons. The Joule power decreased abruptly as the rocket moved over the aurora due to the decrease in the electric field, while the precipitated power peaked over the arcs. The sum of the two was about the same over the arcs as between or south of them. Note that very little power was present north of the auroral arcs, suggesting that a natural boundary was crossed.

The horizontal electrical current can also be obtained by using the calculated conductivities and the measured electric field as $J_{north} = \Sigma_p E_{north} - \Sigma_H E_{east}$ and $J_{east} = \Sigma_p E_{east} + \Sigma_H E_{north}$. The calculated current components are shown in Figure 9. In the lower section the eastward current density is substantial, ~0.6 A/m from 90 to 110 s. It then decreases steadily to ~0.2 A/m at 140 s. This calculated component is weak and erratic in the first auroral arc, recovers to 0.2 A/m between arcs, and is weak and occasionally westward in the second arc. The northward component in the upper section continues at ~0.4 A/m from 90 to 200 s through the first arc, then decreases to −0.4 A/m at 280 s. It increases rapidly to 0.2 A/m at 310 s. The uncertainty in these calculated current densities is principally due to the uncertainties in the ionosphere

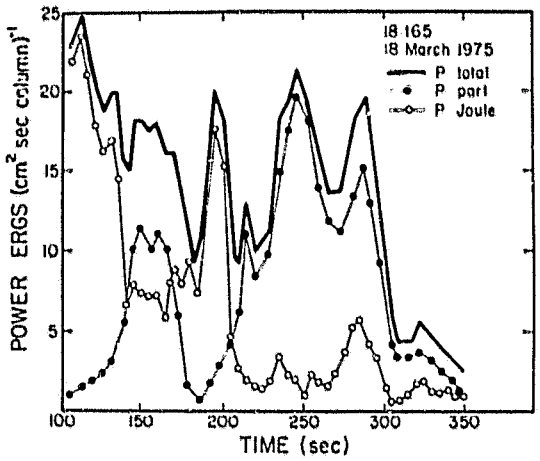


Fig. 8. Power dissipation in the ionosphere. The energy per second deposited by the precipitating electrons is highest in the auroral arcs. The Joule power is strongest outside the arcs where the electric field is higher. The sum of these two decreases abruptly north of the bright arc (300 s).

modeling. We estimate that the current densities may be in error by as much as ±50%.

## Discussion

These rocket measurements provide an accurate comparison between the locations of several auroral zone features: the northern edge of the westward plasma flow, bands of intense electron precipitation and the associated auroral arcs, horizontal ionospheric electric currents, and field aligned currents. We emphasize that the auroral arcs and magnetic field were very stable during the flight, so we interpret observed changes as due to rocket passage through and over stationary structures.

The two arcs were produced by observed fluxes of energetic electrons. *Arnoldy and Lewis* [1977] have shown that the auroral light can be predicted from the observed electron fluxes and vice versa. Two field-aligned sheets of precipitating electron flux stretched from the western to the eastern horizon with bands of auroral light at the lower edges.

The electric field observations show that the auroral arcs were imbedded in the northern edge of a strong westward plasma flow. The decreases in the electric field over the auroral arcs imply polarization charge layers at the edges of the arcs. Similar decreases in electric field over auroral arcs were seen in earlier flights [*Potter*, 1970; *Maynard et al.*, 1973]. Sometimes the electric field does not decrease over arcs, as, for example, during a flight reported by *Kintner et al.* [1974] over a rapidly moving arc in auroral breakup. It appears that only in stable, quiet arcs, like the evening arcs discussed here or the similar arc reported by *Maynard et al.* [1977], are the polarization charge layers established to reduce the electric field.

We must rely on ground magnetic observations and the electric field/conductivity calculations as well as rocket observations to deduce the distribution of the horizontal ionospheric currents. A strong eastward current layer is detected by the proton magnetometer in the upward leg of the flight (40–50 km downrange), while the current is weak or absent on the downward leg (280–290-km range). This establishes that the eastward electrojet terminated between 50 and 280 km north of Poker Flat. The height-integrated current density for the eastward electrojet derived from the change in field magnitude is $\Delta B/\mu_0 \cos I = 0.57$ A/(m in the N-S direction), in good agreement with the calculated value (from measured $E$ and calculated conductivity) of 0.6 A/m at about the same location (Figure 9). Encouraged by this agreement, we note that the calculated eastward current density decreases to zero in the first arc, recovers to 0.2 A/m between arcs, and stays near zero thereafter. These calculated results indicated that the eastward electrojet is greatly reduced in the first arc, 80 km north of Poker Flat, and terminated in the second arc, 175 km north. A third indication of the electrojet extent is obtained from ground magnetometers. Figure 10 shows $\Delta H$ and $\Delta Z$ for several observatories in the Alaskan sector; $\Delta H$ indicates an eastward electrojet with maximum current near Poker Flat and College, and $\Delta Z$ crosses zero just north of Poker Flat, indicating the center of the electrojet current lies there. The shape of $\Delta H$ and $\Delta Z$ curves shows that the current is confined to the region near Poker Flat with the northern edge near Fort Yukon. The southern edge is less certain because of lack of observations between College and Sitka. These ground measurements don't allow a precise determination of the northern edge of the eastward electrojet, but they do support the rocket magnetometer and the calculated results.

Our information about northward current comes solely from the calculations. We had hoped the TFM measurements could be used for these currents, but the rocket attitude changes too rapidly below 120 km to allow reliable modeling. The $D$ component ground magnetometer results in Figure 1 (<25 nT at launch) indicate small and decreasing northward current. The calculated value stays above 0.4 A/m, however, until entry into the second arc 120 km downrange. For a wide northward horizontal current sheet the $D$ component below the current sheet is $D = \mu_0 J_N/2 = 250$ nT, 10 times the observed $D$ component on the ground. The discrepancy is probably due to the solenoidal nature of the meridional currents, downward field-aligned currents south of Poker Flat, northward current south of the arcs, and upward field-aligned currents over the arcs, with the magnetic field confined within the solenoid.

There have been many observations of field-aligned currents with polar-orbiting satellites and by rocket [*Armstrong and Zmuda*, 1973; *Potemra*, 1979; *Cloutier and Anderson*, 1975]. Current densities from 1 to 10 $\mu$A/m² have been re-

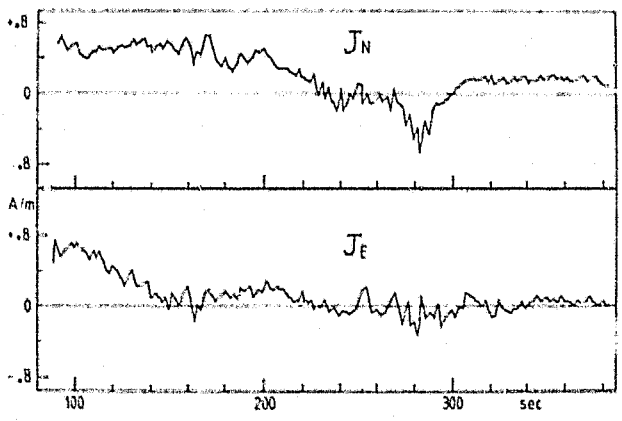


Fig. 9. Horizontal current calculated from electric field and conductivity. The eastward current ($J_E$, in amps per meter; the integrated current from top to bottom of the electrojet in a 1-m-thick sheet, aligned east-west) is the component that can be detected in the proton precession magnetometer record.

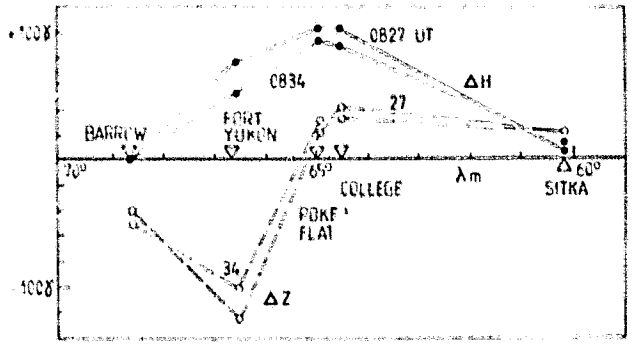


Fig. 10. Profile of the eastward electrojet as seen in the perturbations in the northward and vertical magnetic field components at several Alaskan observatories. Uncertainties in determining these perturbations from ground magnetograms are about ±20γ.

ported. The rocket flight discussed here provided three methods of determining the field-aligned current. The current resulting from the net flux of 25 Ev–15 keV electrons over the auroral arcs (2.5 $\mu A/m^2$ average) is shown in Figure 6 together with the change in east-west magnetic field. The field change implies an average current of 8 $\mu A/m^2$. Over the ~100-km-thick sheet of upward current the integrated current density is ~0.8 A/m. This agrees with the decrease, from +0.4 to −0.4 A/m, in the calculated northward current (Figure 9). Downward field-aligned current is also implied by several increases in northward current density, particularly from 280 to 310 s in Figure 9. Since both the magnetic measurements and the divergence of the northward ionospheric current give an upward field-aligned current larger than the measured electron current (25 eV–15 keV), we attempted to extrapolate the electron measurements to lower and higher energies than those measured. Starting with the measured electron flux at 25 eV, the flux was extrapolated down to 0.1 eV, using a power law decrease of flux with energy $E^{-1}$. The flux of these low-energy electrons is assumed to be isotropic, equal intensities upward and downward. However, in order to find the maximum possible current due to these unmeasured low energy electrons we neglected the upward streaming electrons. This calculation gave an additional upward current density of 2.5 $\mu A/m^2$. Extrapolation upward in energy from 15 keV to 50 keV in a similar fashion gave less than 1 $\mu A/m^2$. We estimate that the average field-aligned current carried by precipitating electrons, including these extrapolated values, was less than 6 $\mu A/m^2$. The remaining discrepancy is perhaps due to unmeasured upstreaming thermal positive ions, to uncertainties in the magnetic measurements, or to uncertainties in the calculated northward current.

One further source of error may be neutral winds, particularly in the interval 210–280 s, when the electric field was less than 10 mV/m. Neutral wind studies by *Brekke et al.* [1973] with the Chatanika radar indicate that neutral winds near 2100 local time are southeast and weak when strong convective ion flow (strong electric field) is absent. In the present case there is, however, strong westward ion flow, thus westward neutral wind due to ion drag, just south of the region of weak electric field and weak ion flow. One might expect, from continuity, that the neutral winds in the weak field region would be south. A weak southward neutral wind should produce a weak southward ion flow by collisions and thus a southward current. This additional current from the neutral wind would add to the calculated southward current in Figure 9 (210–280 s) and would thus increase the upward field-aligned current in this interval.

A model current system is shown in Figure 11 with the eastward, northward, and upward field-aligned components discussed above. Diffuse downward field-aligned currents presumably exist south of Poker Flat, but these have not been included in the model. Field magnitude $\Delta B$ and components $\Delta H$, $\Delta D$, and $\Delta Z$ produced along the rocket trajectory by this model current are also shown. The $\Delta B$ and $\Delta D$ agree approximately with the proton magnetometer and transverse flux gate magnetometer results. The observed $\Delta B$ of Figure 5 does not show the rapid recovery of the model from 100 to 200 s. Bringing the termination of the model eastward current farther north would improve the agreement; $\Delta H$, $\Delta D$, and $\Delta Z$ agree reasonably well at zero seconds with the Poker Flat ground observations. Note that $\Delta D$ is ~0 except above 100 km in the solenoid. Although the model $\Delta H$ at zero seconds, 100 nT, agrees approximately with the ground magnetometer, 90 nT, both are much less than the field, 700 nT/2 = 350 nT, directly beneath the electrojet, inferred from the proton magnetometer assuming an infinite current sheet. In this case, since the current sheet is relatively narrow, $\Delta H$ is only 200 nT beneath the electrojet, as seen in Figure 11, and a change in $Z$ as well as in $H$ contributes to the observed change in $B$ as the

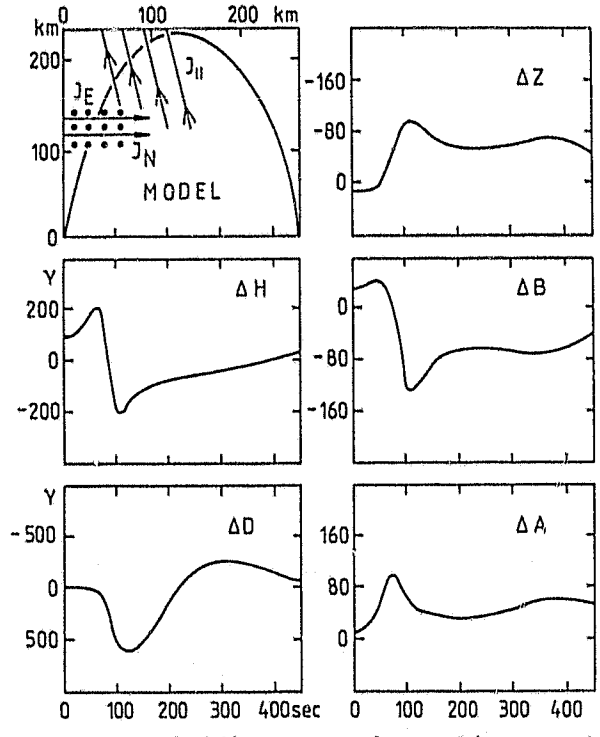


Fig. 11. Magnetic field components from model current calculations. The model is shown in the upper left panel. The $\Delta H$ is the magnetic north component principally due to the eastward electrojet current, $\Delta D$ the magnetic east component due to northward and field-aligned currents, $\Delta Z$ the vertical component due also to the eastward current, and $\Delta B$ the change in total field due principally to the eastward current. The $\Delta A$, the component along the rocket spin axis, was used to compare with the axial flux gate magnetometer records not discussed in this report. The model consists of an eastward current, 12 $\mu A/m^2$, extending from 30 km south of the launch site to 70 km north and from 100 to 150 km in altitude; a northward current, 8 $\mu A/m^2$, extending from 300 km south of launch to 100 km north and 100 to 150 km in altitude; and a field-aligned current, 10 $\mu A/m^2$, extending from 75 to 150 km north of launch and 120 to 700 km altitude. All currents were essentially infinite east-west.

rocket passes through the current sheet. At 440 s, $\Delta H$ and $\Delta Z$ are considerably less than the Fort Yukon values in Figure 10. Rocket impact was about 70 km north of Fort Yukon, so they should be somewhat less. Again, extending the model eastward current farther north would increase $\Delta H$ and $\Delta Z$ at 440 s. Although the model could be improved, it is adequate to show the essential agreement between model, rocket, and ground observations. For example, addition of an induced subsurface current parallel to the electrojet would increase $\Delta H$ and decrease $\Delta Z$ of the model at ground level by as much as 50% but would have less effect on the fields along the upper rocket trajectory.

There is a substantial energy deposit in the auroral ionosphere over the segment traversed by the rocket. The power level by precipitating electrons over the arcs and by Joule heating of the northward current south of the arcs remains near 15 ergs/cm² s until the northern edge of the second aurora. This energy flux (15 ergs/cm² s = 0.015 W/m²) amounts to 1.5 MW for the segment, 1 km east-west and 100 km north-south, that the rocket flew over

Figure 12 summarizes the findings of this flight. The rocket entered the ionosphere at 60 s in a strong westward plasma flow and eastward electrojet (Hall current). The northward electric field, westward plasma flow, and eastward Hall current weakened over one auroral arc and terminated over a second, more intense auroral arc. Field-aligned currents were observed streaming out of the auroral arcs, providing continuity with northward ionospheric currents. The second arc appeared to be a very definite boundary to the plasma flow/current region in that all observed parameters were weak and erratic north of the arc. We are tempted to identify this region as the Harang discontinuity [*Maynard*, 1974; *Maynard et al.*, 1977]. There is no evidence for a westward electrojet, however, and the observations are, at 2100 MLT, a little far west for the Harang pattern. There is no clear evidence of a large-scale eastward plasma flow (southward electric field) in the rocket observations so it isn't clear the rocket entered the polar cap. The region north of the arc may be a local eddy in the plasma flow.

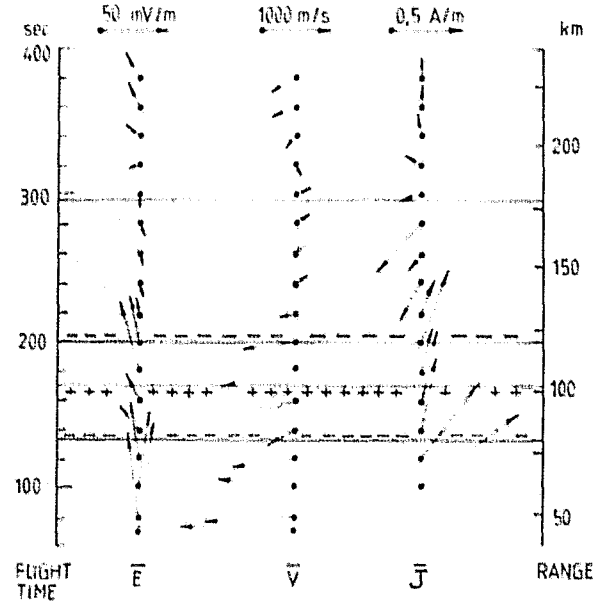


Fig. 12. Schematic view of the electric field vectors at 20-s intervals along the trajectory. E × B drift velocity (obtained by multiplying $E$ by 20 and rotating counterclockwise 90°) and calculated horizontal current are also shown. The scale at right shows the approximate horizontal range of the rocket.

The observations provide a strong confirmation of the earlier similar observations of *Maynard et al.* [1977] and *Evans et al.* [1977]. These two sets of observations provide a detailed description of the northern edge of the westward plasma flow/eastward electrojet/quiet arc region in the evening hours.

*Acknowledgments.* We acknowledge the assistance of Steve Werkema, John Lebens, and Wai Kwok Kwong with data processing and of John Humenansky with payload design and construction at the University of Minnesota. At the University of New Hampshire the efforts of Mark Widholm, Peter Lewis, and Ralph Varney are appreciated. The University of Minnesota was supported by NASA grants NGR24-005-253 and NSG-6005, and the University of New Hampshire by grants NGR30-002-054 and NSG-6013. A portion of this work at TRW was supported by NASA contract NASW-3087. We thank the College Observatory and World Data Center A for ground magnetograms. Laurence Cahill is grateful for the support of Gerhard Haerendel and the people at the Max Planck Institute for Extraterrestrial Physics where this report was completed. Finally, we wish to acknowledge the support given by Richard Vondrak and the Chatanika radar staff for this rocket flight. The Chatanika Incoherent Radar Facility is operated by the Stanford Research Institute and supported by the Defense Nuclear Agency (control number DNA001-74C-0167) and the National Science Foundation (grant DES72-01644-A02).

The Editor thanks H. Anderson and M. H. Rees for their assistance in evaluating this paper.

## REFERENCES

Armstrong, J. C., and A. J. Zmuda, Triaxial magnetic measurements of field-aligned currents at 800 km in the auroral region: Initial results, *J. Geophys. Res.*, *78*, 6802, 1973.

Arnoldy, R. L., and P. B. Lewis, Jr., Correlation of ground-based and topside photometric observations with auroral electron spectra measurements at rocket altitudes, *J. Geophys. Res.*, *82*, 5563, 1977.

Brekke, A., J. R. Doupnik, and P. M. Banks, A preliminary study of the neutral wind in the auroral *E* region, *J. Geophys. Res.*, *78*, 8235, 1973.

Cloutier, P. A., and H. R. Anderson, Observations of Birkeland currents, *Space Sci. Rev.*, *17*, 503, 1975.

Evans, D. S., N. C. Maynard, J. Trøim, T. Jacobsen, and A. Egeland, Auroral vector electric field and particle comparisons, 2, Electrodynamics of an arc, *J. Geophys. Res.*, *82*, 2235, 1977.

Jones, R. A., and M. H. Rees, Time-dependent studies of the aurora, 1, Ion density and composition, *Planet. Space Sci.*, *21*, 537, 1973.

Kamide, Y. F., and G. Rostoker, The spatial relationship of field-aligned currents and auroral electrojets to the distribution of nightside auroras, *J. Geophys. Res.*, *82*, 5589, 1977.

Kintner, P. M., L. J. Cahill, Jr., and R. L. Arnoldy, Current system in an auroral substorm, *J. Geophys. Res.*, *79*, 4326, 1974.

Maynard, N. C., Electric field measurements across the Harang discontinuity, *J. Geophys. Res.*, *79*, 4620, 1974.

Maynard, N. C., A. Bahnsen, P. Christopherson, A. Egeland, and R. Lundin, An example of anticorrelation of auroral particles and electric fields, *J. Geophys. Res.*, *78*, 3976, 1973.

Maynard, N. C., D. S. Evans, B. Maehlum, and A. Egeland, Auroral vector electric field and particle comparisons, 1, Premidnight convection topology, *J. Geophys. Res.*, *82*, 2227, 1977.

Potemra, T. A., Current systems in the earth's magnetosphere, *Rev. Geophys. Space Phys.*, *17*, 640, 1979.

Potter, W. E., Rocket measurements of auroral electric and magnetic fields, *J. Geophys. Res.*, *75*, 5415, 1970.

Rees, M. H., Auroral ionization and excitation by incident energetic electrons, *Planet. Space Sci.*, *11*, 1209, 1963.

Rees, M. H., and J. C. G. Walker, Ion and electron heating by auroral electric fields, *Ann. Geophys.*, *24*, 193, 1968.

Rees, M. H., A. I. Stewart, W. E. Sharp, P. B. Hays, R. A. Hoffman, L. H. Brace, J. P. Doering, and W. K. Peterson, Coordinated rocket and satellite measurements of an auroral event, 1, The satellite observations and analysis, *J. Geophys. Res.*, *82*, 2250, 1977.

(Received June 1, 1978;
revised March 17, 1980;
accepted March 18, 1980.)

# IONOSPHERIC ELECTRICAL CURRENTS IN THE LATE EVENING PLASMA FLOW REVERSAL

D. A. Behm,[1] F. Primdahl,[2] L. J. Zanetti, Jr.,[3,4]
R. L. Arnoldy,[3] and L. J. Cahill, Jr.[1]

Abstract. An instrumented sounding rocket was launched from Andøya, Norway, in January 1977, in the late evening auroral oval. Its trajectory took it northward over a quiet auroral arc and over a region of plasma flow reversal. Horizontal currents were inferred from magnetic field measurements; they were also calculated from the measured electric field and conductivities derived from energetic particle influxes. South of the reversal region the sheet current density of the eastward electrojet was found to be ∿0.1 A/m, while north of the reversal the current density was less than 0.05 A/m. The currents were enhanced in the arc. Current continuity considerations in the meridian plane implied downward field-aligned currents at the southern edge of the arc and upward field-aligned currents at the northern edge.

## Introduction

In January 1977 a sounding rocket, launched from Andøya, Norway, (69.3°N, 16.0°E geographic; 66.5°N invariant magnetic latitude) traversed a region, in the late evening auroral oval, where the plasma flow reversed from westward to eastward. Such plasma flow reversal, often called the Harang discontinuity, has been observed previously through barium ion drift, electric field observations, and radar Doppler measurements [Wescott et al., 1969; Maynard, 1974; Wedde et al., 1977]. In earlier reports on this rocket flight we described the precipitating electron flux and its relation to an auroral arc in the southern part of the flow reversal [Arnoldy, 1977] and the flow reversal itself as simultaneously observed by electric field double probes on the rocket and by the Stare (Scandinavian Twin Auroral Radar Experiment) radar [Cahill et al., 1978b]. In this report we describe horizontal ionospheric currents, flowing near the flow reversal, as inferred from ground and rocket magnetic observations and as calculated from derived ionospheric conductivities and the observed electric field.

## Instruments and Trajectory

The instrumentation, which included several magnetometers, electric field double probes, and curved plate electrostatic analyzers, has been described in earlier reports [Cahill et al., 1978b; Arnoldy and Lewis, 1977]. Two magnetometers were flown to detect the east-west component of the horizontal ionospheric currents. A proton precession magnetometer (PPM) provided total field magnitude measurements once each second with an accuracy, limited by vehicle noise, of ∿10 nanotesla (nT). A three-component flux gate magnetometer was also flown to supplement the PPM measurements and to evaluate the flux gate as a possible replacement for the PPM on future flights. Three perpendicular component measurements were sampled about 360 times each second with a resolution of 30 nT. Only the field magnitude, obtained by combining the three components, was used in this report. Both instruments were sensitive, as described below, to changes in the north-south and vertical field components observed as the rocket penetrated east-west current layers.

The magnetic fields produced by the horizontal current layers were of order 100 nT and horizontal (except near the layer edges), while the earth's field at Andøya was about 55,000 nT and only 12° from vertical. Magnetic north was 10° west of geographic north. An eastward (or westward) flowing horizontal current layer produced a northward (or southward) magnetic field (X) directly below the layer. Such a field made a contribution to the total field magnitude of X sin 12° (20.8 nT when X was 100 nT). This contribution changed sign as the rocket climbed to the topside of the current layer. A northward or southward flowing current layer produced an eastward or westward magnetic field also of order 100 nT but perpendicular to the earth's field. The total field magnitude increased in this case by only about 0.1 nT, an undetectable change.

The electric field double probes provided measurements of the north and east electric field components with an accuracy of ±5 mV/m [Cahill et al., 1978a]. Electron flux measurements, between a few electron volts and 22 keV, were available with energy resolution of 10% and a flux resolution of $10^5$ $(cm^2\ s\ sr\ keV)^{-1}$. With the use of multiple detectors, distribution functions were measured every 5 s of flight time [Arnoldy and Lewis, 1977].

The rocket was launched at 1918:06 UT (∿2200 MLT) on January 23, 1977. The flight lasted 470 s, reached 221-km peak altitude, and travelled 213 km downrange on geographic azimuth 345°. The spin rate was 3.9 Hz, and there was a precession of 3.24° half angle with period 58.55 s.

## Observations

A positive magnetic bay (40 nT) in the northward geographic component, an upward vertical component (20 nT), and almost zero disturbance in the eastward geographic component existed at launch, as shown in Figure 1, while a quiet auroral arc was visible in the north. Observers at the Stare radar reported a westward plasma flow over Andøya and an eastward flow about 100 km

[1]Space Science Center, University of Minnesota, Minneapolis, Minn. 55455.
[2]Danish Meteorological Institute, Copenhagen, Denmark.
[3]Space Science Center, University of New Hampshire, Durham, N.H. 03824.
[4]Now at Applied Physics Laboratory, Johns Hopkins University, Laurel, Md. 20810.



Paper number 9A0536.
0148-0227/79/009A-0536$01.00

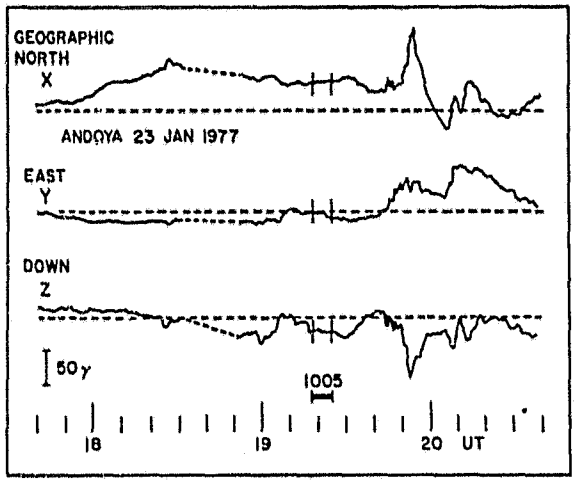


Fig. 1. Andøya magnetogram. X is the north, Y the east, and Z the vertical (down) component. The vertical lines indicate launch and reentry times. The dashed portion of each trace represents a time period when the trace was lost owing to interference.

further north; the conditions were right for flight over the Harang discontinuity [Cahill et al., 1978b].

The magnetic signature of penetration through an eastward electrojet is shown in Figure 2. The proton precession magnetometer record is shown on top and the flux gate record at the bottom. Similar reference fields have been subtracted in each case to emphasize the changes due to penetrating the current layers. Between 90 and 120 km on the upleg a sudden 50-nT decrease in $\Delta B$ was apparent in both records. There were several other smaller features ($\sim$10 nT) in each record, presumably not due to ambient magnetic field changes, since there were no correlations between the two records. Between 120 and 90 km on the downleg there was no field decrease that could be attributed to a possible westward electrojet current layer. The 50-nT change in $\Delta B$ corresponded to a 50/sin 12° = 240 nT change in the X component. For an infinite current sheet, one half of this, 120 nT, would be observed on the ground below. The $\Delta X$ = 240 nT change in the horizontal component through the current layer corresponded to a sheet current strength of $\Delta X/\mu_0 \sim 0.19$ A/m.

The electric field measurements, shown as the top panel of Figure 3, have been reported by Cahill et al. [1978b]; a brief review follows. South of the auroral arc a strong northward electric field produced a westward plasma flow and an eastward (Hall current) electrojet. The field decreased over the arc, decreased again north of the arc, and rotated through an eastward direction (northward plasma flow). Recovering north of this, the field rotated to the south (eastward plasma flow). A sudden increase to over 50 mV/m at 300 s was followed by a direction shift to southeast, an oscillation with 6-s period, and a gradual decrease in magnitude. An eastward electric field (northward plasma flow) is not normally associated with plasma flow reversal in the Harang discontinuity. It is possible that the weak eastward field is a transient feature associated with counterclockwise flow around an auroral loop observed east of the trajectory [Cahill et al., 1978b].

Electron measurements on this flight have also been reported earlier [Arnoldy, 1977]. Briefly, as is shown in Figure 4, there were intense, $10^9$ $(cm^2\ s\ sr\ keV)^{-1}$, electron fluxes with energies of a few hundred electron volts over and near the arc (130-160 s), in the plasma flow reversal region (200-210 s) and in the eastward plasma flow region (250-280 s). Electrons of keV energies were observed only directly over the arc. The electric field magnitude, inverted, is also shown. Note that the field is low when the 0.3-keV flux is high.

## Calculations

The east $J_E$ and north $J_N$ components of the horizontal vertically integrated current density were calculated [Anderson and Vondrak, 1975; Evans et al., 1977; Cahill et al., 1978a]. The electron flux and energy spectrum were used, with models of the ionosphere, to calculate electron densities [Rees, 1963]. Height-integrated Hall and Pedersen conductivities, shown in Figure 3, were obtained from the electron densities and model collision frequencies. In turn, the conductivities and measured north and east electric field components $E_N$ and $E_E$ yielded north and east ionospheric current components $J_N$ and $J_E$.

The height-integrated conductivities were about 2 siemens (S) (1 S = 1 mho) in the westward plasma flow region, south of the auroral arc. The Hall conductivity increased to 20 S over the arc, while the Pedersen conductivity went to 32 S. North of the arc the calculated conductivities remained below 2 S. Since the northward electric field was high in the strong westward plasma flow south of the arc, there was a moderate calculated current density there, $\sim$0.1 A/m for the eastward component and $\sim$0.05 A/m for the northward component. The current densities increased dramatically in the auroral arc, to $\sim$0.5 A/m east and $\sim$0.4 A/m north. North of the arc, including the

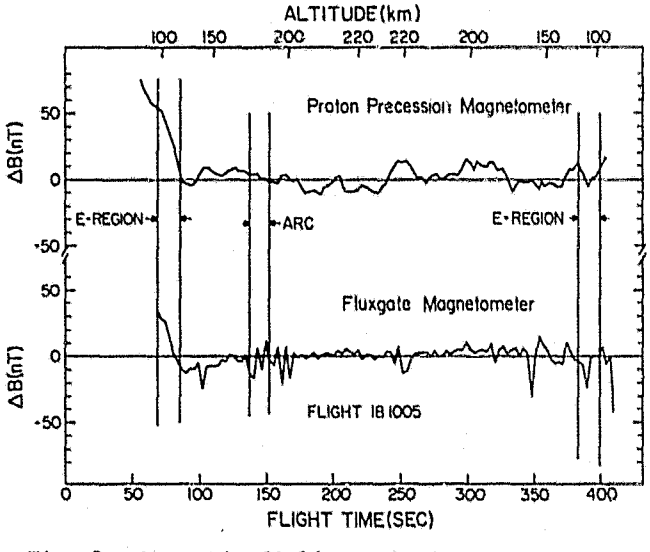


Fig. 2. Magnetic field magnitude measurements. Reference fields have been subtracted from the measured fields. The zero levels are arbitary.

strong eastward plasma flow from 240 to 300 s, the calculated current density components were less than 0.05 A/m.

The Joule power dissipation by horizontal ionospheric current flowing in the direction of $\vec{E}$ was also calculated [Evans et al., 1977]. The Joule power density is compared, in Figure 3, with the power deposited in the same column of the ionosphere by precipitating electrons. The Joule power was ∿3 mW/m$^2$ column (1 mW/m$^2$ = 1 erg/cm$^2$ s) in the eastward electrojet south of the arc, principally due to the northward current component. Over the arc the Joule dissipation increased to ∿8 mW/m$^2$ column, while north of the arc the power was less than 1 mW/m$^2$ column. The precipitating electron power was less than 1 mW/m$^2$, except over the arc, where it rose to 7 mW/m$^2$.

## Discussion

We have two measurements of the magnetic field due to the eastward electrojet current. The northward component at Andøya is 40 nT and the northward component just below the current layer is 120 nT. For a very broad current sheet the full 120 nT should be seen at ground level. The section of the eastward electrojet penetrated by the rocket must therefore be of limited width from north to south. At Andøya the vertical component is -20 nT, indicating that the center of the eastward electrojet is south of Andøya.

An east-west band current of 0.19-A/m strength (inferred from the rocket measurements) approximately 150 km south of the launch site would explain the 40-nT horizontal disturbance and the -20 nT vertical disturbance observed at the ground. The height-integrated current density derived from the rocket magnetometer measurement is 0.19 A/m, while the eastward current density calculated in the eastward electrojet, 20 km south of the arc but 25 km north of the rocket electrojet penetration, is ∿0.1 A/m. The calculated current is about half that derived from the magnetometer measurements. This may be due to variations in current density at the two different locations but may also be caused by uncertainties in the modeling procedures used to calculate the current. Considering the uncertainties in various models used, we estimate the possible error in the conductivities to be less than ±50%. Since the errors in the electric field are smaller, the calculated currents may also be in error by as much as ±50%.

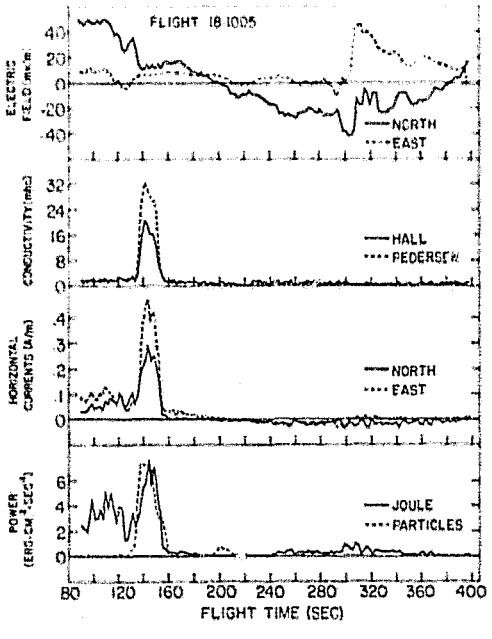


Fig. 3. Measured electric field, calculated conductivities, calculated horizontal currents, and power dissipated by electrons and by Joule heating. The electric field and horizontal current components are given with reference to magnetic north and east. The arc is located between 137 and 152 s.

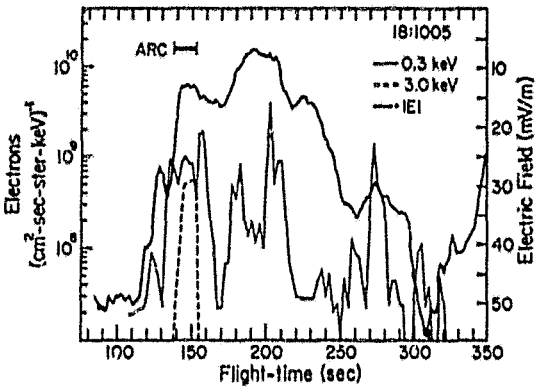


Fig 4. Electron directional intensities at 0.3 and 3.0 keV. The higher energy electrons are seen only over the arc (137 to 152 s). The electric field magnitude is shown with inverted scale at right.

The currents were calculated on the assumption that the neutral winds were negligible. No neutral wind measurements were available during the flight; however, observed neutral winds in the auroral zone during geomagnetically quiet or moderately disturbed times (Kp ≤ 3) have been found by Brekke et al. [1973] to be generally less than or of the order of 100 m/s. Neutral winds of this magnitude, if they were present, would add an effective electric field vector to the observed electric field vector of no more than 5 mV/m. The effects of neutral winds on the calculated currents would be small except in the reversal region, where the measured electric field is small.

The lack of a westward electrojet as observed by the magnetometers on the downward leg agrees with the calculations. A very weak, 0.02-0.04 A/m, calculated westward component is present below the rocket from 250 to 300 s. With the electric field direction change to southeast the calculated currents become southward, 0.02 to 0.04 A/m.

The electric fields, corresponding plasma flow velocities, and calculated horizontal current vectors are shown in a summary view in Figure 5. The weakening of the electric field and of the plasma velocity over the arc is apparent as well as the reversal of the flow velocity north of the arc. The largest current densities, over 0.5 A/m to the northeast, are associated with the arc. Unlike earlier flights over quiet arcs, in this

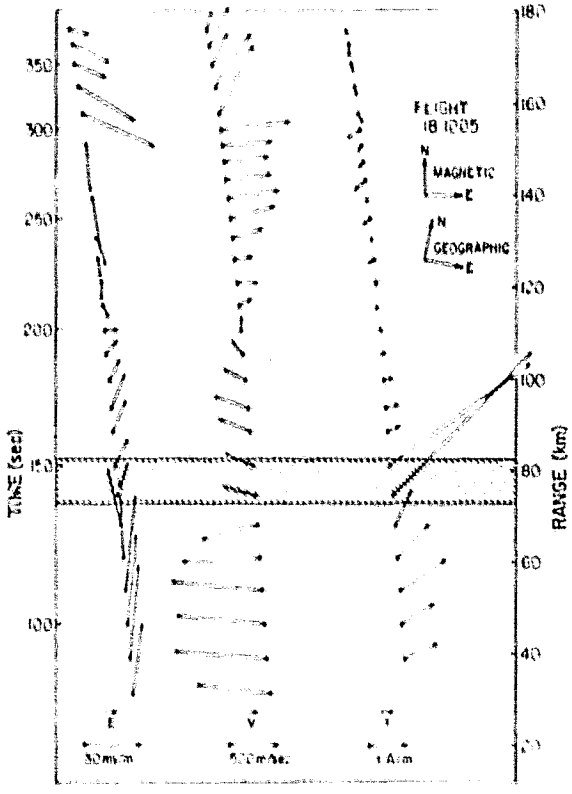


Fig. 5. Summary plot of electric field, plasma convection velocity, and calculated horizontal currents. The shaded region denotes the location of the arc. The trajectory has been projected to 110 km; therefore the time scale on the left is not linear. Scales for the three quantities are given at the bottom.

case the calculated eastward electrojet current is intensified in the arc [Evans et al., 1977; Cahill et al., 1978a]. This is principally because the conductivities increase by a factor of 10 over this arc but only by a factor of 3 or 4 over the earlier arcs.

The total current in the arc is about 4 kA, and the payload flies by it at a distance of about 25 km. The peak magnetic disturbance in the total field at the rocket is then expected to be of the order of 30 nT, which should be detectable by the on-board magnetometers. However, the disturbance increases and decreases gradually over a substantial part of the trajectory, so with the modeling technique used in reducing the magnetometer data the disturbance may not be discernable. The lack of evidence of the line current in the magnetometer measurements could, of course, also be due to errors in the ionospheric modeling procedure leading to a calculated arc current that is too large. As was estimated earlier, the errors may be as large as ±50%.

The electric field was almost constant during the first part of the flight from 83 to 116 s, directed ∿6° west of geographic north. During this time interval the Andøya horizontal magnetic perturbation was also constant and directed toward ∿4° west of geographic north or, within the measurement uncertainties, parallel to the dc electric field. With calculated height-integrated Hall and Pedersen conductivities of ∿1 S in this region the northward Pedersen current should have rotated the horizontal magnetic disturbance 45° to the west. The missing Pedersen current magnetic field component at ground level confirms Vasyliunas' [1970] suggestion that the magnetic fields from the field-aligned currents and the Pedersen currents are confined in regions above the ionosphere. The northward current must be part of a solenoidal current system where current flows down in a field-aligned east-west sheet, then north horizontally, then up in a field-aligned sheet.

Homogeneity along the auroral arc (east-west) being assumed, changes in the northward current density imply field-aligned currents in order to satisfy current continuity [Evans et al., 1977; Cahill et al., 1978a]. The increase from 0.03 A/m at 90 s to 1.0 A/m at 120 s indicates a downward field-aligned current sheet 20-km thick, with an integrated current density of 0.07 A/m. In similar fashion a 0.2-A/m downward sheet is implied in the southern part of the arc, and a 0.3-A/m upward sheet in the northern part.

We are completing a study of field-aligned currents measured by several techniques during this flight: net electron fluxes (from a few eV to 22 keV); ion drift measurement and measurements of changes in the east-west magnetic component when passing through possible field-aligned current sheets. There appear to be some discrepancies between the field-aligned currents measured by the several techniques and between the measured currents and the currents inferred, as above, from the calculated northward current density. A more thorough evaluation of the field-aligned currents will be presented later.

Acknowledgment. The Editor thanks J. R. Burrows for his assistance in evaluating this brief report.

## References

Anderson, H. R., and R. P. Vondrak, Observations of Birkeland currents at auroral latitudes, Rev. Geophys. Space Phys., 13, 243, 1975.

Arnoldy, R. L., The relationship between field-aligned current, carried by suprathermal electrons, and the auroral arc, Geophys. Res. Lett., 4, 407, 1977.

Arnoldy, R. L. and P. B. Lewis, Jr., Correlation of ground-based and topside photometric observations with auroral electron spectra measurements at rocket altitudes, J. Geophys. Res., 82, 5563, 1977.

Brekke, A., J. R. Doupnik, and P. M. Banks, A preliminary study of the neutral wind in the auroral E region, J. Geophys. Res., 78, 8235, 1973.

Cahill, L. J., Jr., R. L. Arnoldy, and W. W. L. Taylor, Rocket observations at the edge of the eastward electrojet, submitted to J. Geophys. Res., 1978a.

Cahill, L. J., Jr., R. A. Greenwald, and E. Nielsen, Auroral radar and rocket double-probe observations of the electric field across the Harang discontinuity, Geophys. Res. Lett., 5, 687, 1978b.

Evans, D. S., N. C. Maynard, J. Trøim, T. Jacobsen, and A. Egeland, Auroral vector electric

field and particle comparisons, 2, Electrodynamics of an arc, J. Geophys. Res., 82, 2235, 1977.
Maynard, N. C., Electric field measurements across the Harang discontinuity, J. Geophys. Res., 79, 4620, 1974.
Rees, M. H., Auroral ionization and excitation by incident energetic electrons, Planet. Space Sci., 11, 1209, 1963.
Vasyliunas, V. M., Mathematical models of magnetospheric convection and its coupling to the ionosphere, in Particles and Fields in the Magnetosphere, edited by B. M. McCormac, pp. 60-71, D. Reidel, Hingham, Mass., 1970.
Wedde, T., J. R. Doupnik, and P. M. Banks, Chatanika observations of the latitudinal structure of electric fields and particle precipitation on November 21, 1975, J. Geophys. Res., 82, 2743, 1977.
Wescott, E. M., J. D. Stolarik, and J. P. Heppner, Electric fields in the vicinity of auroral forms from motions of barium vapor releases, J. Geophys. Res., 74, 3469, 1969.

(Received January 15, 1979;
accepted March 21, 1979.)

# COMPARATIVE ROCKET OBSERVATIONS OF IONOSPHERIC ELECTRIC FIELDS IN THE AURORAL OVAL

L. J. ZANETTI, JR.[1,2], R. L. ARNOLDY[1], L. J. CAHILL, JR.[3], D. A. BEHM[3], and R. A. GREENWALD[4,2]

(Received 3 December, 1979)

**Abstract.** The ion drift technique of measuring ionospheric electric fields is compared to two other simultaneous measurements. Rocket measurements in the evening auroral oval are checked against a dual probe, also in situ, and the ground based STARE auroral radar. The technique is explained thoroughly as well as tested for its dependence on mass.

Two evening auroral oval conditions were observed from Andoya, Norway in January and February 1977. The first flight, 18:1005, measured electric fields over a quiet pre-midnight discrete arc. An interesting plasma convection reversal was observed poleward of the arc. The subsequent flight, 18:1004, samples a breal up phase aurora nearer local midnight.

## 1. Introduction

The intent of this paper is to compare the ionospheric electric field inferred from rocket in situ ion drift measurements with those obtained from dual probe observations made aboard the same rocket and simultaneous ground-based auroral radar soundings during two auroral flights. Such a comparison is necessary to give confidence to the technique of obtaining ion drift, hence electric fields, from measurements of the ion distribution function in the ionosphere. Hanson and Heelis [1] have reported difficulty in making ion velocity measurements with "various kinds of sensors" flown on sounding rockets. Moreover, the first reported use of directional intensity ion measurements from 0 to 5 eV by Whalen *et al.* [2] to obtain drift velocities aboard a sounding rocket flown into an aurora gave unprecedented large transverse electric fields (100–200 mV/m) and strong flow along the magnetic field (~2 km/s).

Multiple electrostatic analyzers detecting ions from 0 to 5 eV/charge are used to measure the thermal ion distribution in energy and space. The ion flow velocity relative to the sensors is obtained by fitting the data to a shifted (due to vehicle potential)-drifting Maxwellian. This technique requires knowledge of the ion mass. One of the analyzers flown on each of the two auroral flights to be discussed in

[1] *Space Science Center, University of New Hampshire, Durham, New Hampshire 03824, U.S.A.*
[2] Now at: *Applied Physics Laboratory, The Johns Hopkins University, Laurel, Maryland 20810, U.S.A.*
[3] *Space Science Center, University of Minnesota, Minneapolis, Minnesota 55455, U.S.A.*
[4] *Max-Planck Institute for Aeronomy, D-3411 Katlenburg-Lindau 3, West Germany.*

*Space Science Instrumentation* 5 (1980) 183–196. 0377–7936/80/0052–0183 $02.10.

this paper was capable of measuring the relative ion abundance of masses 16 ± 2 AMU and 30 ± 3 AMU. The sensitivity of the technique to the ion mass is assessed using these measurements.

A crude test of the ion drift technique has already been reported by Morgan and Arnoldy [3] where data from one detector were used to obtain a distribution function over the duration of the Echo III rocket flight. The inferred electric field compared favorably with simultaneous Chatanika radar observations. This flight was not during an auroral display, therefore, the long period (200 seconds) of data collection to obtain the ion distribution was acceptable. However, since the density dependence on altitude as measured by the ground radar was input into the fit routine, the in situ observations were not totally independent.

Finally, a comparison of the rocket dual probe measurements and the ground auroral radar for one of the flights to be discussed has already been made [4]. Very good general agreement was obtained when the electric field was greater than 20 mV/m, the apparent threshold of the radar technique. A description of the dual probe experiment aboard the rockets and the auroral radar technique has been discussed in the report by Cahill *et al.* [4], hence will not be repeated here.

## 2. Ion Drift Instrumentation

The detection of the drift of ions was accomplished by multiple electrostatic analyzers. These analyzers had 90° cylindrical electrodes ($R = 2$ cm, $\Delta R = 2$ mm) and employed Galileo Model 4025 Channeltron electron multipliers as sensors. Ion spectra from 0 → 5 eV in 32 energy steps were measured every 25.6 ms with an energy resolution of 8%. The acceptance cone of the analyzers was 2° × 7° full angle, larger than the ~ 1.5° angular rotation of the spinning rocket per energy step. Two analyzers were flown, one viewing up the field at 30° with respect to the spin axis of the rocket and the other at 90°. The analyzer design was similar to those flown aboard the Echo III flight [3].

A third analyzer was flown, viewing also at 90° with respect to the rocket spin axis, to measure ion masses of 16 ± 2 AMU and 30 ± 3 AMU. This instrument used the above described analyzer for energy selection with a low-resolution magnetic mass spectometer added between the electrostatic analysis and the channeltron detector [5]. The mass spectrometer consisted of a permanent magnet and post-accelerator. The 16 and 30 AMU mass separation was achieved by post-accelerating the 0–5 eV ions selected by the electrostatic analyzer by the proper amount (153 volts for 16 AMU and 84 volts for 30 AMU) in order to be detected after 90° deflection in the magnetic field by the channeltron sensor. The post-accelerator was set to pass $O^+$ (16 AMU) 90% of the time and 30 AMU masses (predominantly $NO^+$ at rocket altitudes of 200–250 km) the remaining time. The mass resolution of the instrument was 20%, sufficient to separate the two mass groups.

The geometric factor for the three detectors was obtained by laboratory calibration

using a simulated omnidirectional ion beam [5,6]. The electrostatic analyzer had a geometric factor of $9.6 \times 10^{-6}$ cm$^2$ sr eV/eV and the mass analyzer detector was somewhat smaller at $4.7 \times 10^{-6}$ cm$^2$ sr eV/eV.

## 3. Data Reduction

The primary objective of the data reduction was to determine the bulk flow velocity vector. Additional results include ion temperature, ion density and rocket potential. Each data point was assigned a vector direction ($\theta$, $\phi$) in geomagnetic coordinates ($\hat{Z}$ along $\boldsymbol{B}$) and an energy (0–5 eV). Data points were accumulated for two seconds to give adequate representation of the ion distribution. An iterative least-squares fitting routine was applied to this collection, resulting in the energy distribution function parameters of the observed data. Before discussing the fit routine further we would like first to discuss two presentations of the raw data which have proven valuable to help visualize some of the plasma parameters obtained by the fit analysis.

The measured energy spectra are a function of six independent variables: energy, particle pitch angle and azimuth, and the three components of the rocket ram velocity. The parameters needed to determine the electric fields are the magnitude and direction of the $\boldsymbol{E} \times \boldsymbol{B}$ drift vector. The magnitude of this velocity (translated to energy) is nearly impossible to observe in the raw data since the dominant contribution to the energy peak of the ion spectra is due to the drop through the −1.5 V rocket potential. The energy contribution due to the $\boldsymbol{E} \times \boldsymbol{B}$ drift is only about a quarter of an eV. The energy contribution due to the rocket ram velocity is also approximately a quarter of an eV. The direction of relative velocity between the rocket and plasma ($\boldsymbol{E} \times \boldsymbol{B}$ drift plus ram) can, however, be readily viewed in the raw data using a three-dimensional mapping program plotting detector counts vs. ion pitch angle

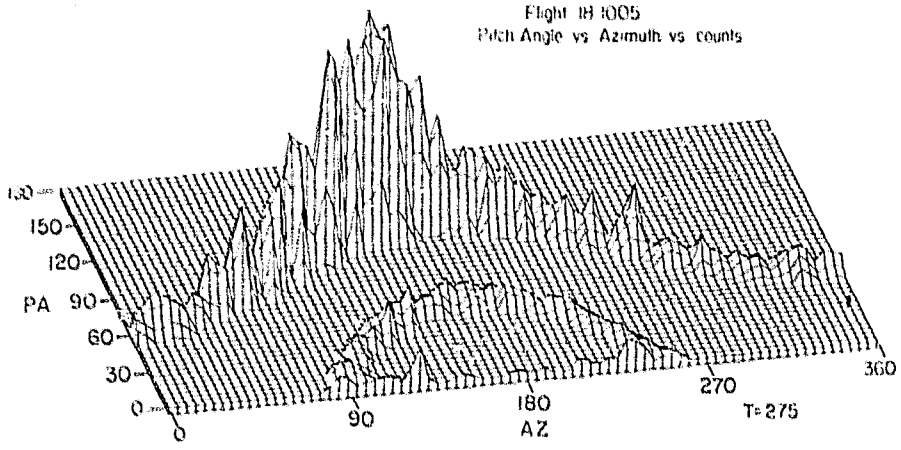


Fig. 1. Example of data display (Flight 18:1005, time 275 seconds) of thermal ion flow velocity relative to rocket. Axes are pitch angle and azimuth, vertical is analyzer response in counts integrated over energy.

vs. ion azimuth (Figure 1). In this figure the dimension front to rear is linear in pitch angle, 0° → 180°. Azimuth is plotted from left to right, 0° → 360°, measured from north through east. The vertical axis is average counts integrated over energy. Essentially what is displayed is the velocity directions observable by the 30° and 90° electrostatic analyzers. Thus the flow direction can be visually located by a peak and compared with the answers obtained by the multiparameter Maxwellian fit to the data. The data shown in Figure 1 were taken on the downleg of flight 18:1005 at a flight time of 275 seconds. As will be shown later, the least-squares fit predicted this time to have a generally southward electric field. This field results in an eastward $\boldsymbol{E} \times \boldsymbol{B}$ drift. Since the rocket ram is included in Figure 1 it must be subtracted. The ram at 275 seconds was south as the rocket was first nearly straight north. The result is an eastward flow combined with a comparably equal south ram velocity or a southeast peak (~ 135° azimuth). This can be seen in Figure 1. These plots are therefore most useful for locating the azimuth of the flow. The limited pitch-angle coverage for two detectors is evident in the figure.

The same plotting package was used to plot detector counts vs. energy vs. pitch angle (Figure 2). In this figure are plotted a series of energy spectra ranging in pitch angle. Consider the energy dimension as a radius arm originating at the center back. From this point along the back to the left is 0° pitch angle. The radius arm pivots about its origin in a right-hand sense with increasing pitch angle. A radius arm starting at center back pointing right would be antiparallel to $\boldsymbol{B}$ or 180° pitch angle. The vertical axis is again counts averaged over azimuth. This plot shows the spectral shift in energy due to the vehicle potential. It also shows that the flow is mostly perpendicular to $\boldsymbol{B}$, in which case the peak flux would occur at 90°, with ram velocity contributing a component greater than 90° pitch angle for this flight time of 275 seconds. Figure 2 is especially useful for detecting noise in the energy

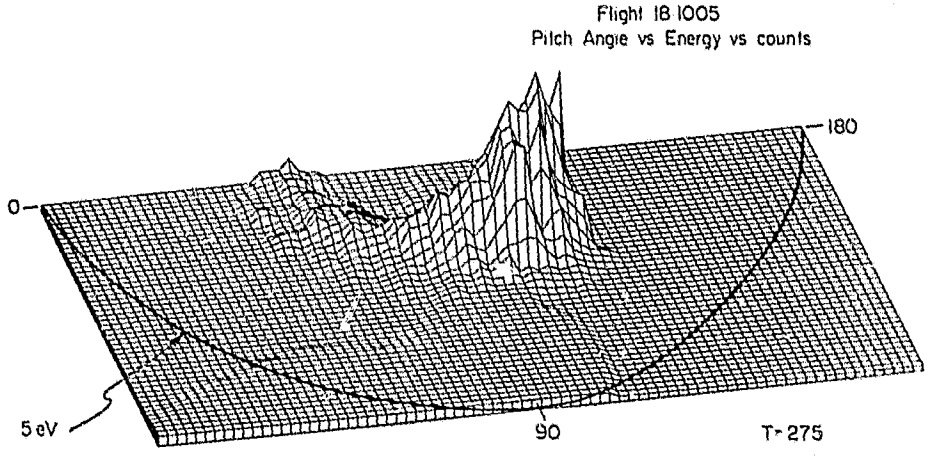


Fig. 2. Similar to Figure 1, showing pitch angle and energy in polar coordinates. A radius arm length starting at the rear center indicates 0–4.5 eV ion energy and its angle from the left rear corner (labelled 0°) is the pitch angle. Vertical is analyzer response in counts. The base line semicircle is 4.5 eV.

sweep. Figures like 1 and 2 have proved invaluable for initial analysis and parameter confidence.

Progressing now to the fit routine, the original thermal ion velocity distribution is assumed to be Maxwellian:

$$f(v') = n\left(\frac{m}{2\pi kT}\right)^{3/2} \exp\left[-\left(\frac{v'^2}{v^2_{th}}\right)\right], \tag{1}$$

where the prime indicates that the independent variable is outside the rocket Debye sheath. The differential directional intensity $J(E')$ is related to the velocity distribution according to:

$$J(E') = \frac{2E'}{m^2} f(v') \left[\frac{\text{particles}}{\text{s cm}^2 \text{ sr eV}}\right]. \tag{2}$$

In passing through the rocket sheath, the unperturbed Maxwellian is shifted according to Liouville's theorem:

$$J(E)/E = J(E')/E'. \tag{3}$$

Finally, including a relative velocity between the rocket frame and the plasma, the final distribution recorded by the detector becomes:

$$J(E) = \frac{2n}{m^2}\left(\frac{m}{2\pi kT}\right)^{3/2} E \exp\left\{-\left[\frac{([2(E-U)/m]^{1/2}\hat{v} - v_0 - v_r)^2}{2kT/m}\right]\right\}$$

$$= \frac{\text{counts}}{G_0 \Delta t E} \tag{4}$$

where $G_0$ = geometry factor = $9.6 \times 10^{-6}$ (cm$^2$ster eV/eV) energy analyzer or $4.7 \times 10^{-6}$ (cm$^2$ster eV/eV) energy mass analyzer, $E$ = selection energy (eV), $\Delta t$ = accumulation time = $8 \times 10^{-4}$ (s), $n$ = density (cm$^{-3}$), $m$ = mass (g), $T$ = temperature (K), $U$ = energy due to rocket potential (eV), $\hat{v}$ = particle direction, $v_r$ = rocket ram velocity (cm/s), $v_0$ = drift velocity (cm/s).

The data are fit to the above function by iteratively adjusting the six parameters (3 components of $v_0$, $T$, $U$, and $n$) and finding the minimum of the least-squares function [7]. Two seconds of data were used for each computation representing blocks of data taken over 78 spectral sweeps or ~2500 data points accumulated over 10 spins of the rocket. A typical pitch-angle vs. azimuth coverage by the two electrostatic analyzers per spin can be seen in Figure 1. Pitch angles greater than 130° were not sampled. A 7° coning angle of the rocket slightly extended the data coverage over pitch angle during the two seconds of accumulation.

The mass of the ions detected is a parameter in Equation (4). The third detector, capable of measuring ion spectra for masses 16 and 30 obtained the ratio of these masses at various altitudes. Figure 3 gives the measured ratio of the number of 30 AMU ions to the total number of ions as a function of flight time and altitude for Flight 18:1005. The rocket was over an 8 kR (3914 Å) arc from 140 to 155 seconds.

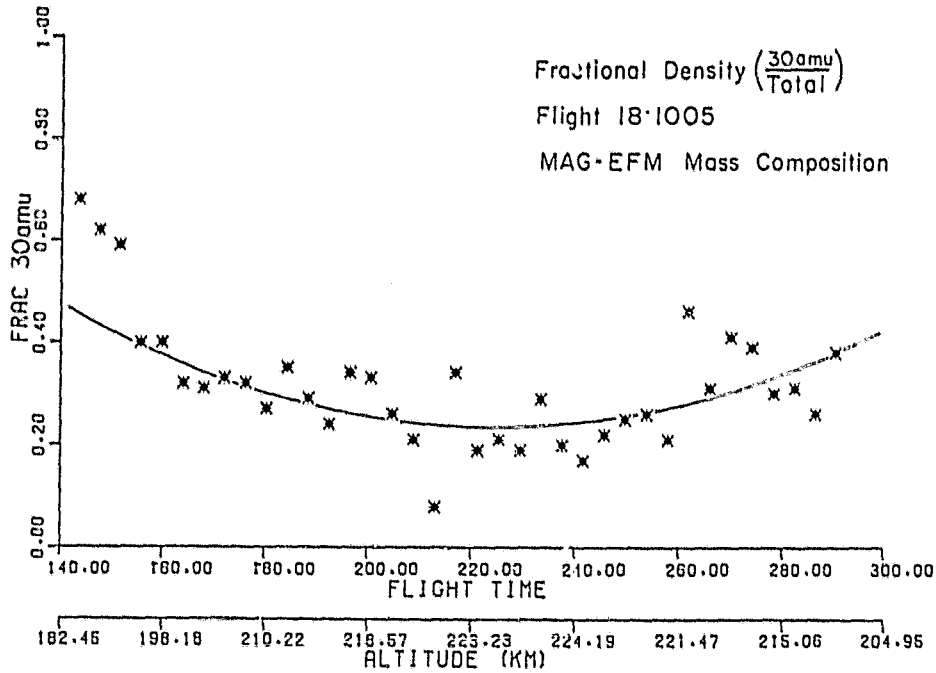


Fig. 3. Measured ratio of 30 AMU ions to total as a function of time (altitude).

Beyond 155 seconds there was no further auroral luminosity, although electrons less than 300 eV with directional intensities exceeding $10^8$ (cm$^2$s sr keV)$^{-1}$ were measured until 280 seconds flight time. The factor of two decrease and subsequent increase appears to be an altitude dependence and is roughly consistent with the altitude dependence of 30 ± 3 AMU ions given by Bauer [8].

Two different fitting routines were used with the data from Flight 18:1005; one assumed that the mass in Equation (4) was $O^+_{16}$ and the other fit the data to a Maxwellian for 16 AMU mass plus a Maxwellian for 30 AMU mass using the measured composition ratio. Table I is a compilation of fit parameters using the

TABLE I
Fit parameters for two fitting routines using data from Flight 18:1005.

| Method | | AMU 30 = 0.35 total | | ALL $O^+$ | |
|---|---|---|---|---|---|
| $v_{ON}$ | (m/s) north | −256 | ± 60 | −289 | ± 64 |
| $v_{OE}$ | (m/s) east | 825 | ± 34 | 919 | ± 34 |
| $v_{O\parallel}$ | (m/s) along $B$ | −257 | ± 66 | −361 | ± 86 |
| Temp | [K] | 1520 | ± 66 | 1670 | ± 72 |
| $U$ | (volts) | 1.72 | ± 0.004 | 1.72 | ± 0.006 |
| $n$ | (m$^{-3}$) | $3.20 \times 10^3$ | ± 800 | $3.07 \times 10^3$ | ± 200 |

two methods for one interval of data. These data were acquired at about 280 seconds flight time at an altitude of 215 km.

Generally there is about a 10–15% discrepancy between the two methods, which is comparable to the error in the parameters. The conclusion is that mass analysis is not essential to the determination of electric fields by this technique in that the accuracy of the spectral measurements cannot resolve the effect of an admixture of mass 16 and 30 ions.

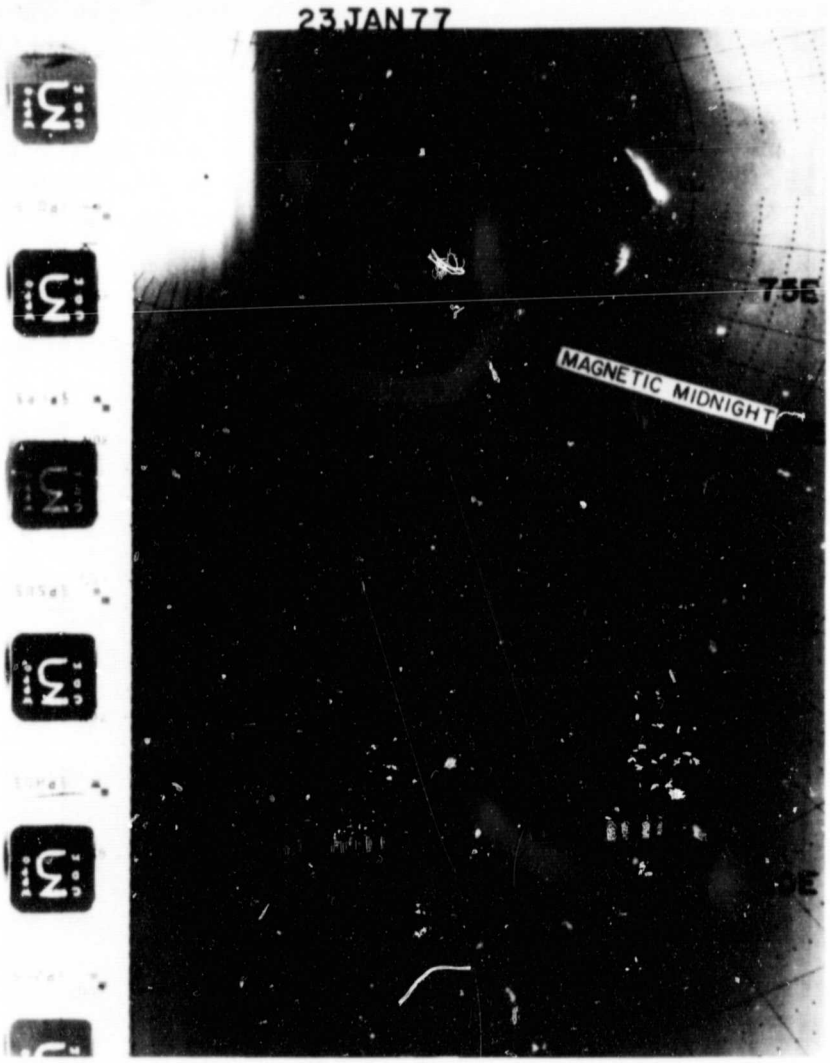


Fig. 4. DMSP photograph, courtesy of Fredrick Rich, Regis College Research Center and Air Force Geophysics Lab taken at about eight minutes after Flight 18:1005. Discrete trajectory is indicated.

## 4. Data Presentation

The object of both flights was to use the high spatial and temporal resolution of rocket techniques to study the premidnight auroral oval environment. In order to make the observation more complete, the two launches were at different magnetic local times, 2118 and 2250.

### *Flight 18:1005*

This flight was launched over a classic premidnight discrete arc. The arc was stable and of wide longitudinal extent shown by the DMSP photograph of Figure 4 taken approximately 8 minutes after the flight. The 'inverted V' in the measured electron spectrogram of Figure 5 locates the arc between 135–155 seconds flight time. The 3914 Å light emission by this arc as measured by onboard photometers and from the ground was about 8 kR. The arc was in the region of an enhancement of the eastward electrojet current, as calculated using conductivity derived from electron flux measurements and the measured electric field [4,9].

Figure 6 gives the simultaneous measurement of $\boldsymbol{E}$ perpendicular to the magnetic field by the ion drift experiment and the dual probe experiment of the University of Minnesota. Figure 7 is the comparison of the dual probe with the STARE ground-

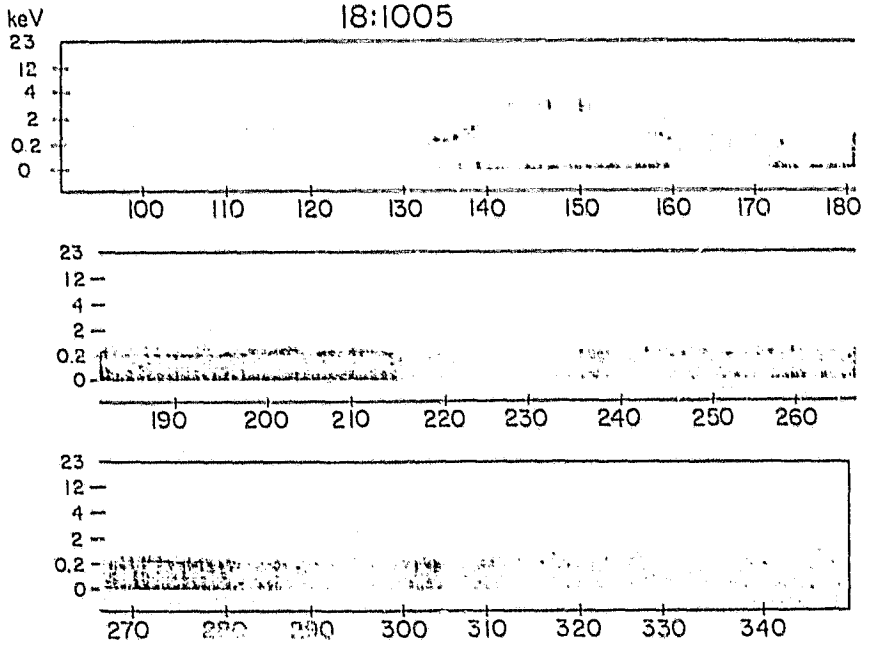


Fig. 5. Suprathermal [illegible] energy-time spectrogram for Flight 18:1005. Rocket arc [illegible] 140–155 seconds flight time.

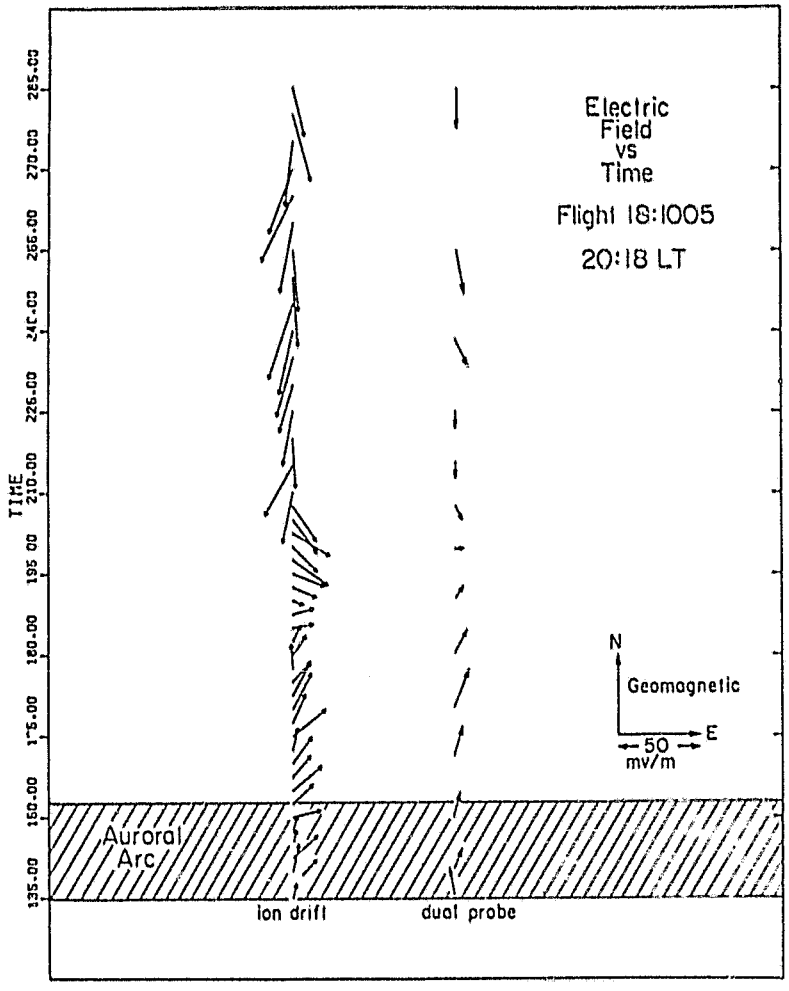


Fig. 6. Perpendicular electric field vector as a function of flight time for the ion drift measurements and the University of Minnesota dual probe during Flight 18:1005.

based radar electric field reported earlier [4]. General agreement can be seen between the three methods, particularly in direction. There is a systematic discrepancy in electric field magnitude between the ion drift method and both the dual probe and STARE measurements. This may be remedied with better pitch angle coverage of the distribution function. (Statistical error in the velocity vector by the ion drift method was about 28%. This would account for the general disagreement in magnitude between the dual probe and ion detector measurements of Figure 6.) Beyond 290 seconds, the count rate of the ion detectors becomes very low due to the change in ram direction during the downleg of the trajectory. Since this was the time when the auroral particle precipitation decreased (Figure 5) the ion density was reduced.

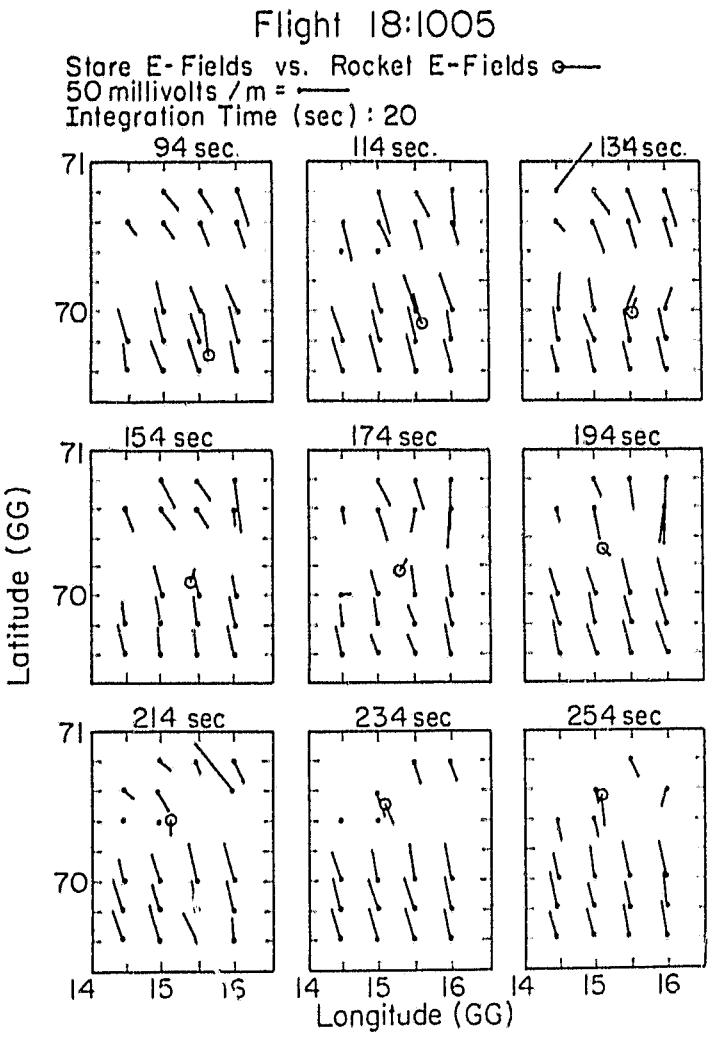


Fig. 7. From Cahill *et al.* [4], comparisons of electric field measurements (Flight 18:1005) by the dual probe and the ground based STARE radar. The STARE *E* field vectors have solid points while the rocket data point in each frame has an open point. Flight time indicated is the time at the beginning of the STARE integration period.

The STARE radar signals dropped to a low signal-to-noise ratio at *E*-region altitudes conjugate to the rocket at this time as well.

Geophysically, a significant event in these data was the flow reversal at about 200 seconds. The electric field reversed from generally poleward across the arc and up to the boundary at 200 seconds to equatorward after 200 seconds. The poleward field was about 25 mV/m while north of the boundary a larger southward field was observed. Note that the STARE observations indicate the reversal to be a spatial structure. These observations are consistent with the transition from sunward to

antisunward plasma convection measured by polar-orbiting satellites [10,11] at the edge of the polar cap.

*Flight 18:1004*

This flight was launched closer to midnight and during the breakup phase of aurora. Although there was strong westward electrojet activity during the flight, the auroral display had faded to very low levels as the rocket was near the top of its trajectory. As might be expected, the aurora became very brilliant after the rocket flight, reaching intensities as high as 50 kR in 5577 Å. The onboard 5577 Å photometer recorded patches of aurora not exceeding 2 kR during the flight.

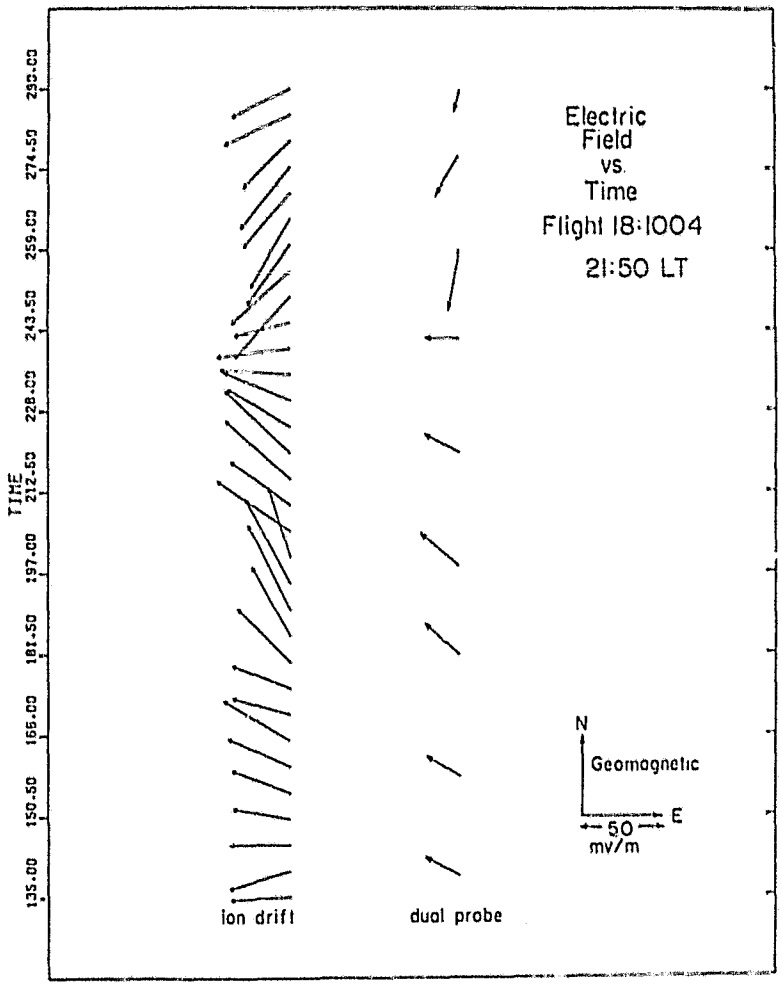


Fig. 8. Comparisons for Flight 18:1004 of the electric field vector as measured by the ion drift detector and the dual probe instrument.

The comparison of electric field inferred from the ion detectors with the dual-probe results is given in Figure 8. Again, the magnitude of the field from the ion-drift detector is larger than that obtained by the dual probes but the directions are in good agreement near the middle of the flight. There is a systematic discrepancy in direction between the ion drift and dual probe measurements at the end of the flight. The STARE measurements during the flight along with the dual-probe data are given in Figure 9. At this time, the rocket trajectory and the STARE radar were not co-located. The westward boundary of the radar field of view is indicated in Figure 9. The measurements to the east of the rocket trajectory support the in-flight electric field measurements.

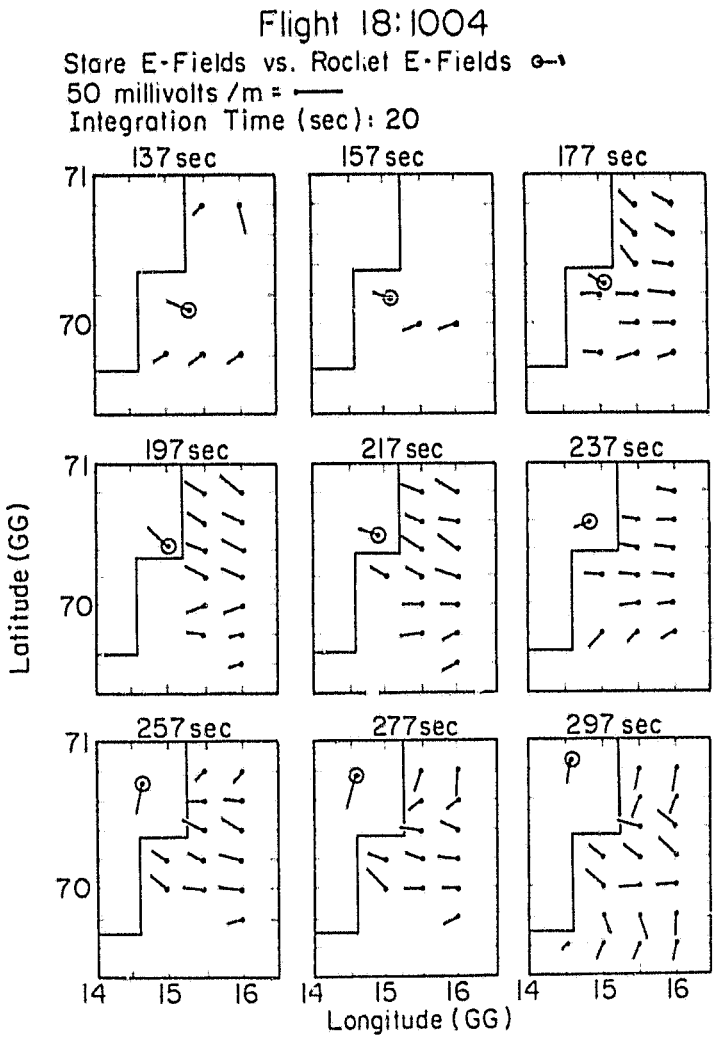


Fig. 9. STARE *E* field observations in comparison to dual probe measurements, Flight 18:1004. The westward boundary of the radar field of view is indicated.

There is an interesting dynamic pattern that seems to be drifting across this section of the oval. The sequence is a slight northward turning of the westward electric field followed by a transition southward. This disturbance appears to be drifting eastward as it is first observed by the rocket and later seen in the STARE field of view. Note in Figure 9 how the rocket measurements at 197 seconds flight time are seen by the STARE at 217 seconds, 217 seconds rocket observation viewed at 237 seconds by STARE, and so on. A rough calculation indicates the eastward flowing perturbation to have a drift of slightly greater than 1 km/s. This is a commonly observed electron drift velocity in the westward electrojet region although the predominantly westward electric field observed at this time indicates a southward drift.

In conclusion, the ion-drift technique of inferring ionospheric electric fields from a rocket platform appears to give results consistent with the more accepted dual probe and auroral radar observations. The large error that we have assigned to the ion-drift technique for the measurements presented in this paper is largely due to the relatively low count rates obtained. The instrument was designed to operate in ambient densities of $10^5$ to $10^6$ cm$^{-3}$. The densities encountered in the two flights were about $10^4$ cm$^{-3}$ as obtained from the fit routine. These densities are quite a bit lower than those normally observed, especially in the auroral regions. This problem is still being investigated. One should note, however, that the drift velocity vector is determined solely from position in $4\pi$ steradians for direction and the location in energy of the peak flux for magnitude. Thus, the drift velocity is independent of density. Recent calibration tests have indicated different efficiencies for low energy electrons or low energy ions impinging on Channeltron cone surfaces. This will effect $G_0$ in Equation (4) and, therefore, $n$, however $nG_0$ is unchanged.

Finally, we would like to briefly describe the other parameters measured by the ion drift detectors, although there is no way to compare them with an independent measurement either from instrumentation aboard the rocket or on the ground. For Flight 18:1005, the vehicle potential rose to $-1.7$ volts in the arc whereas outside the arc it remained near $-1.5$ volts. Inside the arc, the ion temperature was inferred to be $\sim$ 3000 K whereas outside, a value of 1500 K was obtained. For the fading aurora of Flight 18:1004, the temperature was about 2000 K. Near the field reversal seen in Flight 18:1005 at 200 seconds flight time, the ion detectors sensed an enhanced flow of ions out of the ionosphere resulting in an upward field-aligned current of $\sim 2\ \mu$A/m$^2$. This upward current was comparable to that carried by the auroral electrons producing the arc. This point will be further discussed in a subsequent paper when the arc of Flight 18:1005 will be modeled using all the field and particle measurements made aboard the rocket.

Future flights involving the ion drift technique will have additional plasma sensors to measure electron density and temperature and vehicle potential so that a direct comparison can be made for these parameters as we have done here for the electric field. These flights will also use four ion drift detectors giving four simultaneous pitch angle measurements of the distribution function per azimuth increment.

## Acknowledgements

This work was supported by NASA Grants NSG 6013 and NSG 6022. The authors greatly acknowledge all UNH–Minnesota staff and NASA–Wallops Island personnel for the success of the experiment. We also wish to thank the Norwegian ground support and the Tromso Auroral Observatory for data provided. The DMSP data was provided by Fredrick Rich and AFGL.

## References

1. Hanson, W. B., and Heelis, R. A.: 'Techniques for measuring bulk gasmotions from satellites', *Space Science Instrum.* **1**, 493 (1975).
2. Whalen, B. A., Green, D. W., and McDiarmid, I. B.: 'Observations of ionospheric ion flow and related convective electric fields in and near an auroral arc', *J. Geophys. Res.* **79**, 2835 (1974).
3. Morgan, B., and Arnoldy, R. L.: 'A determination of F-region convective electric fields from rocket measurements of ionosphere thermal ion spectra', *J. Geophys. Res.* **83**, 1055 (1978).
4. Cahill, L. J., Jr., Greenwald, R. A., and Nielsen, E.: 'Auroral radar and rocket double-probe observations of the electric field across the Harang Discontinuity', *Geophys. Res. Letter* **5**, 687 (1978).
5. Zanetti, L. J.: *Convective Electric Field Measurements in an Auroral Plasma*, Ph.D. Thesis, University of New Hampshire, 1978.
6. Arnoldy, R. L., Isaacson, P. O., Gates, D. F., and Choy, W. L.: 'The calibration of electrostatic analyzers and channel electron multipliers using laboratory simulated omnidirectional electron beams', *Rev. Sci. Instrum.* **44**, 172 (1973).
7. Marquardt, D. W., 'An algorithm for least squares estimation of nonlinear parameters', *J. Soc. Indust. Appl. Math.* **11**, 431 (1963).
8. Bauer, S. J.: *Physics of Planetary Ionospheres, Vol. 6, Physics and Chemistry in Space*, Springer-Verlag, New York, 185, 1973.
9. Behm, D. A., Primdahl, F., Zanetti, L. J., Arnoldy, R. L., and Cahill, Jr., L. J.: 'Ionospheric electrical currents in the late evening plasma flow reversal', accepted *J. Geophys. Res.* (1979).
10. Gurnett, D. A.: 'Electric field and plasma observations in the magnetosphere', *Critical Problems of Magnetospheric Physics*, Symposium COSPAR, IAGA, and URSI, Madrid, May, 1972, 123, 1972.
11. Heppner, J. P.: 'Electric fields in the magnetosphere, *Critical Problems of Magnetospheric Physics*, Symposium COSPAR, IAGA, and URSI, Madrid, May, 1972, 107, 1972.

JOURNAL OF GEOPHYSICAL RESEARCH, VOL. 86, NO. A2, PAGES 575-584, FEBRUARY 1, 1981

# The Hot Plasma Environment and Floating Potentials of an Electron-Beam-Emitting Rocket in the Ionosphere

ROGER L. ARNOLDY

*Department of Physics, University of New Hampshire, Durham, New Hampshire 03824*

JOHN R. WINCKLER

*School of Physics and Astronomy, University of Minnesota, Minneapolis, Minnesota 55455*

With an extensive array of particle sensors the plasma environment surrounding the Echo III accelerator payload is studied. From measurements of the thermal ion spectrum, negative payload potentials referenced to the unperturbed ionospheric plasma are obtained. Multiple detectors determined the electron population from a fraction of an eV up to 40-keV energy. An intense electron population extending up to the energy of injected electrons by the accelerator is produced when the acceleration is turned on. The energetic tail of this population is returned to the payload principally from directions in which the beam was fired, with the most intense fluxes coming from the atmosphere for downward injections of the beam. The atmospheric-scattered beam and secondary electrons are called 'quick echoes.' Electrons of energy less than several keV down to the detector threshold (0.1 eV) are called the suprathermal component. These electrons are produced isotropically around the payload during gun firings and decay away in approximately 32 ms. The largest directional intensities of this component are observed at the higher altitudes. Quick echo electrons are also observed to produce suprathermal electrons when they encounter the payload. The mechanism by which the suprathermal electrons are produced is discussed but remains unknown at the present time. The hot electrons surrounding the accelerator payload during gun injections bring sufficient charge to the payload to neutralize it provided the loss of charge by secondary production on the payload skin is small, presumably owing to a positive payload floating potential during injection. Since the hot population exists for tens of milliseconds after the gun is turned off, it results in driving the payload up to 4 volts negative during this time. Secondary production on the payload skin apparently prevents much larger negative potentials after gun turnoff when the payload is immersed in the hot population. Quick echo electrons creating suprathermal electrons around the payload also drive the payload to a few volts negative. This is an important consideration when discussing the origin of the suprathermal electrons, since electrical discharge and beam plasma discharge mechanisms do not apply to the quick echo beams.

## INTRODUCTION

The principal purpose of this paper will be to analyze the particle distribution functions measured on board the Echo III electron beam experiment in order to deduce the floating potentials of the vehicle and to identify the source and nature of the hot plasma surrounding the rocket. The subject of passive vehicle potentials in space has been much discussed [*Alpert et al.*, 1965; *Kasha*, 1969], and it is well known that the approximate floating potential of a sounding rocket in the ionosphere may be 1 V negative. But if the rocket is the source of an injected electron beam, such as the University of Minnesota Echo series and numerous other artificial electron beam experiments, then the equilibrium becomes violently disturbed, and a net current must be drawn from the surrounding ionosphere equal to the electron beam experiments, then the equilibrium becomes violently disturbed, and a net current must be drawn from the surrounding ionosphere equal to the electron beam current carried out of the local region considered. Generally, it is expected that during electron beam injection the vehicle potential will rise positively to maintain current balance. An important result of the beam injection is that the ambient plasma becomes heated and may be highly turbulent [*Cartwright et al.*, 1978], and a new plasma environment is in effect created by the beam itself. Even after the end of electron pulses the surrounding medium is found to remain appreciably heated for many tens of milliseconds. The floating potential of the rocket may be considerably altered in this hot plasma medium and be much more negative than in the normal ionosphere.

The term 'vehicle floating potential' will be defined operationally here along the following lines for the Echo III experiment: The ambient ion distribution unperturbed by the presence of the rocket payload is assumed to be Maxwellian. The vehicle potential with respect to this unperturbed plasma is determined for the Echo III flight by measuring the thermal ion spectra reaching the rocket sensors after penetrating the sheath across which the potential drop occurs surrounding the payload. As examples, theoretical ion spectra for floating potentials of +0.5, and −1.2, and −4 volts are given in Figure 1 along with the unperturbed (0 V) Maxwellian. These spectra for a density $2 \times 10^5$ cm$^{-3}$ and a temperature of 1500°K, values which correspond closely to the average ionospheric values during the Echo III flight, are expressed in terms of the differential directional intensity reaching the detector. The effect of a relative velocity of $\pm 10^5$ cm/s between the plasma and the detector on the rocket, also close to actual values, is given for the −1.2- and −4-V spectra. Negative floating potentials are readily identified by the shift in the entire Maxwellian ion spectrum toward higher energy with a sharp minimum energy cutoff resulting from acceleration of the ambient ions in passing through the sheath. Actual measured ion spectra, as we shall show, are consistent with those theoretical predictions for negative floating potentials, and thus there is a clear procedure for evaluating such negative vehicle charging



Paper number 80A0852.
0148-0227/81/080A-0852$01.00

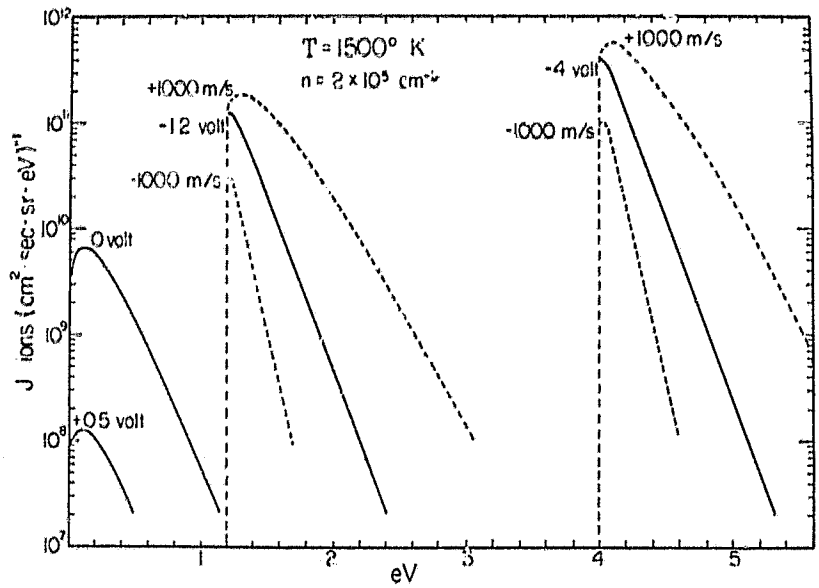


Fig. 1. Theoretical ion spectra ($^{16}O^+$ ions) for an $F$ region temperature of 1500° and a density of $2 \times 10^5$ cm$^{-3}$. Spectra are given for payload potentials of +0.5, 0, −1.2, and −4 V. The solid curves are for zero rocket ram velocity, and the dashed curves for ±1000 m/s ram velocities.

by simply measuring the low-energy spectral cutoff. All necessary details of the ion measurements and analysis for the Echo III experiments have been published by *Morgan and Arnoldy* [1978]. This technique has been utilized with success by *DeForest* [1972] and *Whipple* [1976] in revealing large negative excursions of up to 10 kV for synchronous orbit satellites when exposed to the natural energetic electron component during substorm events. Recently, a special synchronous orbit vehicle has been successfully launched to study such questions [*Stevens,* 1979].

In contrast, without knowledge of the unperturbed ion plasma parameters and the nature of ion drift motions, positive floating potentials cannot be uniquely determined from ion spectra measurements. It might be thought that electron observations should reveal positive potentials also by a minimum energy or cutoff point in analogy with the ion measurements. However, scattering and thermalizing, rocket shielding, secondary production by energetic beam electrons and other effects seriously obscure these measurements; consequently, it has been difficult to interpret the results of retarding potential analyzers when applied to electrons [*Winckler,* 1976]. Recently, by a combination of on-board particle and remote electric field techniques using a mother-daughter payload, some large positive vehicle potentials have been identified with the Norwegian Polar V experiment [*Jacobsen and Maynard,* 1978].

## INSTRUMENTATION

The thermal ion and suprathermal electron distributions surrounding the Echo III rocket were measured by electrostatic analyzers aboard the payload. The ion electrostatic analyzers consisted of 90° cylindrical electrodes (mean radius of 2 cm) and a 'channeltron' multiplier biased to postaccelerate the ions by 1500 V as the sensor. Thirty-two-point spectra from 0 to 5 eV were measured every 25.6 ms by two detectors positioned parallel and perpendicular to the payload spin axis. A more complete description of these sensors has been given by *Morgan and Arnoldy* [1978]. The electron detectors measured the directional intensity perpendicular to the rocket spin axis. Two cylindrical analyzers with different geometric factors and energy ranges were flown. Electrons from 100 eV to 15 keV were measured in 128 windows every 200 ms by an analyzer with a geometric factor of $4.6 \times 10^{-5}$ sr cm$^2$ keV (keV)$^{-1}$. The so-called 'return current analyzer' measured the electron spectrum from 0.1 eV to 1.2 keV in 128 windows every 200 ms. Although three data points were taken below 1 eV, these are to be regarded with caution, since they require very small potentials (<150 mV) across the analyzer. The energy sweep of the detector was accomplished by a 200-V potential across the electrodes decaying to 0 V in 200 ms. Voltages of 200 mV and higher could be substantiated by measurements of the voltage decay curve during the flight; lower voltages remain uncertain. This detector had a very small geometric factor, $2.5 \times 10^{-6}$ sr cm$^2$ keV (keV)$^{-1}$, in order to sense the neutralizing current during gun firings.

Finally, electrons from 10 to 40 keV were sensed by an analyzer having eighth-spherical electrodes making a 256-point spectral measurement every 200 ms. A large geometric factor, $2 \times 10^{-3}$ sr cm$^2$ keV (keV)$^{-1}$, was used to attempt a measurement of gun electrons echoing from the opposite hemisphere. The combined set of three electron detectors covered the energy range 0.1 eV to 40 keV and made directional intensity measurements from $10^4$ to $10^{15}$ electrons (cm$^2$ s sr keV)$^{-1}$. Figure 2 is a schematic showing the acceptance directions of the ion and electron (auroral) detectors and the injection direction of the electron accelerator with respect to the local magnetic field. The Black Brant motor remained with the payload, and the entire vehicle had a spin period of 0.365 s and a coning period of 43 s.

## MEASUREMENTS OF VEHICLE FLOATING POTENTIAL

The electron gun flown aboard the Echo III flight was fired according to a preprogramed sequence of various electron energies (29–43 keV) and pulse duration (2, 8, and 32 ms), with periods of silence between gun sequences. The ion electrostatic analyzers were used during these undisturbed periods

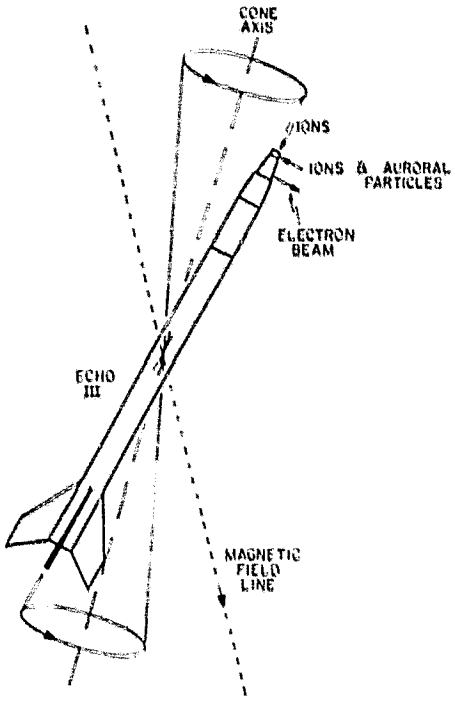


Fig. 2. Schematic showing the acceptance directions of the ion and electron (auroral) detectors and the ejection direction of the electron accelerator with respect to the local magnetic field. The coning half angle was 12°.

to infer the $F$ region electric field from the $\mathbf{E} \times \mathbf{B}$ convection drift imposed by the electric field upon the ambient ion population which appears as a relative velocity between the detectors and the plasma in addition to the rocket ram effect. The ion detector measurements during and just following gun pulses, injecting about 70 ma of 40-keV beam electrons into the ionosphere, will be discussed in this paper.

Figure 3 gives three successive ion spectra measured by the detector looking parallel to the rocket spin axis. Energy increased with time during the spectral sweeps such that 1 eV = 5 ms. The first and third spectra (sweep $N$ and $N + 2$) were measured between gun firings and represent ambient conditions. An 8-ms duration electron injection (heavy horizontal line in Figure 3) occurred during the second spectrum ($N + 1$ sweep) just at the energy (time) where the ambient population would normally have been detected. Some ions were detected during the gun pulse showing that the rocket potential even during beam injection occasionally was close to 0 V. One should note that the voltage applied to the gun was a 1-kHz square wave resulting in a partial or complete beam dropout each millisecond. The 'spikey' appearance of ions during gun-on periods as seen in Figure 3, center panel, may reflect this fact. Several milliseconds after the gun turned off, the main ion population was found between 3 and 5 eV. Note that for the next spectral sweep, ($N + 2$) after 25.6 m, the ion population had returned to its usual position. The nature of the observed spectral perturbation resulting from electron injection depended upon when the gun was fired in the spectral sweep. Figure 4 is an example of a gun firing just after the energy analyzer sweep passed through the region of the ambient population during sweep $N$. The ion population perturbed by the gun firing is now located between 4 and 5 eV and was measured in the same sweep after the gun turned off. In the next sweep, ($N + 1$), the ion spectrum had not yet quite returned to equilibrium conditions.

If we interpret the leading edge and low-energy cutoff of the ion spectra as the vehicle floating potential, we see in the examples presented above that immediately following gun pulses this potential is observed to be several volts more negative than its nominal −1.2-V value. Since the ion electrostatic analyzer sweep was randomly phased with respect to gun pulsing, it has been possible to construct a time profile of ion spectra cutoff and therefore vehicle potential before, during, and after gun pulsing using about thirty 2-ms gun pulses near rocket apogee. The data are shown in Figure 5 and have been separated according to whether the gun electrons were fired down into the atmosphere ($\alpha = 70°$) or away from the atmosphere ($\alpha = 110°$). The payload tended to reach its largest negative potential ~ 5 ms after the end of the gun pulse and then returned to the equilibrium potential of −1.2 V by 10 ms for injection upward. For downward injection the negative payload potential did not decay back to the equilibrium value until about 20-ms after the gun firing. This long-enduring potential for downward injections is apparently due to the immersion of the payload in a population of backscattered beam and secondary electrons from the atmosphere reaching the rocket approximately 12 ms after gun firing. In a detailed study of particle dynamics in the vicinity of a beam-emitting rocket, *Winckler et al.* [1975] have referred to such particles as quick echos. Figure 6 gives an example of such a quick echo (heavy line) registered by one of the Echo III electron detectors following an 8-ms injection of 29-keV electrons down-

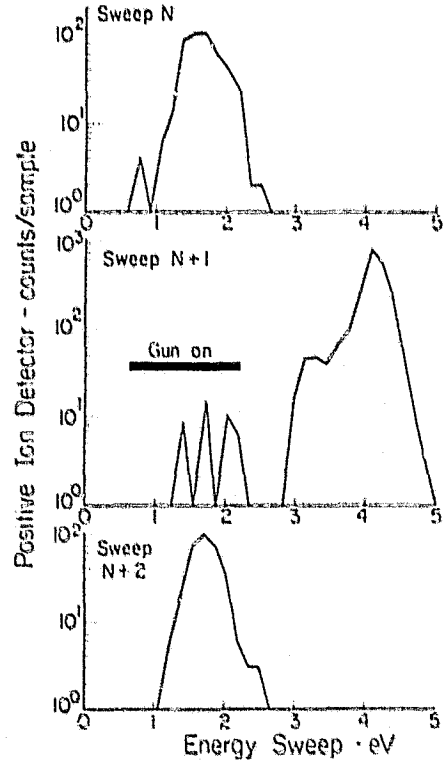


Fig. 3. Measured ion spectra for three consecutive energy Sweeps. The dark horizontal bar in sweep $N + 1$ corresponds to the time of a gun firing. The spectral sweep time was 25.6 ms, sampling from 0- to 5-eV energy. The gun injected electrons at 97° pitch angle, and the ion sensors detected ions having a pitch angle of 53°.

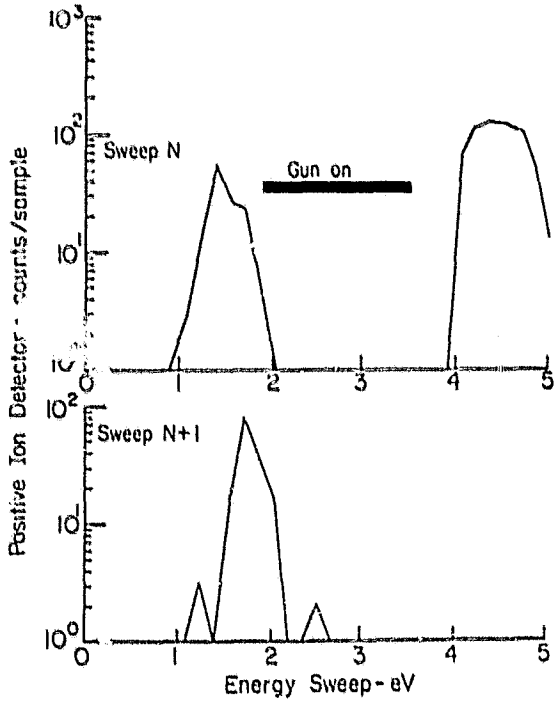


Fig. 4. Ion spectra for two energy sweeps. Gun-on time is again indicated by the dark horizontal bar.

ward into the atmosphere. The detector was in the process of scanning in energy from 19 keV to 14 keV during the echo. The maximum response to the returning electron beam is delayed 12 ms from the center of the gun pulse, which is approximately the time required for a 30-keV electron having a 70° pitch angle at 270 km (which lies in the loss cone) to travel to the 100-km altitude level, undergo atmospheric scattering and magnetic reflection, and return to the rocket. The observed energy is approximately that expected for backscattered 29-keV beam electrons [*Winckler et al.*, 1975]. The light line in Figure 6 shows suprathermal secondaries of 30–150 eV near the rocket generated both by the injected beam and by the quick echo electrons.

One can interpret the increase in negative payload potential following gun pulses shown in Figure 5 as due to a rise in the temperature of the surrounding electron population which we shall now proceed to discuss. Langmuir probe measurements made aboard the Echo II flight [*Cartwright et al.*, 1978] have shown that the electron accelerator heated the electrons of the background plasma to 10,000°K. *Cartwright et al.* [1978] suggested that the high-temperature component of the background plasma represented secondaries produced by the accelerator beam.

## THE HOT ELECTRON POPULATION

The Echo III data are unique among such experiments in that the electron spectrum reaching the payload was measured over a very large energy range, between 0.1 eV and 40 keV. The hot electron population surrounding the payload, necessary information for payload electrodynamic studies during electron injection, is therefore known. Spectra measured at various times with respect to 8-ms duration gun firings and a background spectrum due to natural electrons are given in Figure 7. This figure gives the differential directional intensity of upward moving electrons generated by downward electron beam injections of 8-ms duration, at nominally 40-keV energy and 70-ma beam current. Since the detectors required 200-ms to make a complete spectral measurement, data were compiled over a flight time of ~150 s (fifteen 8-ms gun pulses) in order to obtain the various spectra of Figure 7 measured at the indicated times with respect to gun firings. Limited energy coverage at the desired time with respect to gun pulsing abbreviated some of the spectra at low and high energies. Examples of actual data points are given for the upper and lower curves but not for the remaining spectra to avoid confusion in the presentation.

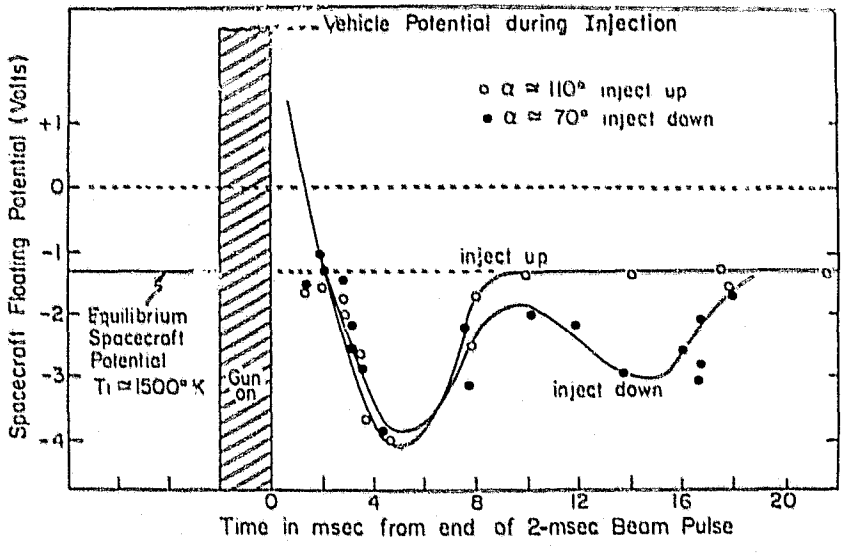


Fig. 5. Floating potentials of the Echo III rocket in the quiescent ionosphere at 250 km before beam injection ($t < 0$), during 2-ms beam pulses (quite likely fluctuating and generally unknown), and after injection, deduced from the low-energy cutoff of the spectra of thermal ions. At 5 ms the rocket reaches an extreme negative potential in the heated plasma created by the beam. At 15 ms another negative excursion is associated with quick echoes returned from below the rocket (only seen for downward injections).

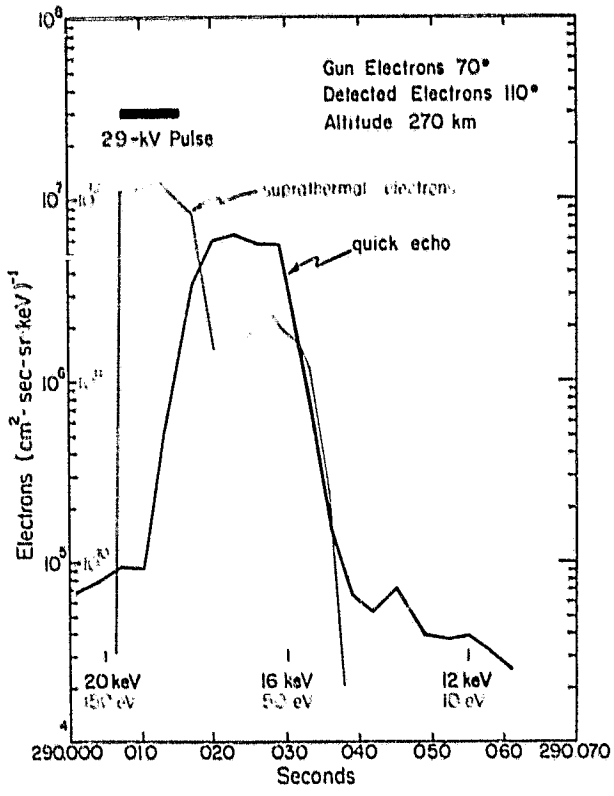


Fig. 6. Directional electron intensities measured by two detectors during and following an injection of 29-keV electrons into the atmosphere. The energies sampled by the two detectors as a function of time are given at the bottom of the figure. The heavy curve is a quick echo. The gun injection and the quick echo electrons both produce suprathermal electrons (light curve).

The low-energy portion of the electron spectrum maximizes during the gun pulse and then decays to background after injection. In contrast to this a significant increase in the flux of high-energy electrons occurs after the gun turns off, reaching a maximum intensity 8 ms after the pulse has terminated. This flattening of the electron spectrum is due to the quick echo electrons discussed above filling in the region above 10 keV. Purely magnetically mirroring gun electrons are not a part of the quick echo beam because they cannot reach the particle detectors as the payload moves off the field line of injection [*Winckler et al.*, 1975]. Only those gun electrons which have multiple-Coulomb scattered in the atmosphere below the rocket to field lines and directions bringing them back to the payload will be detected in the quick echo; hence one should not be surprised at the absence of a peak in the backscattered spectrum at the gun energy. The hypothesis that the spectral flattening is due to atmospheric backscattered electrons is supported by measurements made when the gun fired away from the atmosphere, where the spectral flattening does not occur.

The response of the detector which sampled energies between 150 eV and 10 eV plotted in Figure 6 is a specific example of the time profile of the suprathermal population following a gun injection. The data of Figure 6 are for an 8-ms, 29-kV downward electron injection. For injections upward where no quick echos would be produced, the hot population in this energy range would decay much more rapidly than the ~20 ms given in Figure 6. The secondary peak in the hot population at 290.027 s in Figure 6 is apparently produced by the quick echo electrons. The suprathermal electrons in the secondary peak in turn generate the negative payload floating potential maximizing at 15 ms after gun turnoff as given in Figure 5, while the more intense fluxes measured during and immediately following gun injection are responsible for the prompt (~5 ms) negative payload potential.

## PRODUCTION OF NEGATIVE FLOATING POTENTIAL

At equilibrium, any object in a plasma will adjust its floating potential as defined earlier to keep the total current flowing to the object equal to zero. The thermal ion measurements made between gun pulses aboard Echo III show that to accomplish this, the payload floated at −1.2 V, accelerating ions to the payload and retarding the electrons in compensation for the difference in the thermal ion and electron speeds. However, when the payload was embedded in the very hot electron population following gun injections, we saw above how the floating potential exceeded 4 V negative. Since rather complete thermal and suprathermal electron observations were made above Echo III, we can quantitatively discuss the ambient −1.2-V and the −4-V floating potentials during injection in terms of this suprathermal population. It should be noted here that the Echo III flight was made at night, so photoelectron effects can be ignored.

### *Ambient Conditions, −1.2-V Floating Potential*

A multiparameter fit to the Echo III ion data [*Morgan and Arnoldy*, 1978] inferred an in situ ion temperature of 1500°K.

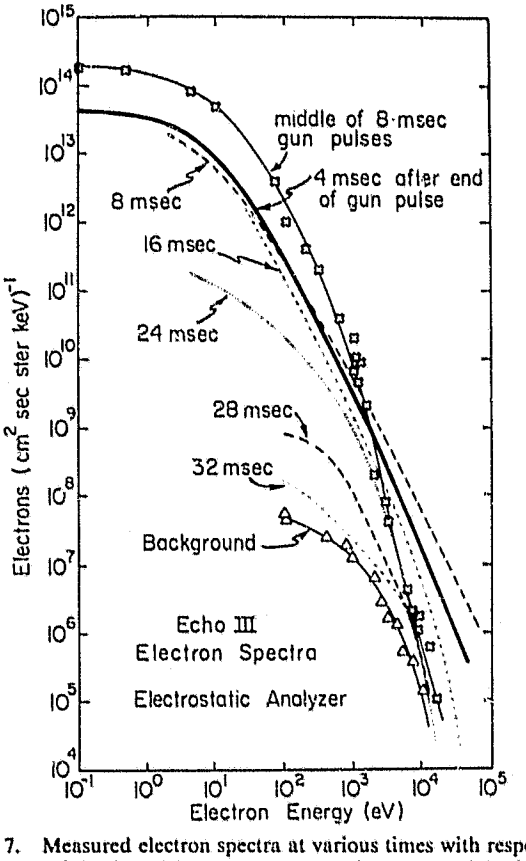


Fig. 7. Measured electron spectra at various times with respect to the 8-ms gun injections. The spectra are compiled over a flight time of 150 s, or fifteen 8-ms gun injections. The spectra are for gun injection downward into the atmosphere and detection of upward moving electrons. Data points are given for only two spectra to eliminate confusion in the presentation.

A density of $2 \times 10^5$ cm$^{-3}$ at rocket apogee was measured during the flight by the Chatanika radar. Figure 1 gives the theoretical, zero plasma potential Maxwellian for these values along with the shifted Maxwellian distribution as it would be observed on a vehicle surface whose floating potential was −1.2 V, which corresponds to the measured value. The shifted Maxwellian is obtained from the 0-V distribution by conserving $J/E$ according to Liouville's theorem, where $J$ is the differential directional intensity, having units of particles (cm$^2$ s sr keV)$^{-1}$. Integrating the $N$ sweep of Figure 3 over energy gives $1.5 \times 10^{10}$ ions (cm$^2$ s sr)$^{-1}$, which compares favorably with the corresponding value of $2 \times 10^{10}$ ions (cm$^2$ s sr)$^{-1}$ obtained by integrating the theoretical curve of Figure 1.

The thermal ion current density incident on the rocket skin can be estimated from the integrated directional intensity by multiplying it by the electronic charge and effective solid angle $\Omega$ over which the ions reach the payload. We assume that the rocket is surrounded by a sheath of 1.2-V potential difference. A thermal $^{16}O^+$ ion moving approximately parallel to this sheath at an energy of $kT = 0.13$ eV will be accelerated as it enters the sheath toward the rocket surface, gaining 1.2 V. The maximum angle measured with respect to the detector view direction (normal to the sheath) that these ions will have as they reach the detector will be 18°. The effective solid angle $\Omega$ is therefore 0.3 sr, and the ion current density becomes $I_{ion} = 10\ \mu$a m$^{-2}$.

A rocket payload moving relative to the thermal ion plasma will record greatly distorted ion energy distributions, as seen in the example in Figure 1, for overtaking and receding velocities of $10^5$ cm/s. From an analysis of the distorted equilibrium ion spectra the $\mathbf{E} \times \mathbf{B}$ drift has been inferred for the Echo III data [*Morgan and Arnoldy*, 1978]. However, the ion measurements presented here made by the detector viewing along the rocket spin axis experienced the least relative velocity near apogee, hence the approximate the zero-velocity case. The current given above is therefore the best estimate of the average ion current density that can be made. A similar ion current is obtained by computing the charge swept up per second by the transverse rocket motion through the plasma, since the transverse rocket ram speed is comparable to the ion thermal speed.

At equilibrium the ion current density should be balanced by the thermal electron current to the −1.2-V payload:

$$I_{\text{electron}} = \frac{nq}{4} \times 10^4 \left(\frac{8kT_e}{\pi m_e}\right)^{1/2} e^{-1.2/kT_e} = 0.1\ \mu\text{a m}^{-2}$$

for a density of $2 \times 10^5$ cm$^{-3}$ and 1500°K temperature. This current is extremely sensitive to the temperature. The temperature need only be increased to 2500°K to produce a current equal to the ion current. In fact, a 2500°K electron temperature is reasonable since there was a diffuse auroral region covering the eastward flight trajectory. Furthermore, the electron background measurement given in Figure 7 shows a substantial flux of hot electrons above 100 eV, and thus the condition $I_{ion} = I_{electron}$ seems attainable.

*Postbeam Injection Conditions, −4-V Potential*

The measured ion spectrum reaching the payload at −4-V potential (Figure 3, $N + 1$ sweep) has quite a different shape than the theoretical shifted Maxwellian of Figure 1. However, the directional intensities integrated over energy in both cases agree to within a factor of 2. The measured value is $3 \times 10^{10}$ ions (cm$^2$ s sr)$^{-1}$ compared with $6 \times 10^{10}$ ions (cm$^2$ s sr)$^{-1}$ from Figure 1. The measured spectrum of Figure 3 is perhaps distorted because the detector energy sweep was not fast in comparison to the time constant of the floating potential; hence the payload potential could have changed significantly between energy steps.

As discussed above, the negative potential will collimate the ions reaching the payload, and for −4-V the effective solid angle is 0.10 sr. The ion current density at the payload becomes 10 $\mu$a m$^{-2}$ for the theoretical directional intensity. Thus despite a higher directional intensity than in the −1.2-V case the collimation reduces the effective solid angle to give equal current densities. In fact, the ~10 $\mu$a m$^{-2}$ current density for both negative potentials is equal, as it should be, to the total thermal ion current density incident on the sheath around the vehicle given by

$$I_{\text{ion}} = \frac{nq \times 10^4}{4} \left(\frac{8kT_i}{\pi m_i}\right)^{1/2} = 11\ \mu\text{a m}^{-2}$$

for a density of $2 \times 10^5$ cm$^{-3}$ and 1500°K temperature. For a thermal sheath interface area not too different from the rocket area (the Debye length at 260 km for ambient conditions is ~1 cm) the above equality simply means that all the ions entering the sheath are attracted to the payload and collected by it.

Integrating the hot electron spectrum measured 8-ms after the gun pulse in Figure 7 gives the directional intensity of the electrons that reach the payload for the −4-V floating potential. This integration gives $3 \times 10^{11}$ electrons (cm$^2$ s sr)$^{-1}$, resulting in an electron current density reaching the payload of 1.5 ma m$^{-2}$, over 2 orders of magnitude greater than the ion current. The electron current can be made equal to the ion current if secondary emission produced by the hot electron bombardment of the payload results in only 1% net electron charge collection. We have further evidence for this from the Echo I rocket flight. During this flight a large aluminized mylar disc was deployed to aid neutralization of the payload. During quick echos this collector was driven positive apparently as a result of secondary emission when bombarded by the quick echo beam and the hot population produced by it [*Hendrickson et al.*, 1975]. From the Echo III data presented in Figure 5 we know that quick echoes produced a hot population similar to that resulting from injections of the primary beam. One can therefore deduce that in the absence of secondary electron emission from the payload the hot electron distribution of Figure 7 would necessarily have driven the payload much more negative than the −4 V observed in order to repel the low-energy electrons and maintain current balance at equilibrium.

## PAYLOAD POTENTIAL AND NEUTRALIZATION DURING GUN INJECTIONS

Integration over energy of the 'middle of 8-ms gun pulse' curve of Figure 7 gives $2 \times 10^{12}$ electrons (cm$^2$ s sr)$^{-1}$ or a current density of 10 ma m$^{-2}$ arriving at the payload during injection. If this current density was uniform over the entire payload area of 10 m$^2$, a total negative current of 100 ma was collected, which agrees well with the 70-ma beam of electrons leaving the payload.

For an ionospheric density of $2 \times 10^5$ cm$^{-3}$ and a temperature of 1500°K the thermal electron current density would be 2 ma/m$^2$, and the thermal current to the payload becomes 20 ma. To neutralize the payload during a 70-ma electron injec-

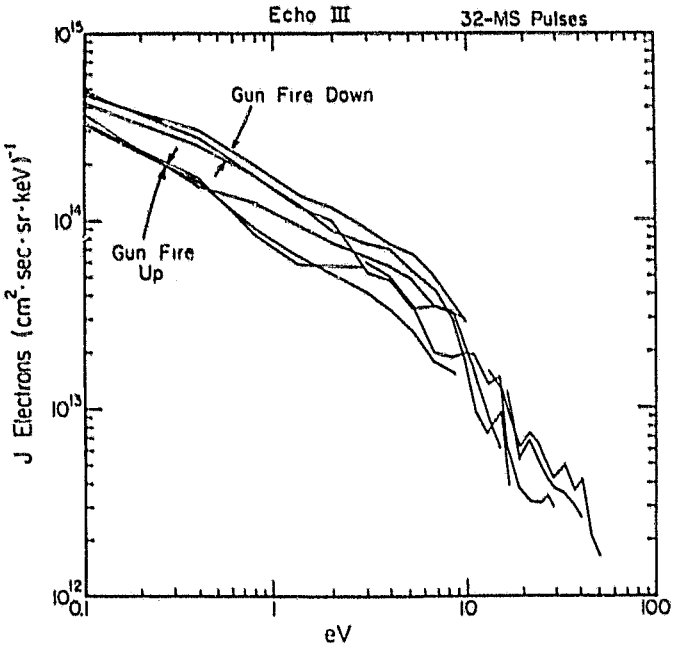


Fig. 8. Segments of measured electron spectra during 32-ms gun firings. Continuous lines are data from the same spectral sweep. At low energies the curves separate according to whether the gun is injecting electrons into the atmosphere or away from it.

tion, a current amplification of 3.5 was therefore needed, and in fact one may consider the suprathermal spectra of Figure 7 to be showing this amplification effect. Secondary emission would not be a factor in this case, since presumably the payload is driven positive during gun firings, thereby returning any secondaries produced back to the payload. It is important to bear in mind that the electron detectors measured particles having pitch angles between 40° and 140°. This combined with the fact that a large percentage of the collecting area could be reached only by flow transverse to **B** means that if the measured electrons neutralized the Echo III rocket, as suggested above, it was accomplished by cross **B** particle motion. No measurements were made to estimate the neutralization current parallel to **B**. Measurements made aboard the Echo IV flight by *Israelson and Winckler* [1979] using metallic collectors, however, showed that there was no appreciable difference in return current collected along the field from that detected perpendicular to the field.

The thermal ion observations presented above clearly show that a few milliseconds after the gun was turned off, the payload potential recovered and in fact swung negative. There remains the question, however, as to whether or how much the Echo III payload charged positively during gun injections to attract the neutralization current. As mentioned before, the thermal ion data during gun pulses cannot measure positive potentials but do not rule out the possibility. The small geometric factor return current electron electrostatic analyzer was capable of measuring the energy of electrons returning to the rocket during gun firings. Portions of a number of electron spectra taken during several 32-ms gun pulses are plotted in Figure 8. Each line segment represents data taken during the same spectral sweep and for one gun pulse. The lack of any spectral cutoff in the curves of Figure 8 essentially leaves the payload potential question unanswered in that it might be interpreted as evidence for (1) a positive potential in which the electrons have undergone complete thermalization before being detected, (2) a positive potential in which there was a strong electron source in the sheath (e.g., beam ionization of neutral gas surrounding the rocket, secondary emission from payload skin, or a plasma discharge around the payload), (3) no potential drop at all, or (4) a rapidly fluctuating potential not capable of being resolved by the measurements made every 3.2 ms. The fact that there is a discernible difference on whether the gun fires up or down indicates that without a thorough understanding of the source of the hot electrons surrounding an accelerator payload they are not a reliable measure of vehicle potential. Ambiguity between two different techniques of determining vehicle potential aboard the Araks rocket utilizing electron measurements [*Gringauz and Schutte*, 1976] further substantiates this conclusion. Measurements of electric fields and electrons on a payload separated from the beam-emitting rocket have produced evidence, however, for large positive potentials in a region of space including the rocket during electron injections [*Jacobsen and Maynard*, 1978].

## PRODUCTION OF HOT ELECTRONS

The hot electron spectrum reaching the payload during and following electron injections undoubtedly has several components. One component might be electrons accelerated to the payload during injections which may be thermalized by local collisions and the generation of secondaries. Another part could be composed of electrons scattered from the beam and the atmosphere (quick echos) and all the secondaries produced by beam and scattered beam electrons. The Norwegian Polar 5 experiment clearly showed the production of a halo of secondary electrons around the beam by detectors on the mother payload physically removed from the daughter payload carrying the electron accelerator [*Maehlum et al.*, 1978]. To explain the increase in secondary electron fluxes with altitude as observed in the Polar 5 experiment, *Maehlum et al.* [1978] have suggested wave-particle interactions as a source of hot electrons at high altitudes.

The spectra of Figure 7 are only for electron injection down into the atmosphere and electrons detected moving up away from the atmosphere. For other injection and view directions they are considerably different. In an attempt to unravel the dependence of detector response on energy, gun pitch angle, and detector pitch angle we have used the phase map presentation developed in the analysis of the Echo II data [*Winckler et al.*, 1975]. In this presentation the measured directional intensity is plotted on a pitch angle of gun injection versus pitch angle of detection grid. The magnitude of the directional intensity is four-level-coded by the size of the data point. The phase map of Figure 7 is made for the average directional intensity of electrons having any energy between 5 and 25 keV sampled during four time intervals: during any gun pulse, 0–8 ms after, 8–16 ms after, and 15–24 ms after the pulse. Two of the three electron detectors flown contributed to this map. Since the detector energy sweeps were not synchronized to the gun firings, the energies sampled for any gun pulse were random. Although electrons from 5 to 25 keV were accepted for the plot, for any given time segment the energy changed by less than 1 keV over the averaging time. Finally, injection at all altitudes were used in constructing the phase map of Figure 9.

The Figure 9 phase map substantiates the conclusion

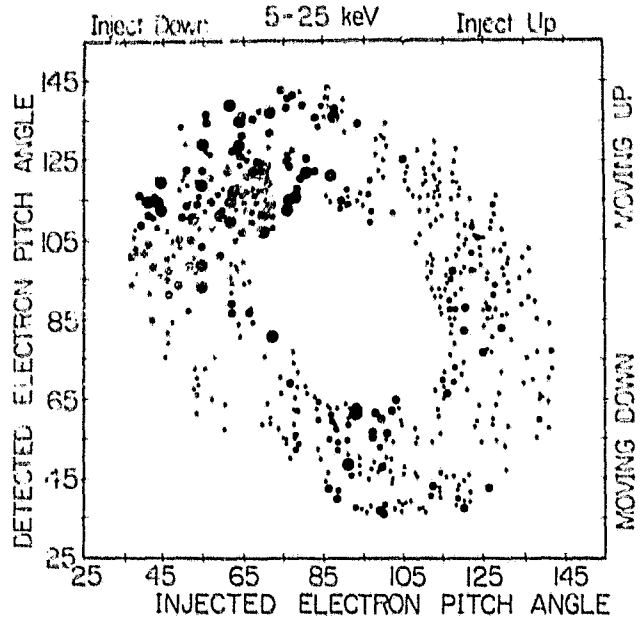


Fig. 9. Phase map (explained in text) for electrons between 5 and 25 keV. The size of the dot increases with the directional intensity measured.

reached in the earlier analysis of the Echo II data [*Winckler et al.*, 1975] that energetic electrons whose trajectories clear the payload return from directions in which the electron gun has just injected beam electrons. Quick echoes predominate and lie in the "inject down-detect moving up' quadrant of the phase map. A significant but still unexplained return of energetic electrons occurs when the gun injects up and the detectors view electrons moving down the magnetic field.

The phase maps of Figure 10 are for the 0.1- to 1.2-keV suprathermal component. The data for these maps are further selected according to time segments measured with respect to beam injection and the altitude at the time of injection. The two maps on the left are for altitudes below 200 km, and those on the right between 200 and 260 km. The top panels of each set include the time segment during the injection and the first 8-ms segment after gun turnoff. The bottom panels are for the 8- to 16- and 16- to 24-ms segments after gun turnoff. Average directional intensities during each time segments are plotted as in the phase map of Figure 9.

The range of average directional intensities included on a given phase map is given in the lower left corner. The maximum intensities measured have an altitude dependence, increasing with altitude. The phase maps also show that as a function of time after gun injection the suprathermal electrons decay in intensity as the spectra of Figure 7 show. During and immediately following injections the suprathermal electrons show little dependence on injection and detection pitch angles as given by the top two phase maps. Apparently, the suprathermal electrons form an isotropic cloud around the payload during this time. As the intensity decreases with time, however, there is an indication in the high-altitude data of a longer time constant for the decay in the quick echo quadrant apparently due to their delayed production by the energetic quick echo electrons as seen in Figure 6.

The altitude dependence of the suprathermal electrons first seen in the Polar V data [*Maehlum et al.*, 1978] has led these investigators to rule out secondary production by beam ionization as a principal source of the suprathermal electrons at high altitudes. A beam-plasma interaction mechanism was postulated, since it would become more efficient at high altitudes and explain the observed altitude dependence. One such mechanism, beam-plasma discharge originally discussed by *Getty and Smullin* [1963], has recently been observed in plasma tank experiments by *Bernstein et al.* [1979]. The results of the plasma tank experiments, however, suggest that the Echo III electron gun was not capable of igniting the discharge [*Winckler*, 1979]; hence the interaction was probably not the source of the hot population. Moreover, the fact that quick echo beams (orders of magnitude less intense than the injected beam) also produced suprathermal electrons clearly requires alternative sources.

Can one rule out the possibility of secondary production by beam ionization of the neutral gas around the rocket? The study of auroral light produced by the Echo III beam as a function of altitude by *Israelson and Winckler* [1975] shows that the neutral density surrounding the payload is not significantly enhanced above ambient values as a result of payload outgassing; hence the ionization must occur only in the ambient neutral atmosphere. Since the neutral atmospheric density decreases by 2 orders of magnitude over the altitude range 130–260 km, the ionization rate near the rocket will do likewise. If equilibrium conditions are assumed, then the decrease in the recombination coefficient as a function of altitude does compensate for the drop in production rate to give nearly constant secondary densities as a function of altitude. It is not at all evident, however, that the equilibrium conditions should prevail during and immediately following gun injections.

The observations of a visible light glow around the Zarnitza payload [*Lyachov and Managadze*, 1977] suggest that an electrical discharged occurred owing to the high positive payload potential during injection. Such a discharge might produce the suprathermal secondaries observed by the Echo III electron detectors during and immediately following injection. Photometers flown aboard the Echo III flight, however, give no evidence for any light produced by such a discharge [*Israelson and Winckler*, 1975]. Moreover, this mechanism could not produce the suprathermal electrons associated with quick echos, since the payload potential was measured to be only a few volts negative at these times. Finally, the isotropic distribution of suprathermal electrons during injections requires a rapid thermalization of the hot electrons. Since strong wave emissions have been measured during gun injections [*Cartwright and Kellogg*, 1974], it is quite likely that wave-particle interactions must enter the picture to accomplish this and could also be instrumental in producing the suprathermal component.

## SUMMARY

1. From measurements of the thermal ion spectrum, negative excursions of the payload potential referenced to the unperturbed plasma up to −4 V were observed several milliseconds after gun firing.

2. A hot electron population existed around the Echo III payload during beam injections, decaying to background intensities in a few tens of milliseconds. The hot population extended in energy up to the injected electron energy. The energetic electrons of this population returned to the payload principally from directions in which the beam was fired. From

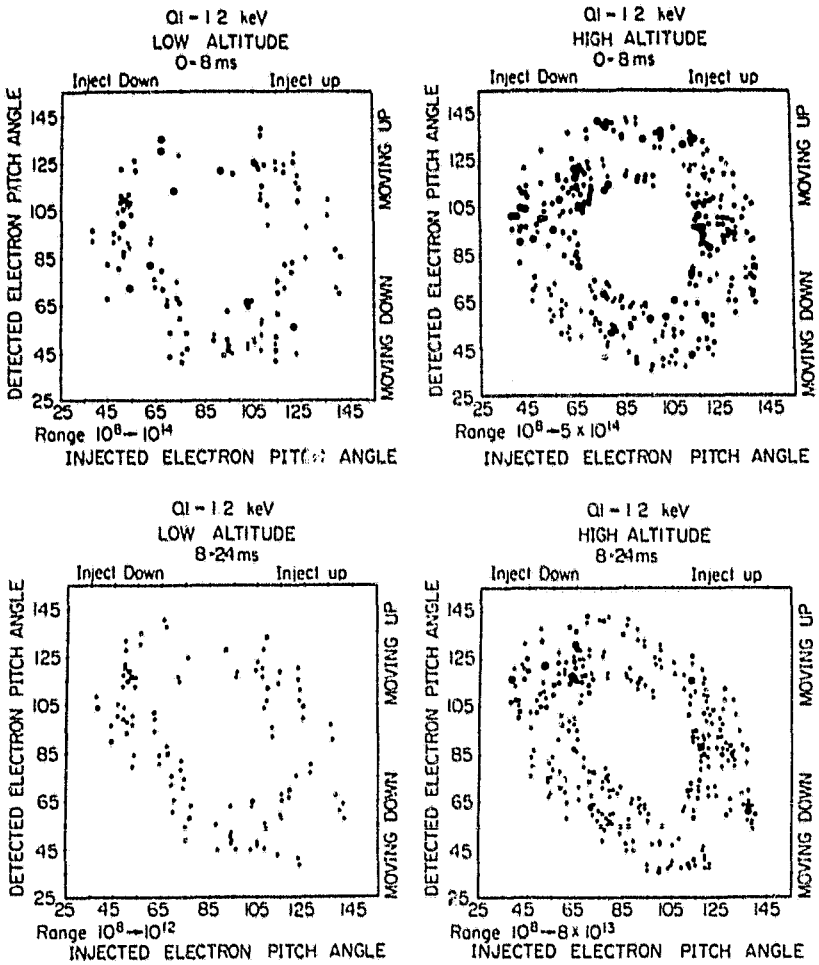


Fig. 10. Phase map of suprathermal (0.1–1.2 keV) electrons separated according to altitude (left maps are for altitudes below 200 km, and right maps are for altitudes between 200 and 260 km) and time after gun injections. Top two maps are for the time segment during injection and the first 8-ms segment after injection. The bottom maps are for the 8- to 16-ms and 16- to 24-ms segments after gun turnoff. The range of directional intensities plotted in each map is given in the lower left corner beneath each map.

the atmosphere the energetic electrons were beam and secondary electrons Coulomb-scattered onto the rocket field lines (quick echos) and were delayed in arriving at the payload after beam injection by their transit time to go down to the atmosphere and come back to the payload. The downward return of energetic electrons for upward injections resembles the Echo II result and is not as yet understood.

3. The suprathermal component (less than a few keV) of the hot population appears to have been produced isotropically about the payload during gun injection. The intensity of this component increased with increasing altitude.

4. The suprathermal component of the hot population was responsible for driving the payload negative several milliseconds after gun turnoff.

5. Energetic quick echo electrons also produced a suprathermal component when they intercepted the payload, resulting in a second negative excursion in the payload potential for downward injections.

6. Setting the electron current collected by the payload equal to the measured ion current several milliseconds after the end of gun injections requires that the measured suprathermal electrons were only 1% efficient in bringing negative charge to the payload. One might interpret this in terms of a rather large secondary emission from the payload when bombarded by the suprathermal electrons.

7. The Echo III particle measurements give no information about positive payload potentials during injections. If the payload were sufficiently positive to prevent the loss of charge by secondary emission, the measured hot electron intensities surrounding the payload were more than adequate to provide the beam neutralization current during injections.

8. The positive dependence of the suprathermal component on altitude makes it difficult to interpret its origin in terms of beam ionization of the neutral atmosphere. Wave-particle interactions, beam-plasma discharge, and electrical discharge of a highly charged payload should be studied further. However, the suprathermal electrons produced by quick echo electrons could not have been generated by the beam-plasma discharge of an electrical discharge around the payload. Upon completion of this work we received a manuscript accepted for publication authored by *Johnstone and Sojka* [1980] dealing with the heating of ambient thermal electrons to temperatures as high as $10^5$ °K by the passage of a field-aligned beam of suprathermal auroral electrons. Since the

measurements were made at altitudes above 600 km, where collisional effects are negligible, Johnstone and Sojka suggest that they represent evidence for beam-plasma interaction.

*Acknowledgments.* The Echo III program and the analysis of data were supported at the University of Minnesota under NASA grant NSG-07005 and at the University of New Hampshire by subcontract from the University of Minnesota and by NASA grant NSG-6022. We wish to acknowledge the efforts of Barry Morgan in building the University of New Hampshire instruments and his major role in the analysis of the data. Also at the University of New Hampshire the data analysis work of Daniel Mead is appreciated. Much credit for the overall success of the Echo III program must go to Richard Hendrickson as Program Scientist at the University of Minnesota.

The Editor thanks D. Reasoner and A. G. Rubin for their assistance in evaluating this paper.

## REFERENCES

Al'pert, Ya. L., A. V. Gurevich, and L. P. Pitaevskii, *Space Physics With Artificial Satellites*, translated by H. H. Nickle, Consultants Bureau, New York, 1965.

Bernstein, W., H. Leinbach, P. J. Kellogg, S. J. Monson, and T. Hallinan, Further laboratory measurements of the beam plasma discharge, preprint, Natl. Oceanic and Atmos. Admin., Space Radiat. Lab., Boulder, Co., 1979.

Cartwright, D. G., and P. J. Kellogg, Observations of radiation from an electron beam artificially injected into the ionosphere, *J. Geophys. Res., 79*, 1439, 1974.

Cartwright, D. G., S. J. Monson, and P. J. Kellogg, Heating of the ambient ionosphere by an artificially-injected electron beam, *J. Geophys. Res., 83*, 16, 1978.

DeForest, S. E., Spacecraft charging at synchronous orbit, *J. Geophys. Res., 77*, 651, 1972.

Getty, W. D., and L. D. Smullin, Beam-plasma discharge: Buildup of oscillations, *J. Appl. Phys., 34*, 3421, 1963.

Gringauz, K. I., and N. M. Shutte, Altitude changes of electrical potential of the 'Eridan' rocket during Araks experiment, *Preprint 223*, Space Res. Inst. (IKI), Acad. of Sci., Moscow, USSR, 1976.

Hendrickson, R. A., R. S. McEntire, and J. R. Winckler, Echo I: An experimental analysis of local effects and conjugate return echoes from an electron beam injected into the magnetosphere by a sounding rocket, *Planet. Space Sci., 23*, 1431, 1975.

Israelson, G. A., and J. R. Winckler, Measurements of 3914-Å light production and electron scattering from electron beams artificially injected into the ionosphere, *J. Geophys. Res., 80*, 3709, 1975.

Israelson, G. A., and J. R. Winckler, Effect of a neutral $N_2$ cloud on the electrical charging of an electron beam-emitting rocket in the ionosphere—Echo IV, *J. Geophys. Res., 84*, 1442, 1979.

Jacobsen, T. A., and N. C. Maynard, Evidence for significant spacecraft charging by an electron accelerator at ionospheric altitudes, *Intern. Rep. E-292*, Norw. Def. Res. Estab., Kjeller, Norway, Dec. 1978.

Johnstone, A. D., and J. J. Sojka, A beam/plasma interaction in the high altitude auroral ionosphere, *Planet. Space Sci., 28*, 467, 1980.

Kasha, M. A., *The Ionosphere and Its Interaction with Satellites*, Gordon and Breach, New York, 1969.

Lyachov, S. B., and G. G. Managadze, Beam-plasma discharge near the rocket (Zarnitax II Experiment), *Preprint 310*, Space Res. Inst., Acad. of Sci., Moscow. USSR, 1977.

Maehlum, B. N., B. Grandal, T. A. Jacobsen, and J. Troim, Scattering of an artificially produced electron beam in the atmosphere, *Tech. Note E-950*, Norw. Def. Res. Estab., Kjeller, Norway, Feb. 1978.

Morgan, B. G., and R. L. Arnoldy, A determination of *F* region convection electric fields from rocket measurements of ionospheric thermal ion spectra, *J. Geophys. Res., 83*, 1053, 1978.

Stevens, J. R., Description of the Space Test Program's P78-2 spacecraft (abstract), *Eos Trans. AGU, 60*, 922, 1979.

Whipple, E. G., Jr., Observation of photoelectrons and secondary electrons reflected from a potential barrier in the vicinity of ATS-6, *J. Geophys. Res., 81*, 715, 1976.

Winckler, J. R., A summary of recent results under the 'Echo' program for the study of the magnetosphere by artificial electron beams, *Cosmic Phys. Tech. Rep. 168*, Univ. of Minn., Minneapolis, 1976.

Winckler, J. R., The application of artificial electron beams to magnetospheric research, *Cosmic Phys. Tech. Rep. 183*, Univ. of Minn., Minneapolis, 1979.

Winckler, J. R., R. L. Arnoldy, and R. A. Hendrickson, Echo II: A study of electron beams injected into the high-latitude ionosphere from a large sounding rocket, *J. Geophys. Res., 80*, 2083, 1975.

(Received March 25, 1980;
revised June 11, 1980;
accepted June 12, 1980.)